Insights relating to octane rating and the underlying role of autoignition

André Swarts

Thesis presented for the degree
DOCTOR OF PHILOSOPHY
in the Department of Mechanical Engineering
UNIVERSITY OF CAPE TOWN

February 2006

Abstract

The methods prescribed by the ASTM for Research and Motor octane number ratings are generally accepted as indicative of the anti-knock properties of gasoline when applied in spark ignition engines. However, it has been shown by the author that the manifestation of autoignition in the CFR engine that is used for octane rating differs significantly from that which is typically experienced in a modern production engine under knocking conditions (SAE paper 2005-01-2081).

The present research examines the knock measurement system prescribed by the ASTM method and demonstrates how knock intensity is defined by the pressure rise associated with bulk autoignition heat release and that it is insensitive to the high frequency pressure fluctuations. Significantly, the extent of pressure fluctuations present during octane rating at "standard knock intensity" was shown to vary considerably between fuels of different composition.

In a production engine, potentially damaging knock arises from a localised and near-instantaneous autoignition phenomenon involving a relatively small fraction of the trapped mass (less than 10%) and is characterised by significant pressure fluctuations. In the CFR engine however, it was found that the autoignition that occurs during octane rating could involve anything from 30% to 80% of the trapped gas, depending on the octane value of the fuel being tested. This manifestation of autoignition is characterised by a rate of heat release exceeding the rate associated with normal flame propagation, but which is insufficient to produce a substantial localised pressure discontinuity and the associated characteristic pressure fluctuations. It is therefore believed to be an example of cascading autoignition similar to the phenomenon associated with Homogeneous Charge Compression Ignition (HCCI) type combustion. A pre-requisite for such a cascading autoignition is a non-uniform end-gas temperature profile that was found to be a unique function of the engine geometry and independent of the fuel tested. The profile of the inferred thermal gradient was quantified by theoretical calculation and the hypothesis was validated for the primary reference fuels and the toluene standard fuels, as well as for gasoline surrogate blends.

The research findings have important implications for octane modelling and prediction, HCCI combustion research and engine performance simulations.

Acknowledgements

I wish to acknowledge the following people:

- My fellow students at the Sasol Advanced Fuels Laboratory and colleagues from Sasol for their assistance in different facets of the research.

- Mr. Trevor Cloete from the University of Cape Town, for the original suggestion of combining three exponential functions as a descriptor for autoignition delay, as well as for his suggestions about modelling the bouncing pin.

- Mr. Ting-Pang Hsiao from the University of Cape Town, for performing the CFD analysis and making the results, presented in Appendix C, available.

- Mr. Carl Viljoen for his patient response to countless requests to try and elevate my understanding of fuel chemistry. His provision of ignition delay data and the chemical kinetic model results was central to the success of this project. Mr. Viljoen played another critical role in the preparation of the fuel blends for the engine tests.

- Prof. Kevin Bennett for his consistent support of the fuels research effort at the University of Cape Town.

- The management of Sasol Technology Fuels Research, in particular Dr. Johan Botha and Dr. Hein Strauss who gave me the opportunity and support to pursue this research.

- My colleague and supervisor, Prof. Andy Yates, for his guidance, encouragement and inputs throughout the pursuit of this research.

This thesis is dedicated to my wife, Joey and sons Edu and Kehan for their love, patience and support. They made innumerable sacrifices, in the absence of which, I would not have been able to conclude this work.

SOLI DEO GLORIA

Table of Contents

Appendices

List of Figures

List of Tables

1. Introduction

This chapter serves as a general introduction to the thesis and highlights the relevance of, and need for, the research conducted. The last section covers the problem statement, research objectives and approach to the research, as well as the structure of the thesis.

1.1. General introduction

There is little doubt that the internal combustion engine has changed the face of the planet and the way people live. The development of the engine technology was followed closely by the development in fuel technology: what was formally a by-product of heating fuel production became a sought after commodity. Increasingly stringent environmental regulations have forced a marriage between engine and fuel technology. The advent of well-to-wheel analysis has necessitated the fuel life-cycle to receive attention.

From a fuel producer point of view, two often opposing needs must be satisfied. Firstly to produce fuels that conform to internationally recognised or local specifications and secondly to do so in the most economical manner possible. In the case of an integrated fuels-chemicals business, the challenge is more severe, since streams or even particular molecules may be directed to either the fuel or chemical pools.

Of all the fuel properties, the octane rating of a fuel is probably the single biggest challenge to address. Since the first fuel specification came into being, there has been a definite and unequivocal increase in the octane number requirement. This increase has stabilised at a level collectively found to yield the lowest overall cost per distance travelled. The phase-out of octane enhancing, heavy metal, fuel additives has forced fuel producers to invest in technology to produce fuel streams with intrinsically higher octane numbers. This approach is also under threat by virtue of pressure from Original Equipment Manufacturers (OEMs) to reduce levels of certain fuel components, such as aromatic and olefins, because of environmental concerns. This view was recently challenged in a paper by Kalghatgi (2005) who presented a case against the reduction of aromatics from current levels.

South Africa represents a unique automotive market and is characterised by the following features:

- More than half of the vehicle population reside at altitudes of more that 1200 m above sea level (4000 feet above sea level) in the interior of the country. Mexico and Colorado two other locations in the world with a significant vehicle population at altitude. (Yates and Cilliers, 2002)
- The interior region of South Africa is characterised by particularly hot and dusty summers and moderate winters.
- About a third of the country's fuel is synthetically produced in a coal based Fischer-Tropsch plant operated by Sasol. This fuel is distributed predominantly in the interior, high altitude regions.
- There is a distinct divide between brand new and very old vehicles in the demographics of the vehicle population. The average vehicle age is 12 years and increasing. (Stone and Bennett)
- The country as a whole has no vehicle emissions legislation, although legislation, equivalent to Euro2, is expected to be implemented on newly homologated vehicles by 2006. The phase-out of lead was instituted only at the beginning of 2006. (Arendse, 2004)

In this context, fuels research at Sasol has always focussed on fit-for-purpose studies in an effort to match the fuel requirements of the diverse vehicle population with the challenges of operating an integrated, synthetic fuels and chemicals business.

The increasing demand for un-additised high octane fuel, combined with increasing compositional limitations, has placed a premium on the ability to accurately predict octane numbers based on a molecular composition. The benefits are apparent, not only from an operational point of view but also when it comes to the strategic planning of molecule allocation, be it to the fuel or chemicals pool.

Although octane measurement has existed in its current form for many years, it is surprisingly poorly understood at a fundamental level. This study was commissioned to investigate underlying details of octane measurement and particularly the nature of autoignition during the octane rating of gasoline fuels.

1.2. Current relevance of octane numbers

There is sufficient empirical evidence that octane rating is successful in describing the knock resistance of gasoline fuels. There has been an industry wide convergence to an octane rating of gasoline fuels at a Research Octane Number (RON) of between 92 to 95 starting with early studies by Corner and Cunningham (1971) and Van Gulick (1975). This octane level has formed the design basis for modern production engine manufacture.

Electronic control units (ECU) on modern engines allow for the detection of incipient knock and the adjustment of the spark advance via feedback control, which allows these types of engines to operate over a wider variety of octane number fuels. A quantification of this effect was presented by Yates and Mkwanazi (2002). A comprehensive study by Kalghatgi (Kalghatgi, 2001a and Kalghatgi, 2001b) has shown that the octane requirement of these modern vehicles was no longer the average of the RON and the MON values, but that the higher pressure and lower temperature conditions of modern engines made the RON more descriptive of the vehicle octane appetite. In fact, Kalghatgi's analysis found a lower motor octane number (MON) and increased octane sensitivity (numerical difference between RON and MON) to be beneficial. Yates et al. (2005) similarly found that forced induction engines operated in a region of higher pressure and lower temperature than normally aspirated contemporaries.

Interest in octane numbers is not only limited to the high end of the scale. Research into Homogeneous Charge Compression Ignition (HCCI) engines and fuel requirements has revealed the requirement of a readily ignitable fuel, characterised by an octane number lower than that required for spark ignition engine operation (Ryan, 2005). A second facet of intermediate octane number measurement relates to blending octane number behaviour. This is typified by the American Petroleum Institute Research Project 45, where the blending behaviour of individual molecules was assessed by measuring their octane effect in a Primary Reference Fuel (PRF) 60 base (Bood et al., 1950).

It is therefore clear that the understanding of octane measurement, both RON and MON, at all levels of the octane scale, is relevant to fuel production and application.

1.3. *Chemical and physical attributes of octane rating*

A common point of departure in literature has always been to attribute all observed differences in octane numbers to the autoignition characteristics of the fuel. Leppard (1990) for example, attributed octane sensitivity to the differences in low temperature chemistry between PRF and non-PRF fuels. It was suggested that *"Olefins and aromatics do not exhibit NTC (*negative temperature coefficient) *behaviour, and therefore, do not enjoy enhanced Motor octane qualities which accounts for their high octane sensitivities"**.

The comprehensive understanding of octane measurement requires knowledge of, not only the fuel autoignition quality, but also the operating envelope provided by the conditions in the engine. This envelope describes the changing pressure, temperature and time to which the end-gas is exposed and is affected, in broad terms, by the inlet pressure and temperature, compression ratio, engine speed and normal flame development. There are of course a host of secondary considerations that will extenuate the propensity to autoignition, either directly or by affecting some of the aforementioned primary causes. The conditions in the engine are prescribed unequivocally by the ASTM test methods for octane number measurement.

1.4. *Research and thesis overview*

Problem statement

The pressure development in the CFR engine used for octane rating has been shown to be distinctly different to other engines during knocking operation and the reasons for it are not fully understood. The quantification of "knock intensity" during octane rating is similarly different to any other metric used for the quantification of the severity of knock. The exact role that autoignition plays in both facets is as yet not fully understood or quantified.

Research objectives

The main objectives of the research can be summarised as follows:

* In this study it was found that the differences in NTC behaviour between PRF and non-PRF fuels are more relevant to the conditions encountered during the Research octane number test than the Motor octane number test.

- To develop an intimate understanding of octane rating by performing a variety of tests in the octane rating engine. This understanding relates, in particular, to the measurement of knock intensity using the prescribed measurement equipment.
- To develop and apply a theoretical interpretation of the measurements to highlight any anomalies between the observations in the octane rating engine and the expected behaviour for knocking engine operation.
- To reconcile any anomalies found during the experimental study by further exploration of the role of autoignition during knocking engine operation.
- Where appropriate, to explore any unique interaction between the fuel composition and the features of the CFR engine. The conclusion thereof should be a consistent fit between experimental data and empirical observations.
- Finally, to propose the basis for theoretical prediction of all the observed phenomena. This will constitute the genesis of a tool with which octane numbers can be predicted.

Research approach

In order to achieve the objectives, a series of experimental measurements were performed on the CFR octane rating engine under the conditions relevant to octane rating over a wide range of octane numbers. In-cylinder data was captured and analysed to establish the basis for quantifying the measured knock intensity.

The hypothesis was explored by means of theoretical modelling, which included an initial interpretative part, where measured data will be subject to an interpretative model to derive thermal conditions and autoignition phenomena likely to be responsible for the observed pressure development. The subsequent predictive modelling combined all the hypothesised features to replicate the expected pressure development.

Thesis outline

The thesis begins with a literature review covering a wide range of relevant topics, including knock in spark ignition engines and autoignition, since there is general consensus that knock is an autoignition phenomenon. The literature review also covers certain aspects of the development of knock intensity measurement for octane measurement, as it sets the scene for the experiments performed. The review is concluded with some examples of different approaches to octane prediction.

The third chapter describes the experimental methods and the tests performed. The chapter includes the experimental set-up, the test conditions and fuels tested, as well as instrumentation and data acquisition. To ensure the relevance of the data, measurements were made in the engine appropriate to octane measurement under the prescribed operating conditions.

Chapter four gives the most important experimental results, including the effects of fuel composition and engine operating conditions on pressure development in the engine during octane measurement. The same data is utilised to infer the effect of autoignition on knock intensity and ultimately, octane numbers. This chapter also deals with variability in the measured quantities.

Chapter five proposes a theoretical modelling treatment for the interpretation of the experimental results. A fuel autoignition delay model was applied to the experimental data in an attempt to account for the underlying interaction between the engine and the fuel autoignition.

The sixth chapter applies the theoretical interpretation to engine conditions relevant to octane number determination. The applications include different fuel types, as well as the RON and MON test conditions. The chapter is concluded by illustrating the principles of a predictive model.

Chapter seven serves as a conclusion to the thesis and contains appropriate recommendations for future work.

2. Literature review

This chapter provides an overview of the literature relevant to the octane determination and knock intensity measurement.

2.1. Knock in a spark ignition engine

2.1.1. General description

With the benefit of hind-sight it is evident that no other feature has directed the development of spark ignition combustion engine technology as did knock-free operation. Swarts et al. (2005) provided a historical overview of the early research into knock in a spark ignition engine.

Some of the earliest research into knock, conducted by Professor Hopkinson at Cambridge University, revealed that knock was not a pre-ignition phenomenon, but in fact a pressure disturbance that occurred after the ignition by the spark plug. It was furthermore concluded that the knock was a characteristic of the gasoline fuel, as the phenomenon could not be replicated when running the engine on gas (Ricardo, 1953). Moreover, the knocking noise could be alleviated by either retarding the spark timing, changing the air fuel ratio or throttling the engine.

For the purpose of the ensuing discussion, "knock" will refer to "spark-knock" according to the definition provided by Obert (1973) and echoed by Heywood (1988). Other types of abnormal combustion fall outside of the scope of this thesis. The typical characteristics of spark knock are shown with the aid of Figure 2-1, replicated from Heywood (1988). This graph reveals the high frequency pressure fluctuations, the amplitude of which decays with time. It is also clear that the pressure fluctuations begin close to peak cylinder pressure.

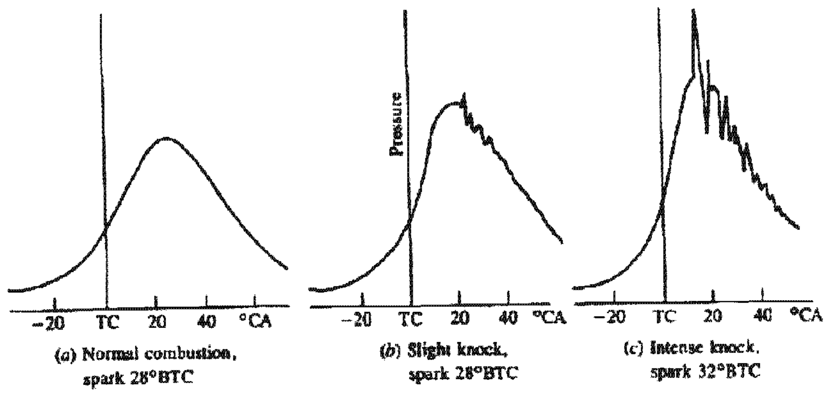

Figure 2-1: A replication of Figure 9-59 from Heywood (1988) showing, from left to right, pressure traces for normal combustion, slight knock and intense knock.

2.1.2. Autoignition and detonation theories

Although knock was phenomenologicaly understood and empirically managed, particularly through the application of metal additives, by the 1960 there was still no clear fundamental understanding to the nature of knock. Two theories were proposed to explain the origins of knock:

- The autoignition theory suggested that the rapid pressure increase was due to the spontaneous autoignition of the end-gas. One of the first references to this was by Taylor (1934)
- The detonation theory postulated a transition of the deflagration wave to a detonation wave that led to the observed rapid increase in pressure. This theory was founded in the observations made by Miller (1947)

In spite of any uncertainties concerning the exact origins of knock, there was early consensus on the effects thereof. Localised high pressures caused pressure waves that would impact against the cylinder walls causing a ringing knock "*as though they had been struck by a light hammer*". The rate of heat flux to pistons and cylinder walls would also increase dramatically due to the destruction of the protective thermal boundary layer (Ricardo, 1953).

This relationship between knock and engine damage received attention, particularly with respect to geometrical dimensions to the damage experienced (Nates, 1995, Nates and Yates, 1994). Fitton (1995) similarly found that knock damage correlated exceedingly well with pressure at the initiation of knock. Moreover, he concluded that the extent of damage was a function of the degree of confinement of the end-gas.

Today it is generally accepted that knock is due to autoignition of that part of the end-gas that had not been consumed by the normal flame front, following the explanations offered by Taylor and Taylor (1948). This point of view is entrenched in main stream literature on the subject of internal combustion engines (Heywood, 1988, Miller and Fisk, 1987) and the unfortunate reference to detonation has been dropped in favour of knock. The latter was previously reserved for reference to mechanical noise caused by loose bearings or pistons. (Taylor and Taylor, 1961)

This work will adopt the terminology proposed by Konig and Sheppard (1990) which states that "***autoignition*** *refers to chemical reaction accelerating to spontaneous ignition of the mixture*" whereas "***knock*** *is restricted to the physical manifestation of the abnormal oscillations in the cylinder pressure*"

2.1.3. Inhomogeneous autoignition

There are a number of references to the details of autoignition during knocking operation. These relate in particular to the inhomogeneous nature of the autoignition as well and the finite heat release rates in the end-gas during knocking operation. Selected examples include:

- The landmark publication by Rassweiler and Withrow (1938) that revealed that autoignition does not occur uniformly throughout the end-gas region of an internal combustion engine.
- Male (1949) demonstrated that autoignition is not a homogeneous reaction of the end-gas but rather initiated at several discrete nuclei.
- Adbel-Gayed et al. (1989) attributed the temperature gradients in an internal combustion engine to the effects of turbulence. Evidence of thermal segregation in the end-gas and the existence of a thermal boundary layer is a well known phenomenon. (Heywood, 1988)
- Konig et al. (1990) described the existence of exothermic centres in the end-gas of a knocking engine. Conditions in these centres were more favourable for autoignition development when compared to its surroundings. The local heat release and pressure increase caused adiabatic compression of the surrounding end-gas, speeding up their autoignition development and setting off a chain reaction of autoignition events.
- Konig and Sheppard (1990) observed *"several definite areas of autoignition in the end-gas region"*. Moreover it was observed that in some instances, the autoignition process required comparatively long periods to complete and did not necessarily result in knock. This established the notion of having autoignition without knock.

- Brussovansky et al. (1992) concluded that the autoignition centres can be treated as adiabatically compressed based on the ratio of the characteristic cooling time and the adiabatic temperature rise time.
- Measurements by Griffiths et al. (2002) in the Leeds University rapid compression machine (RCM) revealed that temperature and mixture inhomogeneities were present even in the single stroke rapid compression machine.

Obert (1973) made one of the earliest distinctions between "explosive autoignition" and "non-explosive autoignition". In the former, the rate of chemical reaction exceeds the rate of expansion of reacting elements. During non-explosive autoignition, the rate of expansion exceeds the rate of reaction, possibly due to the sparse nature of molecules *"poised on the brink of autoignition"*. Konig et al. (1990) expanded the concept and proposed the distinction between three modes of autoignition: *"deflagration", "developing detonation"* and *"thermal explosion"*. The developing detonation is characterised by a strong coupling between gas-dynamics and chemical reactions and is most likely to cause high localised pressures. It posses the greatest risk for engine damage. Bradley et al. (1996a) built on the work done by Pan and Sheppard (1994) and found through the application of a model of autoignition, that the more reactive mixture is more conducive to the establishment of a developing detonation, whereas a less reactive end-gas reverts to a continuation of the deflagration mode.

As early as 1955, Livengood and Wu (1955) highlighted the dilemma of assigning an ignition delay to the end-gas of a knocking engine that is clearly non-homogeneous. Today, there are numerous examples of modelling approaches to quantify the behaviour in an inhomogeneous end-gas:

- By et al. (1981) utilised a two part unburnt zone comprising an adiabatic core and a boundary layer. The application of an autoignition model revealed this event to occur in the hotter, adiabatic part.
- Bradley et al. (1996b) utilised a three zone model comprising of "burned", "unburned" and "autoignited" parts. A temperature difference, over-and-above that of the burned zone, was applied to the autoignited zone to account for the heat liberated by the autoignition reactions in the same.
- Pan et al. (1998) quantified the extent of the temperature gradient by the application of a gas dynamic/chemical code for each of the three modes of autoignition described above.

- There are numerous other examples of multi-zone engine models and multidimensional engine models aimed at revealing the detail of the end-gas thermal behaviour (for example Hajireza et al. (1999)

Inhomogeneous autoignition reactions have come to the fore in a strong way with the focus on heat release in HCCI type engine deployments. Bradley et al. (2002) revisited the concepts originally proposed by Zel'dovich (1980) and suggested that autoignition can in fact occur in one of five modes. These were:

- near-instantaneous thermal explosion
- supersonic autoignitive deflagration, requiring a favourable spatial distribution of mixture reactivity and characterised by an autoignitive wave ahead of the acoustic wave
- developing detonation, where the autoignition front moves into the unburnt mixture at approximately the acoustic speed.
- subsonic autoignitive deflagration, where the pressure pulses run ahead of the autoignition front, and
- conventional flame propagation, limited by molecular transport processes and conductive mechanisms.

Gu et al. (2003) descriptively referred to the second, forth and fifth modes listed above as *"rapid autoignitive deflagration", "slow autoignitive deflagration"* and *"laminar burning deflagration"*, respectively.

There are a myriad of publications on the subject referring to the presence of "*sequential, progressive or heterogeneous*" autoignition and "*propagating autoignition*" (SAE HCCI conference, 2005). Sheppard et al. (2002) for example, applied an analysis, similar to that for SI engines, to the lean conditions encountered in HCCI operation.

2.1.4. Normal flame propagation effects on engine knock

Flame propagation affects autoignition and knock by altering the envelope of pressure, temperature and time to which the end-gas is subjected. The role of variability of flame propagation on the knock onset was recognised by Chomiak and Skold (1995). This yielded a positive correlation between the early flame development and the onset of knock.

Air-fuel ratio effects

The effect of mixture strength on engine knock was recognised and quantified as early as 1961 by Gluckstein and Walcutt (1961). The mechanism of knock mitigation was said to be the less severe end-gas conditions, due to be slower burn rates, which in turn was a result of the effect of air-fuel ratio changes on the flame speed. Dimpelfield and Foster (1986) found that for propane, for instance, the most severe knock was at a fuel-air equivalence ratio† of 1.05. This corresponded to the maximum laminar flame speed, typically found to be just on the rich side of stoichiometric. (Heywood, 1988)

The observations were confirmed by comprehensive knock-limited-spark-advance (KLSA) tests performed by Millo et al. (1995). Typical results are presented in Figure 2-2 and the reveal a significant speed effect, with minimum KLSA occurring closer to stoichiometric conditions as the engine speed increases.

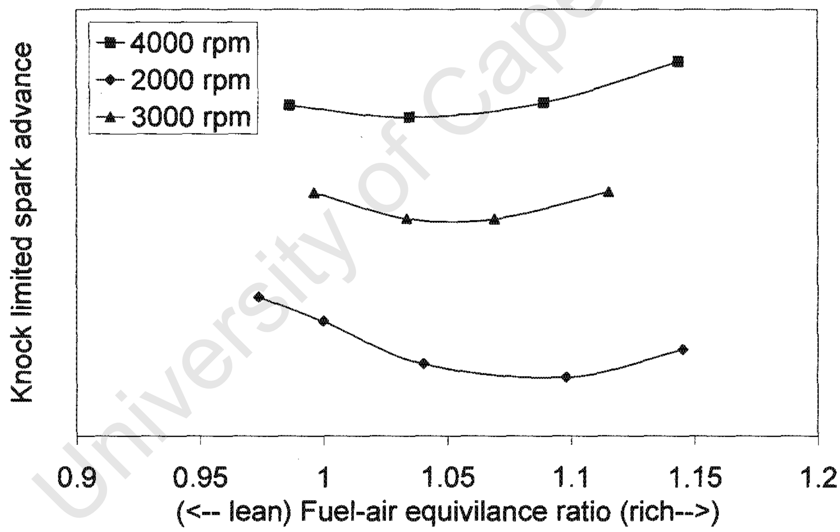

Figure 2-2: Knock limited spark advanced for different fuel-air equivalence ratios and engine speeds taken from Millo et al. (1995).

The effect of air-fuel ratio on knock is firmly entrenched in the ASTM octane testing methods that state, that the air-fuel ratio *"shall be that which maximizes the K.I."* (ASTM, 2004a). This aspect will receive further attention in this thesis.

† The fuel-air equivalence ratio is defined as the ratio between the actual fuel-air ratio and the stoichiometric fuel-air ratio. Values greater than unity indicate rich conditions.

Chemical composition effect

When a quiescent but explosive mixture is combined in an enclosed vessel at room temperature, no appreciable reaction occurs, even for the longest temporal observation window. With the aid of a spark of sufficiently high energy intensity, a flame can be established which is able to travel, spontaneously, through the mixture. The laminar flame is the result of a self-sustaining, exothermic chemical reaction, the speed of which is a measure of the rate of the reaction, all other things being equal (Warnatz, 2000).

Laminar flame speeds are usually measured and calculated at ambient conditions and include the effects of transport phenomena in the propagating flame front. A sensitivity study of the rate coefficients of a kinetic model, performed by Warnatz (2000), revealed that only two reactions (those between atomic hydrogen and molecular oxygen on the one hand and carbon monoxide and the OH radical, on the other) govern the rate of reaction. This explains the rather similar flame velocities for a variety of alkanes and can be extended to explain the rather similar flame velocities for a wide range of hydrocarbons.

The direct application of laminar flame speeds at ambient conditions to the expected performance in the internal combustion engine is questionable and is compounded by two issues:

- Firstly, the laminar burning velocity changes with pressure and temperatures and although augmentation correlations are available, lack of reliable high pressure and temperature data would caution against the generalisation of the correlations. Numerous empirical correlations exist to perform this transformation, usually in the form of a power law function. (Obert, 1973, Heywood, 1988)
- The second complication is the fact that the flame propagation performance is strongly influenced, if not governed, by the transport phenomena in the engine, such as convection and diffusion. Enhancement of turbulence combustion occurs through the increase of the flame front area via distortion thereof and bodily entrapment of unburnt pockets.

A final complicating factor is that the relative ranking of fuels in the autoignition and flame propagation regimes is not necessarily consistent. A long delay in one regime may not necessarily mean a long delay in the other. Measurements performed by Burluka at el. (2004) revealed that the laminar burning velocity, determined at elevated temperature and pressure in the Leeds Mk2 fan-stirred bomb, is not significantly different for toluene containing fuels when compared to iso-octane or unleaded gasoline. Westbrook (1992) also concluded that flame propagation depends only weakly on fuel properties and that predicting knock in a SI engine reduces to calculating the autoignition rates of the end-gas.

This effect of fuel composition, and the underlying laminar flame velocities, on the normal combustion performance was assessed for a range of model fuels blends, comprising molecules from representative chemical families (Swarts et al., 2003). Despite subjecting the results of burn duration and combustion development features to rigorous statistical analyses, no significant correlations could be found with the fuel composition only.

2.2. Autoignition

2.2.1. General description

In the spark ignition internal combustion engine, autoignition typically occurs at temperatures above about 950 K and at pressures in excess of 20 bar. The conditions are brought about by the compression of the piston, in the first instance, as well as compression by the flame front.

The chemistry and kinetics that govern the autoignition of automotive fuels are highly complex and outside the scope of the study. It is however important to highlight the most important features as described by Miller and Fisk (1987).

- Low temperature ignition is a two stage process. In the first of these, occurring at temperatures of 500 to 800K, the co called "cool flame" reactions raises the temperature by 100 to 200 K. The first stage produces organic peroxides The equilibrium reaction between the alkyl radicals and molecular oxygen may favour, at increasing temperatures, the reactants, thereby slowing down the overall reaction rate, giving rise to a phenomenon known as the negative temperature coefficient (NTC) behaviour (Westbrook, 1992). Earlier studies by Westbrook and Pitz (1987) concluded that the tendency to knock is directly related to the level of low-temperature heat release and serves to explain the lower octane rating of, say n-heptane, with its pronounced low-temperature chemistry, when compared to iso-octane.
- Hot ignition occurs at temperatures in excess of 900K and is characterised by the production and eventual dissociation of hydrogen peroxide, H_2O_2.

The ignition delay (ID) of a particular fuel is often expressed on an exponential plot against the inverse of temperature. A typical result for n-heptane data is shown in Figure 2-3 and the NTC region is indicated. The origin of the data, as well as the correction to a pressure of 12 bar is described in Appendix B.

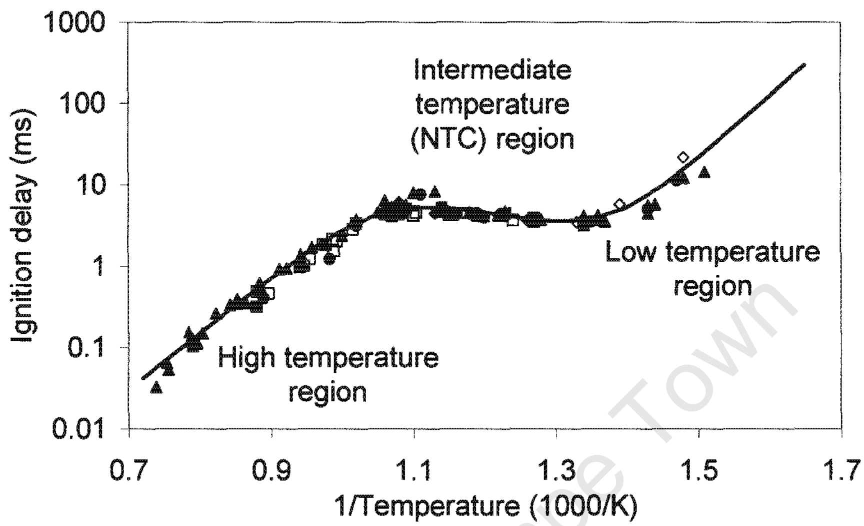

Figure 2-3: Ignition delay data for n-heptane, showing the NTC region. Data is taken from Appendix B and corrected to 12 bar.

There are two rather elusive challenges that face the study of autoignition. The first challenge is to make reliable measurements over the required range of pressures and temperatures relevant to the internal combustion engine. Four types of devices are traditionally used to perform global kinetic experiments (Miller and Fisk, 1987). These are:

- Static reactors
- Plug-flow reactors
- Continuously stirred reactors
- Laminar flames

The bulk of fuel autoignition data relevant to internal combustion engines has however been provided by shock tubes, rapid compression machines and motored engine experiments. A few of the challenges when using these devices are highlighted below:

- Data from shock tubes are typically limited to high temperatures (greater than 1000 K). Maximum ignition delay times are also limited by the length of the tube.

- Rapid compression machines are well suited to low temperature measurements, but reactions during the compression stroke are a concern, especially for reactive fuel mixtures with short ignition delays.
- Motored engines make the target pressures and temperatures accessible, but introduce uncertainties about the temperatures and composition.

The second challenge is to produce kinetic models of the autoignition reactions.

2.2.2. Kinetic models of autoignition

The goal of a comprehensive and consistent chemical kinetic model, which is to describe the complex autoignition chemistry in a gasoline blend, is one that has been eluding researchers for a long time. Kinetic schemes for single components are still being refined and suffer mostly from a lack of accurate temporally resolved species and temperature information.

Despite the rapid growth in computing power, there is as yet no prospect for the calculation of even a simple combination of the best described fuel components This has led researchers to explore means of reducing the comprehensive kinetic schemes to a more manageable size. The two requirements of such a reduced autoignition model are:

- Economy: The model needs to run in a reasonable amount of time
- Accuracy: The model needs to be sufficiently accurate to encompass the most critical features of the autoignition development.

Probably one of the best known examples of autoignition model reduction is the one developed at the Shell Thornton Research Centre in the 1970's (Halstead et al., 1975). The Shell model consists of eight reactions and was designed to capture the most important steps that lead to the appearance of the negative temperature coefficient. These are the initiation, propagation, branching and termination reactions. The kinetic parameters were originally derived for a range of primary reference fuels (Halstead et al., 1977) using RCM data. One of the central features of the Shell model is that the model requires 26 parameters, and since the model does not describe elementary reactions, these parameters need to be empirically assessed for each fuel. This particular feature, as well the apparent inconsistencies in the parameters and the assignment of the parameters, was highlighted previously by Yates et al. (2003)

Another well-known reduction effort followed from measurements done on the RCM at Massachusetts Institute of Technology by Hu and Keck (1987). It was found that some of the parameters in the Shell model were "required to take values different from those expected from the original hydrocarbon oxidation mechanism" in order to match experimental results. The results of their effort was a 18-reaction kinetic scheme. Schreiber et al. (1994) provided yet a further simplification to kinetic modelling that yielded a model comprising of six reactions. A feature of all of the reduced models is that the reactions involve "pseudo-species", so the model is not molecularly conserved and thermodynamic data for the pseudo-species is at best approximated by the nearest actual species.

There are references, too numerous to mention, to the utilisation of kinetic models to study autoignition in spark ignition engines. The biggest limitation, highlighted by Viljoen et al. (2005), is that detailed, validated, prediction models are at best available for a handful of molecules and selected binary and ternary combinations. Moreover, the calculation time for these complex kinetic schemes are prohibitively long in the context of a simple interpretive and predictive model. To remedy this limitation, the fuel autoignition ignition delay calculation was considered for this research.

2.2.3. Ignition delay models

A simplistic description of knock in a SI engine is the competition between consumption of the end-gas by the flame front and the evolution of the autoignition reactions in the end-gas. In this view, the problem reduces to two time-scales: that of the flame front passage time and the autoignition delay time.

It is well known that the ignition delay time varies with pressure, temperature and air-fuel ratio. The earliest expression for the ignition delay took the form of an exponential function of temperature:

$$\tau = c\exp(-b/T)p^{n} \quad \textbf{(2-1)}$$

where T = temperature

p = pressure

c, b, n = empirical constants

The formulation stemmed from the notion that the ignition delay progress can be reduced to a single overall reaction with undeniable similarities to the Arrhenius expression of the temperature dependence of the reaction rate of an elemental reaction.

In a landmark paper by Livengood and Wu (1955) it was proposed that an equivalent aggregate reaction may describe the concentration, x, of pertinent reaction products and that the change in the concentration is a function of pressure, temperature, time, air fuel ratio and fuel composition. Livengood and Wu further suggested that there is a critical concentration, x_c, where the reaction proceeds to completion, signified by the ignition delay time, τ. The results of their mathematical manipulation revealed the "ignition delay integral" which reaches unity at critical time, t_c:

$$\frac{x}{x_c} = \int_{t=o}^{t=tc} \frac{1}{\tau} dt = 1.0 \tag{2-2}$$

The formulation proved to be immensely powerful in dealing with the autoignition development in the changing conditions present in the internal combustion engine. Today, many of the reputable commercial engine modelling software packages include this type of autoignition model (Ricardo software, 1999)

The ignition delay model was parameterised for iso-octane by Rifkin and Walcutt (1957) and Gluckstein and Walcutt (1961). Possibly the best known application of the framework developed by Livengood and Wu is the paper by Douaud and Eyzat (1978). They performed a series of engine tests in a CFR engine to parameterise the overall ignition delay model for a commercial fuel as well as primary reference fuels with octane numbers from 80 to 100. The authors recognised the simplicity of the single exponential function by conceding that this *"can be attempted through an overall reaction rate for a limited pressure and temperature range"*. Their insightful proposal for fuel characterisation was to utilise four octane measurement conditions that would allow for the estimation of the parameters in the exponential ignition delay expression.

Douaud and Eyzat (1978) did however conclude that the temperature and pressure sensitivity of different fuels can be markedly different and that the magnitude can be assessed by perusal of the b and n parameters. One contemporary example of addressing this feature is the work by Burluka et al. (2004). and Bradley et al. (2004) In it, the pressure coefficient of the single exponential function was changed to better fit the experimental observations.

Shock tube studies by Gauthier et al. (2004) also found that a power law serves to align the ignition delay data at different pressure:

$$\tau = \tau_{ref}\left(\frac{P}{P_{ref}}\right)^{-n} \quad \textbf{(2-3)}$$

The extent of the exponent varies significantly. For low pressures, a scaling factor of n=0.55 was adopted for n-heptane by Gauthier et al. (2004). For high pressures, the factor was found to be n=1.64, based on a collection of measurements. The same authors found the scaling factors to be 1.05, 0.83 and 0.96, for a gasoline and two surrogate gasoline fuels, respectively. The latter two were ternary blends of iso-octane, n-heptane and toluene.

A recent duet of papers (Yates et al., 2004 and Yates et al., 2005) revealed that the single exponential function can be improved upon and proposed the combination of three exponential functions to describe more accurately the complex ignition delay response to pressure and temperature, according to:

$$\tau_{overall} = \frac{1}{\left(\frac{1}{\tau_1 + \tau_2} + \frac{1}{\tau_3}\right)} \quad \textbf{(2-4)}$$

Where each of τ_1, τ_2, τ_3 takes the form of Equation (2-1)

2.2.4. Autoignition reaction rates

In addition to thermal and mixing inhomogeneities described previously, there are undeniable influences of the composition on the reaction rates during autoignition in a spark ignition engine. Taylor and Taylor (1961) stated that the intensity of detonation (autoignition) is related to the intensity of the pressure wave energy. This intensity is dependant on (1) the mass of end-gas that autoignites and (2) the rate of reaction in the autoignition process.

Non-explosive autoignition is exemplified by the reaction of benzene, where the rate of pressure increase has been observed to increase very uniformly, giving rise to the anecdotal observation that knock in an engine running on benzene resembles a “thud” or a “bump” (Obert, 1973). The slower reaction rate of benzene was said to be responsible for lack of appreciable pressure waves and associated high knock resistance. Downs and Wheeler (1951) also concluded that with single stage fuels (i.e. those with little of no NTC behaviour) there is no pre-sensitising of the end-gas and the slower reaction mechanism causes autoignition without knocking. Benzene and methane were both identified as exhibiting single stage characteristics.

Bradley et al. (1996b) focussed on the calculation of the volumetric rate of heat release as a measure of the severity of knock. Significantly, they found that the maximum volumetric heat release rate was lower for aromatic than for paraffinic fuel types. As such, aromatic fuels are said to be less prone to severe knock. Results for the TOLHEP fuel (85% toluene, 15% n-heptane), presented by the same authors, showed increasing levels of knock intensity, quantified as difference between the maximum and minimum filtered pressure signal, for the same notional level of heat release rate, as one progresses from TOLHEP to lower octane number primary reference fuels. It was eventually concluded that the toluene-containing fuels were much closer to the deflagration zone (when presented on a plot of volumetric heat release versus apparent activation energy) than their paraffinic counterparts.

A chemical kinetic study utilising Chemkin™ software (Viljoen, 2005) and applying kinetic mechanisms form Djurisic (1999) showed that the rate of heat release was noticeably more gradual for aromatics (toluene) than for paraffins (iso-octane). These differences are shown in Figure 2-4 below with the presentation of the temperature and hydrogen peroxide concentrations. The more gradual dissociation of the latter for toluene is thought to be responsible for the more gradual heat release.

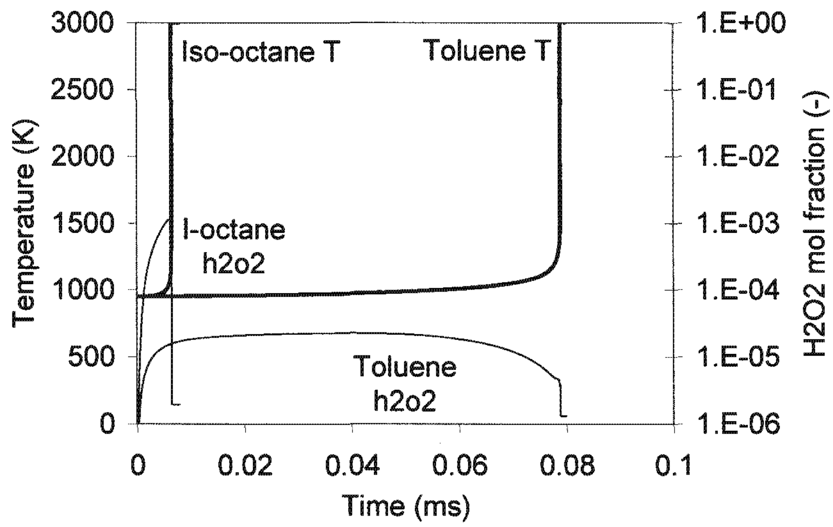

Figure 2-4: Temperature and peroxide concentrations for Toluene and Iso-octane. Calculated for a fixed volume at 950K and 12 bar, from detailed chemical kinetics calculations (see text for details).

As such it is to be expected that the severity of knock in a spark ignition engine relates not only to achieving to the onset of the autoignition but also to the rates of the chemical reactions.

2.3. Octane measurement

2.3.1. Early history of octane rating

With the intensification of research into engine knock after the turn of the 20th century, there was an increasing need to define a measure of the anti-knock resistance of gasoline fuels that would allow for the comparison of fuels from different parts of the world. Ricardo devised an early method whereby the detonation quality of gasoline was expressed as the relative toluene content, since the latter compound was found to exhibit a particularly high resistance to autoignition (Ogston, 1981). The dependable link between compression ratio and knocking formed the basis for the proposal of Sir Harry Ricardo to use the Highest Useful Compression Ratio (HUCR) as a measure of a fuel's autoignition resistance (Ricardo, 1953). His proposal required, however, that all the testing equipment should adhere to very tight tolerances to ensure repeatability and reproducibility.

In 1928, the Cooperative Fuel Research (CFR) committee assigned the challenge of developing a test method to the Detonation Sub-Committee. Their charter contained three requirements: (1) a standardised engine, (2) a common reference fuel and (3) a uniform testing procedure. The first requirement was fulfilled by the Waukesha Motor Company who produced a single cylinder, variable compression unit. Although the Cooperative Fuel Research committee was later superseded by the Coordinating Research Council (CRC) the engine is still known today as the CFR engine. The second requirement introduced the use of iso-octane (2,2,4-trimethyl pentane) and n-heptane with defined octane numbers of 100 and 0, respectively.

The third requirement underwent an early evolution as it was found that the original research octane method yielded a poor correlation with on-road knock experience and the more severe motor octane test condition was introduced. The original research method was replaced by a more convenient CFR Research method in 1939. (Waukesha Motor Company, ca. 1946)

Research octane number (RON) and Motor octane number (MON) remain to this day as the absolute metric for the quantification of knock resistance of gasoline fuels.

2.3.2. Knock measurement system

Early research into octane rating went hand-in-hand with the detection and quantification of knock intensity. Since the measurement of knock is critical to understanding the octane scale in total, an overview will be given of the evolution of knock intensity measurement during octane rating. The parallel development of the octane rating test methods is also discussed. For a comprehensive overview of the early history of knock detection, refer to Swarts et al. (2005).

The first quantification of severity of knock was done using the bouncing pin, developed by Thomas Midgley, Jnr. The pin was isolated from the cylinder cavity by a diaphragm which deflected due to pressure in the cylinder and in turn, acted upon the pin.

By 1948, the measurement of Research and Motor Octane Numbers (RON and MON) had been adopted by the American Society for Testing Materials (ASTM) (ASTM, 1948). The 1948 manual contained a description of a bouncing pin based on the Midgley design and detailed instructions for its usage. The instrument included another innovation in the form of an electrical integrator. When elevated, the pin would close two contact breakers at the top of the device, causing an electrical current to flow in the detection circuitry. The electrical current was used to heat up a thermal element and the extent of heating up was directly proportional to the time the contact breakers were closed. A thermocouple contained within the thermal element provided the signal for a suitably sensitive voltmeter and provided the readout of knock intensity[‡] (KI). The latter instrument was designated as the "knockmeter" and was calibrated from 0 to 100. A value of 55 was chosen as *"standard knock intensity"*.

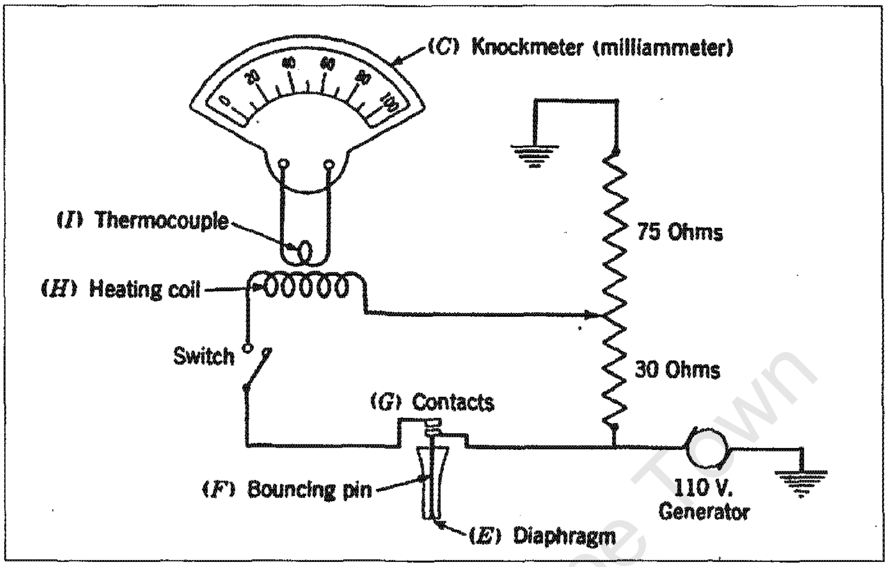

Figure 2-5: Knockmeter circuit used in conjunction with the bouncing pin (circa 1940). Taken from Jennings and Obert (1944).

The bouncing pin remained as the preferred device for measuring the knock intensity and was specified as the standard instrumentation on the single cylinder CFR engine until it was superseded, in circa 1970, by an electronic knock measurement system. The system comprised of a detonation pick-up, detonation meter and knockmeter, as shown in Figure 2-6.

‡ The term "knock intensity" will henceforth refer to the output of the ASTM knock measurement system only.

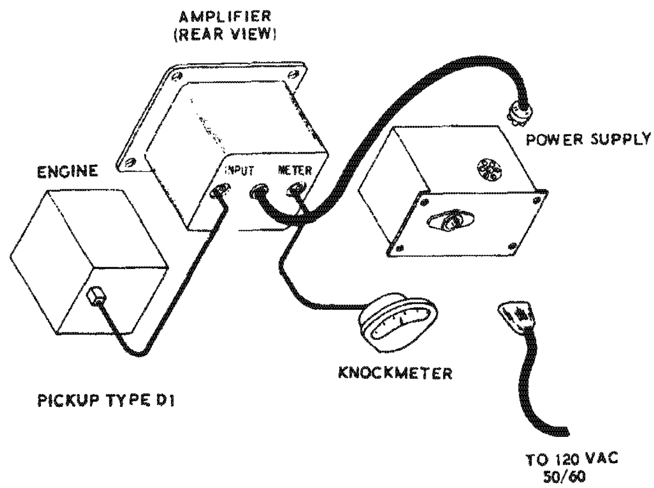

Figure 2-6: Elements of the knock measurement system in use on the CFR octane rating engine. Taken from ASTM (2004a).

By the 1970's, the Research and Motor octane rating of automotive fuels were being done under the now familiar designations ASTM D-2699 and D-2700, respectively (ASTM, 1973) and included a subtle relaxation of the threshold value for standard knock intensity, from the previously used 55 to a value of 50.

More details of the elements of the knock measurement system are given below:

Detonation pickup

The model D1 magnetostrictive pressure transducer was designated the "detonation pick-up". The detonation pick-up generated a voltage proportional to the pressure rise rate inside the cylinder. The detonation pick-up was installed in the same position and exposed to the same conditions as the original bouncing pin. The choice of name for this component was particularly unfortunate as the current consensus is that knock is in fact not a detonation phenomenon.

Detonation meter

The detonation meter included circuitry to effect input signal attenuation and amplification. By 1978 there had been an evolution of at least four models: 501, 501-A, 501-AP and 501-T (ASTM, 1978). The methods and equipment remained unchanged during the 1980's and

1990's, although an updated detonation meter, model 501-C, became available by 1982 (Waukesha, 1982).

The operation of all these variants of the detonation meter was similar in so far that the circuitry would split the signal into the rate of pressure rise due to the "combustion wave", i.e. normal combustion, and the "knock pulse". The signal due to normal combustion was subtracted to provide a final output voltage proportional to severity of knocking. The block diagram of the operation of the model 501 detonation meter, taken from the detonation meter operating manual is shown in Figure 2-7 below. The diagram shows the evolution of the input signal and the role of the adjustments for METER and SPREAD settings.

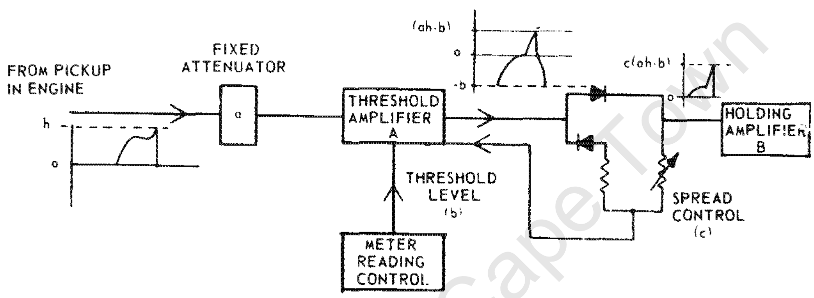

Figure 2-7: Block diagram showing the operation of the Model 501 detonation meter used on the CFR octane rating engine. Taken from the detonation meter operating manual (Waukesha Engine Division, 1982).

Knockmeter

The knockmeter was nothing other than the sensitive voltmeter originally used with the bouncing pin, producing a reading of the detonation meter output.

Input filter circuit

The inability of the electronic knock measurement system to discern the high frequency fluctuations observed during knocking, received attention in the text book by Obert (1973). The pressure rise rate signal for the detonation pick-up was compared to the output from the detonation meter filter circuitry and the figure from Obert is reproduced below as Figure 2-8. It is clearly evident that all remnants of high frequency signals are absent from the output of the detonation meter filter circuit.

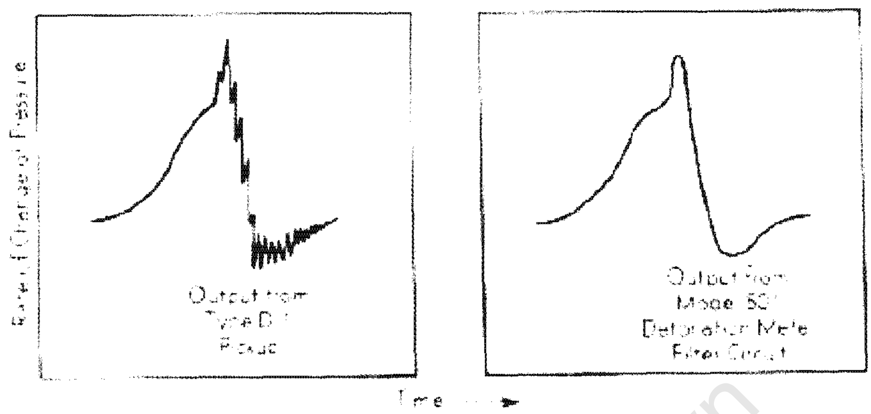

Figure 2-8: Rate of pressure change values from the Type D-1 pickup (left) and the Model 501 detonation meter (right). The results show the absence of the higher frequency fluctuating components in the output from the Model 501 detonation meter. Taken from Obert (1973).

The existence and characteristics of an input filter is an undeniable reality in the instrumentation used on the CFR engine, given the explicit reference to it in the most recent versions of the ASTM octane rating procedures (ASTM, 2004a and ASTM, 2004b). Current versions of the octane rating methods actually provide the frequency response of the low-pass input filter and this is reproduced in Table 2-1 below. The response is clearly designed to provide maximum attenuation at the frequencies characteristic of knock at about 6.5 kHz.

Table 2-1: Frequency response of the low pass filter present in the ASTM knock measurement system as fitted to the CFR engine. (ASTM, 2004a)

Input frequency (Hz)	Output Frequency Response (dB)
Dc to 2000	-0.5+-1.0
2250	-3.0+-0.2
2500	-6.5+-0.3
5000	<-40
6500+-100	Point where dB drop maximizes and reverses (point of minimum output)

2.3.3. Octane rating conditions

The methods, equipment and testing materials have remained largely unchanged since 1939 and testing in the CFR engine continues to this day as the de-facto standard for the octane rating of gasoline fuels (ASTM, 2004a and ASTM, 2004b). The operating conditions applicable to RON and MON ratings are given in Table 2-2:

Table 2-2: Operating conditions relevant to octane rating

Parameter	RON test	MON test
Engine Speed	600 rpm	900 rpm
Spark Timing	13 °BTDC	19 to 26 °BTDC§
Inlet air temperature	51.7 °C	38 °C
Inlet mixture temperature	Not controlled	149 °C

For both rating scales, the methods require that standard knock intensity be achieved for a sample fuel by adjusting the compression ratio and air-fuel ratio on the CFR engine. The knock intensity must then be matched by operating the engine under the same conditions on a blend of primary reference fuels, iso-octane (2,2,4-trimethyl pentane) and n-heptane. The octane number of the sample is defined as the volume percentage iso-octane in the primary reference fuel (PRF) blend for which this parity occurs.

Over limited ranges of RON and MON, the methods allow for the octane number of the sample fuels to be established directly from the compression ratio using the so-called "guide tables"**, provided in the ASTM documentation.

2.3.4. CFR engine design features

Several design features of the CFR engine which distinguishes it from modern internal combustion engines are highlighted below. Additional information is given in Table 2-3:

§ Spark timing in the MON test is varied as a defined function of compression ratio

** The guide tables relate the compression ratio to the octane number. It can be regarded as a listing of the critical compression ratios of the CFR engine associated with the standard knock intensity.

- The inlet valve is fitted with a 180° shroud.
- The engine has a flat top piston and, given the low compression ratios at which it operates, lack of squish.
- The engine has a side mounted spark-plug, giving rise to a long flame propagation path.
- There is limited valve timing overlap between exhaust and intake.

Table 2-3: Key parameters of the CFR octane rating engine

Parameter	Value
Bore	82.55 mm
Stroke	114.3 mm
Inlet Valve Closure	146 °BTDC
Exhaust Valve Opening	140 °ATDC
Inlet Valve Opening	10 °ATDC
Exhaust Valve Closure	15 °ATDC
Compression ratio	Variable

Taylor and Taylor (1961) showed that the inclusion of a shrouded inlet valve more than halved the maximum brake torque ignition advance, indicating a reduction in combustion duration when compared to plain valve operation. This is attributed to increased flow velocities entering the cylinder. Knock limited mean effective pressure is similarly improved by the introduction of squish and the shroud. The former effect is attributed to the enhanced heat transfer, brought about by large surface to volume ratio, in the squish zone. Similarly Tabaczynski (1977) quantified the effect of the shroud as increased levels of turbulence (expressed as gas mean velocity and turbulence intensity), leading to faster burn rates when compared to a standard valve.

2.4. Autoignition in the CFR engine

2.4.1. Measurement in CFR engine

Test results from the CFR engine arguably represent the single biggest engine experimental data set in the world: thousands of octane ratings are done in refineries across the world every day. Scientific measurements are however limited. Some examples are given below:

- Rifkin and Walcutt (1957) and Gluckstein and Walcut (1961) performed a range of experiments on a CFR engine in an attempt to reconcile fuel ignition delay times and engine behaviour.
- By et al. (1981) performed tests on the CFR engine for primary reference fuels of octane numbers 80, 90 and 100, as well as two high boiling range multi-component hydrocarbon (certification) fuels. Noticeable deviations from the ASTM method were higher speeds (greater than 1000 rpm), varying inlet temperatures and non-standard ignition timing.
- Leppard performed a variety of autoignition experiments on a CFR engine, but these were with a modified engine under non-standard conditions. (Leppard, 1987 and Leppard, 1992)
- Flowers et al. (2000) performed HCCI engine experiments on the CFR engine.

Very few of these experiments were performed at the prescribed conditions for octane rating and moreover, no explicit reference to the use of the CFR knock measurement equipment could be found. The exception was the measurements performed at the Sasol Advanced Fuels Laboratory at the University of Cape Town. These included tests performed under the octane rating conditions, including the simultaneous measurement of knock intensity using the equipment prescribed by the ASTM.

2.4.2. Pressure development in the CFR engine

The paper by Swarts et al. (2004) revealed that the pressure trace from the CFR engine contains a very distinct change in slope prior to the peak pressure and the pressure oscillations normally associated with knock. The associated pressure rise rate was however below that of volumetrically homogeneous autoignition. Moreover, there was diminished evidence of any acoustic phenomena, when compared to Figure 2-1. Figure 2-9 below shows several successive pressure traces for a PRF90 fuel captured in the CFR engine under standard knock intensity conditions. Although the exact cause of the transition was not clear, the instant of the change in pressure signal was termed the “knock-point”, since it was sufficiently clear that the transition was associated with “knocking” engine operation.

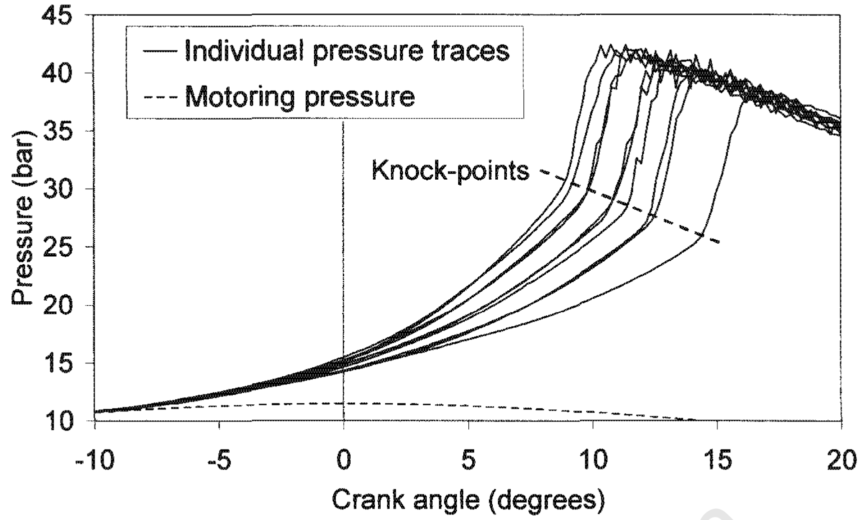

Figure 2-9: Several successive pressure traces for standard knock intensity in the CFR engine. The fuel is a PRF90 blend at a compression ratio of 6.65:1. Adopted from Swarts et al. (2004).

Similar pressure development profiles have been reported by other researchers:

- Indicator card results for a CFR engine at 1200 rpm at the Sloan Automotive Laboratories suggested a similar change in slope of the engine operating with "detonation". (Taylor, 1985)
- A reference by Broeze (unknown) also refers to the "some 40% of the end gas detonating" in a CFR engine operating under knock-rating conditions. Figure 74 of this reference very clearly shows a change in combustion pressure slope, although it is thought to be an illustrative graph.
- In 1974, Arrigoni et al. (1974) illustrated the knock-point in the pressure signal from the CFR engine.
- The work done by Löhner and Müller in 1967 (Maly and Ziegler, 1982). showed a similar change in the pressure slope under knocking conditions, as well as the characteristic pressure oscillations, from measurements made in an L-head engine. This type of engine shares a similarly long flame propagation path to that of the side sparkplug mounted CFR engine.

No literature references could be found that allowed for the distinct pressure development in the CFR when performing an autoignition calculation. Even though Swarts et al. (2004) had identified the knock-point, the application of an ignition delay model followed the standard methodology of predicting autoignition onset near peak pressure. This paper did however include the pressure development features as a flame propagation phenomenon.

Bradley et al. (2004)) similarly calculated ignition delays to correspond to the peak pressure position during octane rating. Although admitting to the uncertainties about turbulent burning velocities, there is no indication, from Figure 4 of that paper, of accounting for the pressure development features.

2.4.3. Mass fraction burnt

Early assessment of the amount of trapped mass that participates in the autoignition phenomenon found that the reaction of less than even 5% off the trapped mass is "*sufficient to produce a very violent knock*" (Ricardo, 1953). Contemporary studies would classify the autoignition of similar fractions of the end-gas as moderate knock, with increasing fractions relating to more severe knock .

By et al. (1981) concluded that the knock intensity was related to the unburned charge mass at the time of knock, but knock intensity was defined as the magnitude of the pressure oscillations. Moreover it was shown that the mass fraction burnt at knock varied from 30 percent (for the greatest intensities) to just under 90 percent (for the lowest intensities).

Work by Bradley et al. (1996b) also alluded to the fact that, for largest knock intensity, about 40% of the original mass was consumed in the autoignition reactions (i.e. at a MFB of 60%). This value dropped to about 10% for the lowest knock intensity. A more recent study by Elmqvist et al. (2003) indicated that if autoignition occurs after 93% of the trapped mass has been consumed, no knocking occurs.

Swarts et al. (2004) calculated the mass fraction burnt at the instant of the knock-point in the CFR engine and found that this varied from 30 % to 80 % of the trapped mass for the different octane number PRF blends tested under RON conditions. Very significantly, all of these tests were performed at standard knock intensity (according to the CFR system), indicating a lack of correlation between the mass fraction consumed during autoignition and the knock intensity.

2.4.4. Possible explanations of the knock-point

Obert (1973) discussed conclusions reached by Curry wherein he attributed the initial acceleration of the flame front, and the continued high flame speed, to the formation of free radicals in the end-gas. Similar speculation was made by Swarts et al. (2004) where the "pre-conditioning" of the end-gas was said to be one of the possible explanations for an accelerated flame front.

This possible role of free-radicals was assessed with the aid of detailed chemical kinetic modelling utilising Chemkin™ software (Viljoen, 2005) but no consistent presence of free-radicals at the knock-point was found that would serve to explain an accelerated flame propagation beyond the knock-point.

Konig and Sheppard (1990), found that the normal flame propagation speeds were unaffected by end-gas autoignition, so on the balance of the evidence at hand, it must be concluded that the pressure development in the CFR following the knock-point can be nothing but a manifestation of autoignitive deflagration. This is further supported by the similarity of the pressure development in the CFR engine to HCCI engine pressure records. Numerous examples of these pressure developments were contained in presentations at the 2005 SAE HCCI conference.

2.4.5. Knock intensity on the CFR engine

There are numerous metrics in existence to quantify the knock intensity following autoignition of the end-gas in a SI engine. A review of some of the methods was provided by Swarts et al. (2005), but suffice it to report that most of these metrics were based on the strength of the pressure fluctuations. By natural extension, it was assumed that the knock intensity during octane rating is also based on the strength of the pressure fluctuations caused by knocking. This view is in fact entrenched in reputable text books on the subject of internal combustion engines (Heywood, 1998).

The paper by Swarts et al. (2005) concluded, however, that the knock intensity metric used on the CFR engine was insensitive to the pressure fluctuations and was rather responding to a bulk pressure increase due to autoignition. It further revealed that there was no consistent relationship between pressure fluctuations, if present at all, and the knock intensity value measured by the CFR engine instrumentation. Moreover, it was concluded that the pressure fluctuations and post knock-point pressure increase both varied with octane number, test method (RON or MON) and fuel composition (PRF or non-PRF).

Since the issue of knock intensity is such a critical facet of the current study, results of a solid body analysis of the bouncing pin, first presented by Swarts et al. (2005) will be recalled. The discussion provides not only a historical perspective, by also an elegant mechanical metric of knock intensity quantification. The analysis comprised of an elastic, circumferentially clamped diaphragm supporting the rigid free bouncing pin. Figure 2-10 below shows the idealised depiction of the solid body model used.

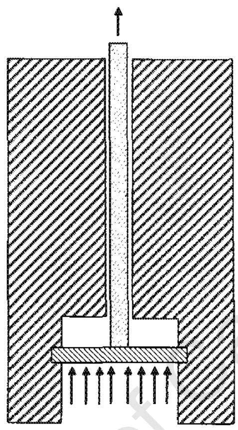

Figure 2-10: Depiction of the idealised solid body analysis of the bouncing pin. Taken from Swarts et al. (2005).

The bottom of the diaphragm was subjected to the forces exerted by pressures experienced in the CFR engine during octane rating. The results of one such simulation is shown in Figure 2-11, where the force applied to the diaphragm represented the measured pressure at standard knock intensity. The results suggest that the diaphragm follows the pressure development faithfully with maximum deflections typically less than 1 mm. The rigid bouncing pin can be seen to lose contact with the diaphragm just prior to peak pressure. Displacement of the pin is typically more than twice that of the diaphragm.

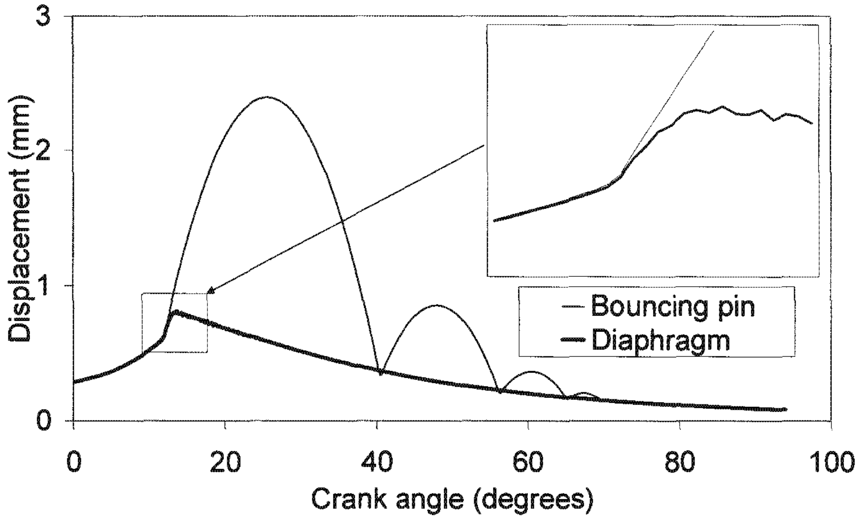

Figure 2-11: Simulated displacement of the diaphragm and pin as a function of crank angle position when subject to pressures typical of the CFR engine during octane rating. Taken from Swarts et al. (2005).

The most significant result of the bouncing pin analysis is that movement of the pin is oblivious to the pressure fluctuations due to knock (visible near the top of the displacement of the diaphragm). One can therefore deduce that, since the ASTM knock intensity is proportional to the time the pin spends in the elevated state, knock intensity is a measure of the bulk increase in pressure prior to peak pressure and not the pressure fluctuations.

This simple analysis of the bounding pin kinetics raised sufficient suspicions to warrant further study of the knock measurement system employed in the current day CFR engine. To this end, Swarts et al. (2005) quantified the knock intensity as the best fit gradient to the pressure data after the knock-point, to what visually appear to be a linear pressure increase. A typical pressure signal and best fit gradient line is shown in Figure 2-12. The smoothing brought about by fitting was thought to sufficiently mimic the low-pass filtering described by the ASTM manual. The results were however found to be inconclusive and it was deduced that the knock intensity measurement appears to be more sensitive to the early autoignition development immediately following the knock-point.

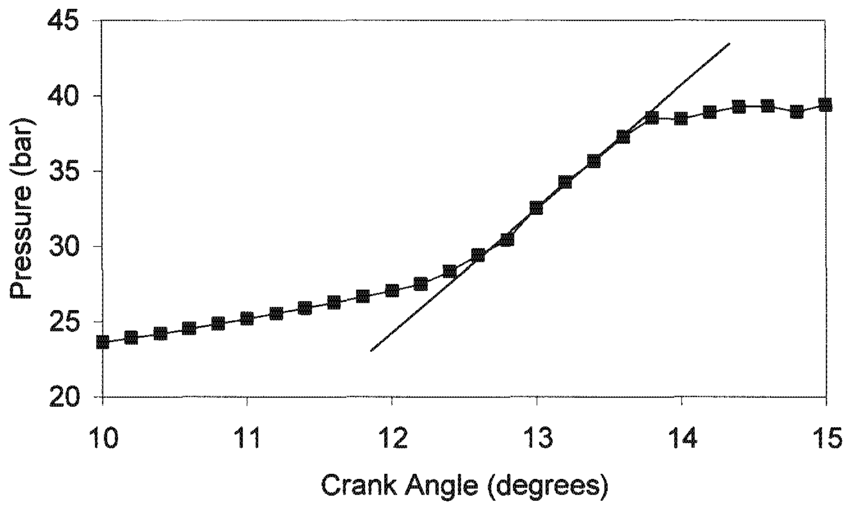

Figure 2-12: Pressure data and best fit gradient taken from Swarts et al. (2005).

The reconciliation between the pressure development and knock intensity measurement in the CFR engine will receive further attention during this thesis.

2.5. Octane number prediction

2.5.1. Empirical octane number prediction

Prediction of octane numbers have been in the realm of empirical calculation for the longest time. The simplest approach is a linear by volume addition of the octane number of blend components which yields varying results depending on the composition of the blend components.

The source of the discrepancies stemmed from the chemical bias of the octane rating scale, as eloquently put by Westbrook et al. (1998): *"By defining octane numbers in terms of alkane fuel oxidation, non-linear and complex reaction paths are built into the rating scale, and non-alkane fuels with inherently simpler oxidation mechanisms appear, erroneously, to be unusual in their ignition properties"*

Efforts by Stewart (1953) and Twu and Coon (1997) are noteworthy examples of adding blending component composition information to the blending of octane numbers.

3. Experimental methods

This chapter details the experiment part of the investigation, including the measurements performed and treatment of the experimental data. Selected illustrative results are given.

3.1. *Experimental set-up*

Details of the instrumented CFR engine used during this project are contained in Appendix A.

Tests were performed according at both RON and MON test conditions as described by the ASTM methods D2699 and D2700, respectively. The engine was checked to ensure adequate performance in terms of compression pressure and the detonation meter pickup output and the knock measurement system tracking accuracy was confirmed.

Two deviations from the ASTM standard methodology were allowed:

- The air-fuel ratio was changed in discrete intervals of 0.05 relative air-fuel ratio[††]. This allowed for comparison between different fuels and for replication of test conditions.
- Inlet air tuning (IAT) was not performed for any of the tests. This ensured that the same inlet conditions were used for all RON and MON tests, respectively. To compensate for this, small variations in compression ratio were allowed to match the required knock intensity.

All tests were limited in compression ratio to that corresponding to 100 octane for two reasons:

- Bracketing with PRF blends above 100 octane require the addition of TEL which is incompatible with the exhaust oxygen sensor.
- An earlier modification to allow for optical access to the top of the cylinder limits the clearance volume.

Data was acquired using one of two synchronisation clocks:

- Angularly resolved: this data was clocked against the shaft encoder at 0.2 °CA increments. This data was utilised where positional information was more relevant, such

[††] The relative air-fuel ratio, λ, is defined as the ratio between the actual air-fuel ratio and the stoichiometric air-fuel ratio. Values greater than unity indicate fuel lean conditions.

as the checking of the spark advance, as well as during interpretative model assessment, where it yielded a manageable amount of data.

- Temporally resolved: data acquisition was clocked against the internal clock at 50 kHz, and was typically used for engine speed independent analysis, such as the calculation of quantities with respect to time.

Further details of the data acquisition and data management are contained in Appendix A.

3.2. Model fuel components

This choice of fuel components was limited by the availability of reliable fuel ignition delay and kinetic information, with the eventual goal of model prediction in mind. Natural first choices for fuel molecules were the primary reference fuel blend components, n-heptane and iso-octane.

In addition to the PRF blends, toluene was added to the matrix for a number of reasons:

- Toluene is used in binary and ternary blends with the primary reference fuel components to make up the toluene standard fuels (TSF). These standard fuels are used during the inlet air tuning procedure prescribed for the octane rating of gasoline fuels (ASTM, 2004a and ASTM, 2004b). As such, the toluene containing blends are widely used and the octane numbers are well established.
- Toluene is chemically unlike the paraffinic reference fuels and has been found to exhibit autoignition resistance far beyond that of iso-octane.
- Toluene has been used widely, in conjunction with the primary reference fuels, to blend up gasoline surrogate fuels. Example are those by Gauthier et al. (2004) and Golovitchev and Ogink (2003). Moreover, the ignition delay character of these blends have been characterised to some extent.
- Many of the features exhibited by toluene are thought to be indicative of the behaviour of aromatics in general. There are numerous examples of the peculiar autoignition behaviour of benzene. For example, the slow reaction rate after the initial induction period observed in a rapid compression machine (Obert, 1973).

Details of all the fuel blends, including composition and properties are contained in Appendix A.

3.3. *Calculation of cyclic variability and average pressure trace*

Swarts et al. (2003) quantified the extent of cycle-to-cycle variation in the CFR engine under non-knocking conditions in terms of the position and magnitude of the peak pressure point.

The variability in terms of indicated net mean effective pressure (IMEP) was further studied for the current data measurements. Descriptive statistics were employed to quantify the extent of variability in a sample of typically 250 engine cycles. The average and standard deviation for a number of tests at standard knock intensity under RON operating conditions are shown in Table 3-1 below:

Table 3-1: Descriptive statistics of indicated net mean effective pressure for selected PRF blends at standard knock intensity under RON conditions

	PRF65	PRF76	PRF85	PRF93	PRF100
Average (bar)	6.77	6.88	6.95	7.23	7.36
Standard deviation (bar)	0.11	0.13	0.13	0.04	0.08
Coefficient of variation (%)	1.64	1.85	1.85	0.60	1.12

It was clear from the data that variability in IMEP in the CFR engine under the conditions tested was exceedingly small, probably due to the low load and speed under which the tests were performed.

To find a pressure trace that represents the "average" for a particular test condition, one is tempted to simply take the ensemble average of a number of pressure traces in the time (engine position) domain. This would however introduce serious errors, since the combustion evolution (or MFB) at any instant in time varies significantly for individual pressure traces.

An alternative solution is to pick a single pressure trace that represents the average behaviour. The methodology can be further expanded to visualise variation in the pressure development for any test condition, by selecting individual pressure traces corresponding to the average, maximum, minimum as well as the 68 % confidence level (average +- one standard deviation). The mathematical implementation was done according to:

$$\begin{array}{|l|}\hline IMEP_{representative} = IMEP_{goal} \\ where \\ IMEP_{goal} \in \begin{pmatrix} IMEP_{average} \\ IMEP_{average} + \sigma \\ IMEP_{average} - \sigma \\ IMEP_{\max} \\ IMEP_{\min} \end{pmatrix} \\ and\ \sigma = std\ deviation\ of\ sample \\ \hline \end{array} \quad (3\text{-}1)$$

Figure 3-1 below shows a typical result of the application of equation **(3-1)** above for a PRF93 blend under RON conditions at standard knock intensity.

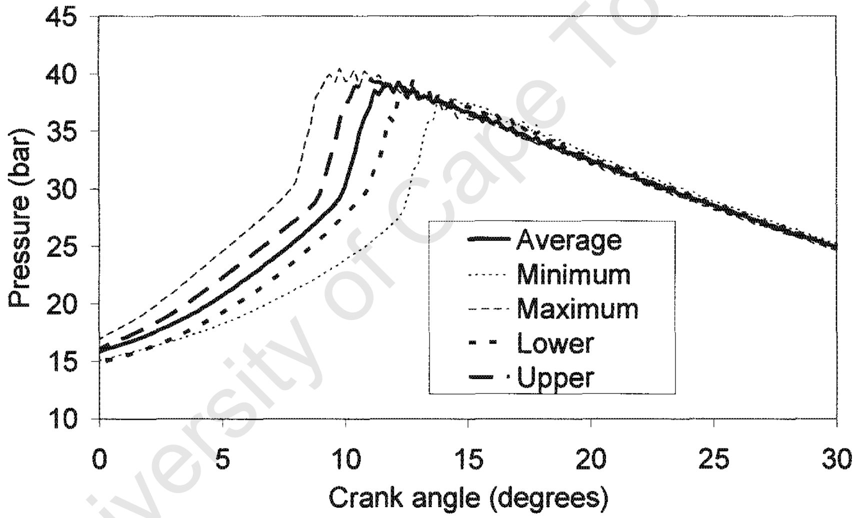

Figure 3-1: Variation in the cylinder pressure of PRF93 blend at standard knock intensity under RON conditions. The upper and lower limits are shown at the 68% confidence level and the calculations are based on the IMEP.

3.4. Mass fraction burnt

Cumulative mass fraction burned was calculated from thermodynamic considerations (Gogan et al., 2003, Heywood, 1988).

A typical result for the mass fraction burnt is shown in Figure 3-2. The data presented is for the representative pressure trace of PRF93 blend tested under RON conditions at standard knock intensity. The presence of the knock-point is clearly visible in both the pressure trace and the MFB line.

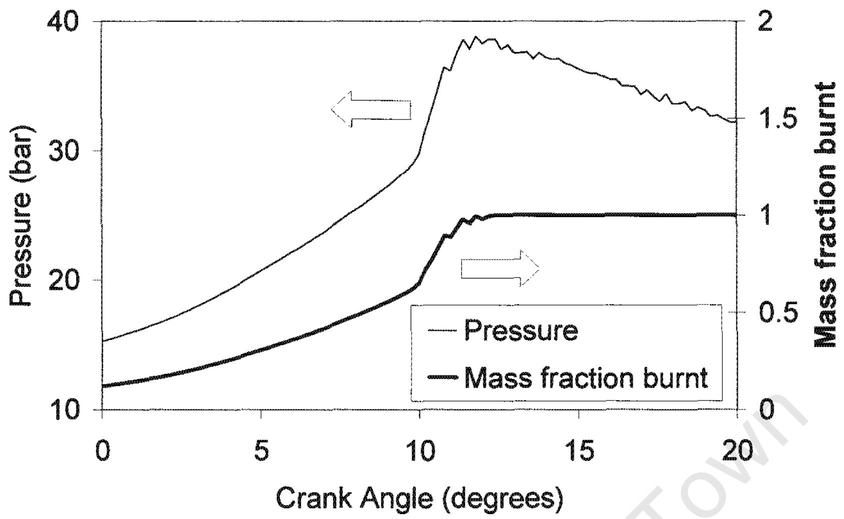

Figure 3-2: Pressure signal and calculated mass fraction burnt for PRF93 blend tested under RON condition at standard knock intensity. Spark discharge is at 13 ° BTDC.

The identification of the knock-point was based on the methodology developed and presented by Coetzer et al. (2006) and utilised a weighted mean square error criterion. The bootstrap method was applied for estimating the mean square error.

3.5. Emulation of the knockmeter

Input filter design

In an attempt to fully understand the nature of the ASTM knock intensity measurement, the operation of the model 501 knockmeter was emulated using Labview^{TM} software used in conjunction with National Instruments data acquisition hardware. Firstly, pressure data from the piezoelectric transducer was captured on a time basis. The derivative of the pressure signal was taken with respect to time to produce a rate-of-change of pressure signal, similar to the output from the magnetostrictive pressure transducer (Barton et al., 1970).

The derivative was then subject to a low-pass filter, exhibiting the same frequency response as prescribed in the ASTM manual and presented in Table 2-1. The characteristics of the filter was synthesized by using an 11th order Butterworth filter with a cut-off frequency of 2200 Hz (Horwitz and Hill, 1986). The resultant frequency response is graphically represented in Figure 3-3 against the ASTM requirement.

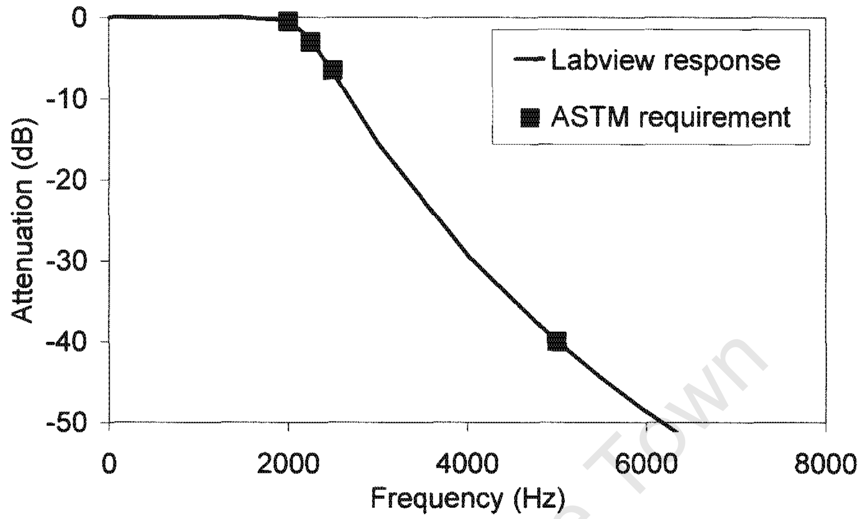

Figure 3-3: Required frequency response of the low-pass filter circuit of the knockmeter shown as symbols. Solid line represents the resultant software filter as implemented in the data acquisition system.

The filtered rate-of-change of pressure data was captured as an additional analogue channel and saved for further manipulation. An example of the filtered signal is shown in Figure 3-4 below for a single random pressure trace of a PRF93 blend tested under RON conditions.

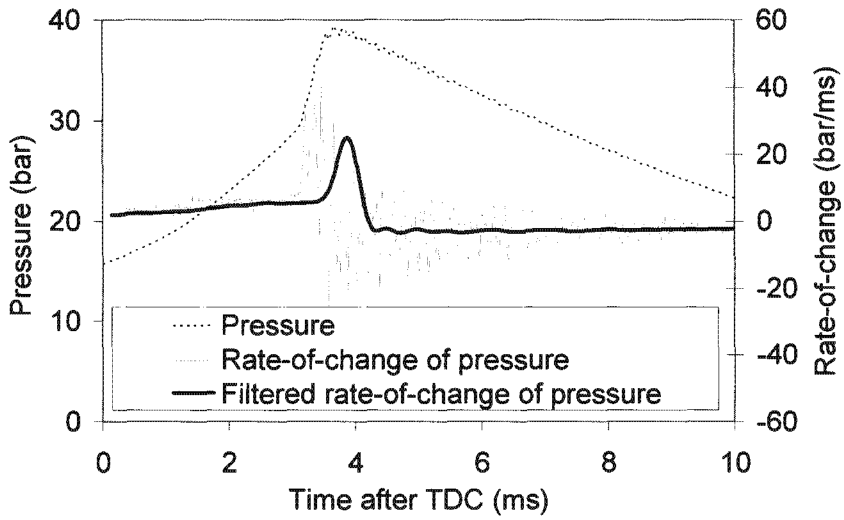

Figure 3-4: The effect of the low-pass filter on the rate-of-change of pressure. Results are shown for a random sample of PRF93 under RON conditions at standard knock intensity.

The filter exhibits two significant effects in addition to smoothing the derivative signal. The first is signal attenuation and the second is a delay in the peak value. The maximum positive value of the filtered rate-of-change data was taken to present the pressure rise rate for an individual cycle.

Variability of filtered signal

Since the pressure rise rates vary due to the cycle-to-cycle variation of the underlying pressure traces, descriptive statistics were performed on the pressure rise rate data. Results for some of the fuels tested are given in Table 3-2. The coefficient of variation was generally below 10%, although variability did increase with increasing octane numbers.

Table 3-2: Descriptive statistics for the pressure rise rate data.

	Average (bar/ms)	Standard deviation (bar/ms)	Coefficient of variation (%)	Comments
PRF100	17.6	2.7	15.1	
PRF93A	26.9	1.5	5.5	
PRF93B	27.1	1.4	5.2	Repeat of PRF93A test
PRF65	39.4	1.5	3.8	
TSF998	20.3	2.3	11.1	
TSF934A	22.1	1.9	8.6	
TSF934B	22.1	2.2	10.1	Repeat of TSF93A test
TSFnatref	22.7	1.6	7.0	Reproduction of TSF934A/B tests
TSF852	29.4	2.1	7.2	
TSF651	36.8	2.0	5.4	
Blend5	29.2	2.1	7.1	RON=90
Blend6	24.0	1.6	6.7	RON=95.6

The table further serves to show the repeatability of analysis methodology: PRF93A and PRF93B and TSF934A and TSF934B are two pairs of successive tests on blends prepared on-site using the graduated burettes, and show remarkably similar results. Reproducibility of the fuel blend preparation was also investigated by testing the TSFnatref sample. This particular blend of the same 74:26 toluene:n-heptane standard fuel blend was sourced from the motor laboratory attached to the Natref refinery in Sasolburg, South Africa. The difference in the average pressure rise rate was found to be well within the standard deviation of the data.

4. Experimental results and discussion

This chapter provide selected details of the experiment results.

4.1. Knockmeter settings

In order to develop a detailed understanding of the knock measurement system and adjustments thereto, the METER and SPREAD adjustments were studied for the range of RON PRF blends from 40 to 100. Details of the adjustment procedures are contained in the ASTM manuals, but an abridged description is as follows:

- Set up the engine at the required compression ratio for the particular PRF blend.
- Operate the engine at an air-fuel ratio that yields the maximum knock.
- Adjust the METER setting to attain a standard knock intensity
- Adjust the SPREAD setting to ensure a change in knock intensity of about 12 per octane number.

As described previously, the METER setting can be regarded as the threshold value of the pressure rise rate due to normal combustion that must be subtracted to reveal the contribution of the autoignition. The SPREAD adjustment aims to achieve a reasonable variation in knock intensity value for changes in octane number at all octane levels. The detailed procedure for making these adjustments are contained in the ASTM operational manuals.

Figure 4-1 shows typical results of the METER and SPREAD settings noted during RON tests. Above 60 octane, the response of both the meter and spread settings are both notionally linear. The increasing METER setting is to compensate for the progressively larger contribution of the normal combustion pressure increase, whereas the decreasing spread counters the large changes made in compression ratio required to discriminate a change of one octane number at the high octane levels. This feature is also apparent from the ASTM guide curves.

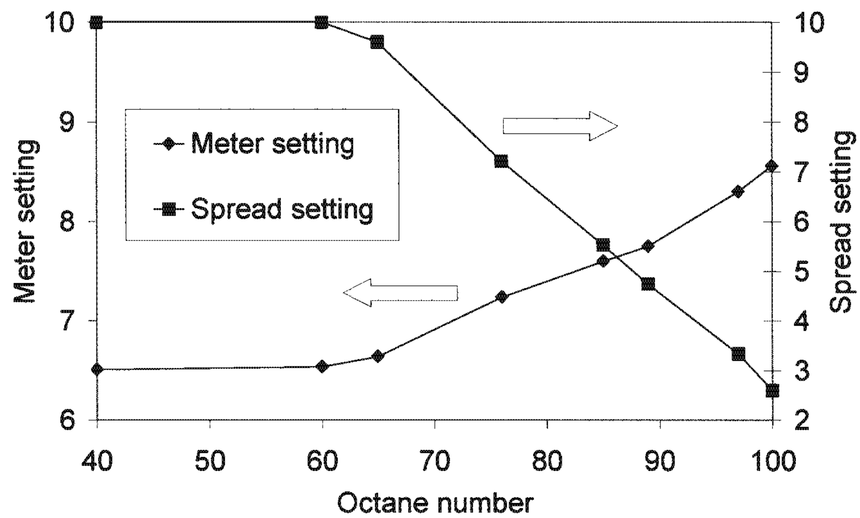

Figure 4-1: Typical METER and SPREAD setting from the knock measurement system on the CFR engine.

From the graph it is clear that there is no further adjustment possible below a 60 octane number since the SPREAD is at the maximum possible setting of 10. It is not clear whether this adjustment is typical or unique to the particular knock detection system used. The observation does caution against inferences drawn from the low octane knock intensity data information.

4.2. Angular results

4.2.1. Typical pressure traces

Typical pressure traces for selected fuels and test conditions are given in the following section. All the data correspond to the engine operating at standard knock intensity. Figure 4-2 below compares a PRF40 and PRF100, both at standard knock intensity, in the RON test. The lower compression pressure, as well as the greater visibility of the autoignition heat release can be seen for the PRF40.

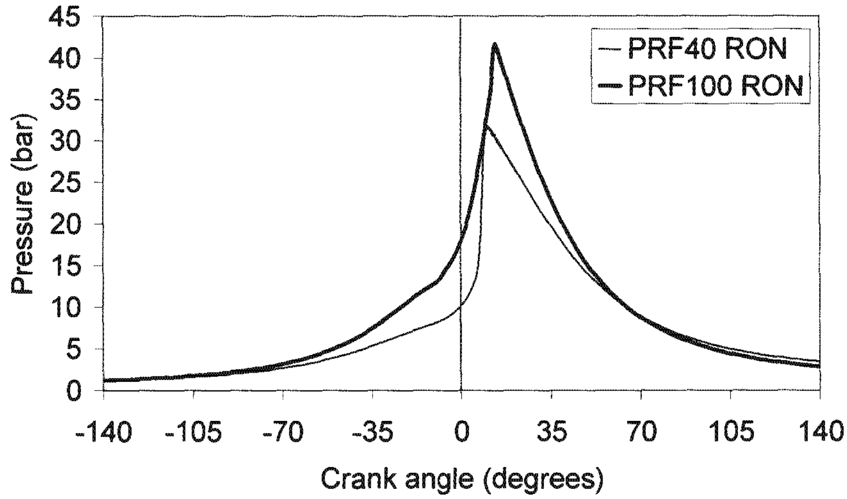

Figure 4-2: Typical pressure traces for a PRF40 and PRF100 blends at standard knock intensity for the RON test condition.

Figure 4-3 shows further results for the RON test condition with a comparison between a PRF and TSF blend. Given the similar octane number, the compression part of the engine cycle is the same, although pressure development during the combustion and autoignition differs.

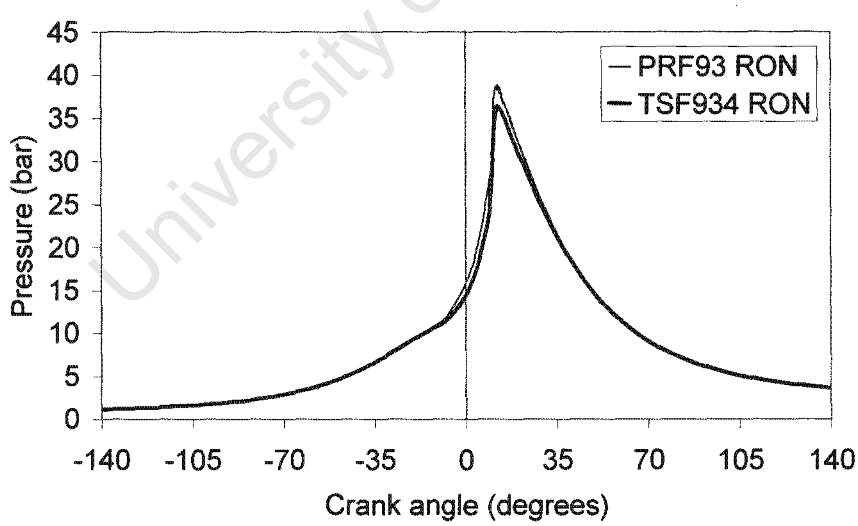

Figure 4-3: Typical pressure traces for a PRF93 and TSF934 blends at standard knock intensity for the RON test condition.

Finally, the RON and MON test conditions were compared. Figure 4-4 shows the PRF40 result from which it is clear that, because of the far advanced ignition timing for the MON test, the pressure development is very early compared with the RON test. For a 40 octane fuel, the prescribed spark advance is 26 ° BTDC and resulted in autoignition and peak pressure prior to TDC.

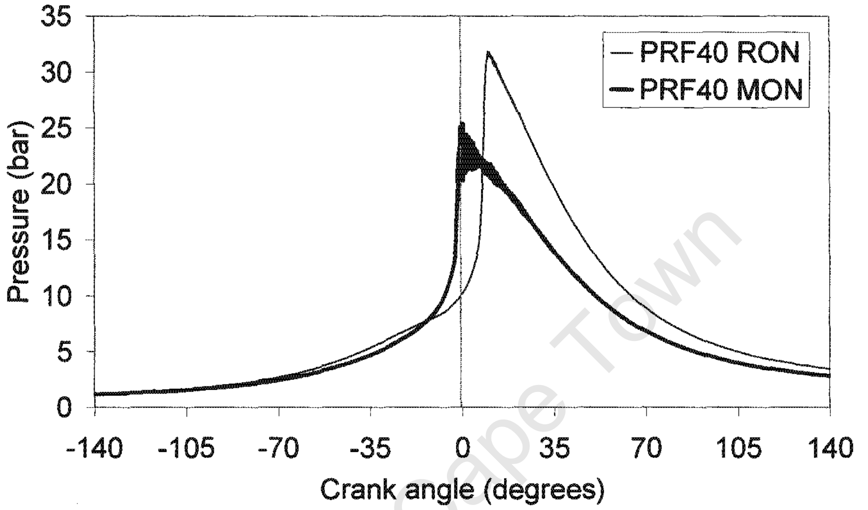

Figure 4-4: PRF40 at standard knock intensity: RON and MON results compared.

Figure 4-5 gives similar results for PRF100. In this graph, the difference in compression pressure is clearly visible. This difference stems from the difference in compression ratio prescribed by the ASTM guide tables for the testing of 100 octane fuel (7.82:1 for RON versus 8.03:1 for MON). It is also clear from all of the preceding graphs that the peak pressures for MON are consistently lower than for RON. This follows from the higher inlet temperature for the MON test.

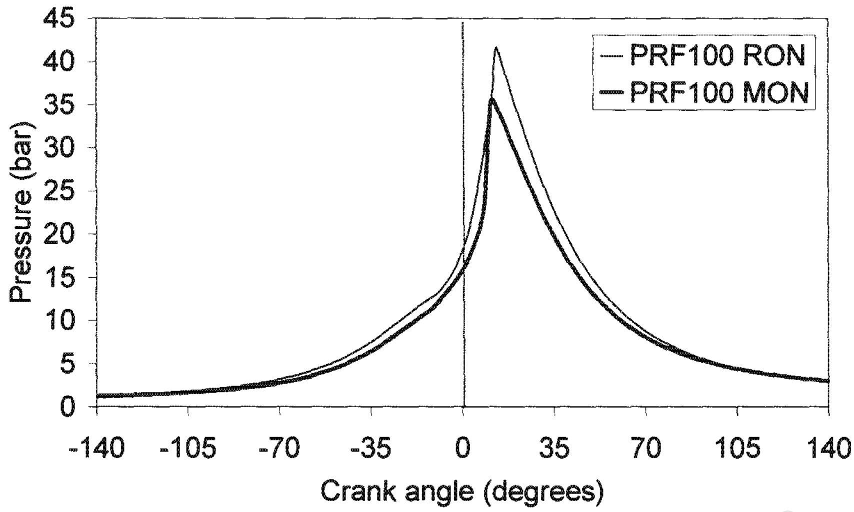

Figure 4-5: PRF100 at standard knock intensity: RON and MON results compared.

4.2.2. Knock-point location

Results for the angular position of the knock-point for PRF blends tested under RON conditions were presented in the paper by Swarts et al. (2004). The same paper calculated and presented results for the mass fraction burnt at the knock-point and revealed that a significant fraction of the end-gas participates in the autoignition, especially for low octane PRF blends.

Using the methods described in Section 3.4, the mass fraction burnt and knock-point was identified for tests performed at standard knock intensity, for both RON and MON. Figure 4-6 reveals that the mass fraction burnt for non-PRF blends under RON conditions are slightly lower than the PRF of similar octane, indicating a larger proportion of trapped mass involved in the autoignition. The trend identified by Swarts et al. (2004) for PRF blends under RON conditions remains unmistakable.

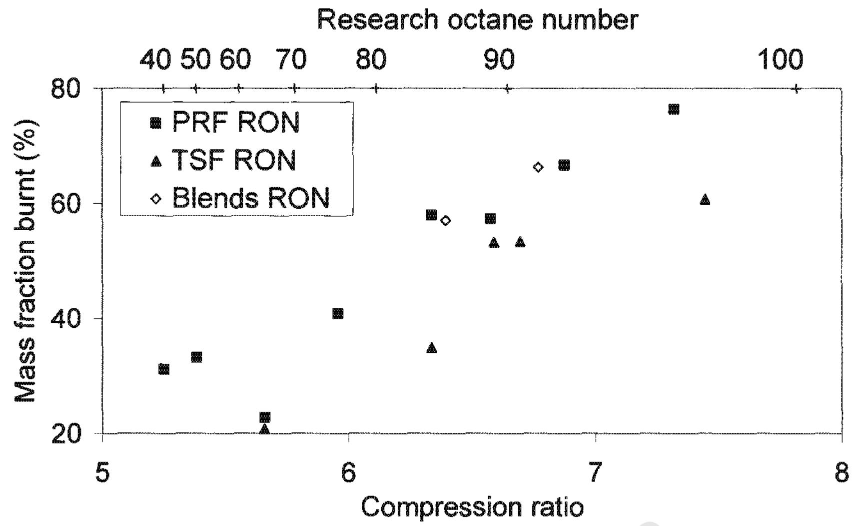

Figure 4-6: Mass fraction burnt at knock-point for RON conditions.

A similar analysis of the MFB at the knock-point was performed for tests performed under MON conditions at standard knock intensity and these results are shown in Figure 4-7.

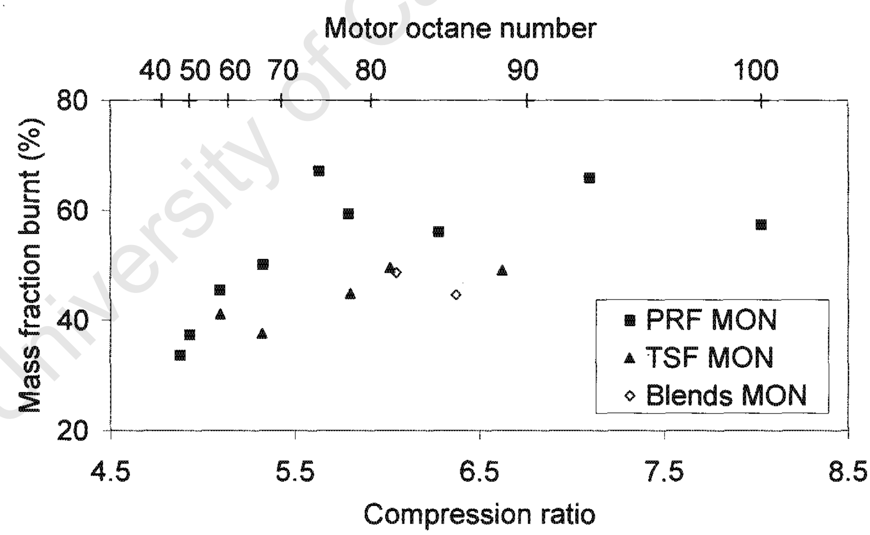

Figure 4-7: Mass fraction burnt at knock-point for MON test conditions.

In comparison to RON, the general increasing trend of MFB at knock-point for increasing compression ratio remains visible for MON. The range of MFB values from the MON results fall within a much narrower band, with much of the data at the 50 % MFB level. The MON data does however reveal an anomaly in the PRF data for octane numbers between 60 and 80 with MFB value excursions to 60%.

4.3. Temporal results

4.3.1. RON PRF blends

The pressure rise rates‡‡ for a range of PRF blends at standard knock intensity is shown in Figure 4-8. These measurements were performed under RON conditions and at the standard inlet air temperature of 51.7 °C and compression ratios from the guide table in the ASTM manual.

The general trend observed during the measurements was that of decreasing pressure rise rate values as octane number increases. More severe conditions of temperature and pressure were expected to lead to greater values for the pressure rise rate at higher octane numbers. However, owing to the diminishing fraction of fuel participating in the autoignition as octane numbers increase, the severity of the autoignition, as measured by the rate-of-change values, diminishes.

‡‡ Any further reference to the pressure rise rate will imply the average of the minima of the filtered rate-of-change of pressure data

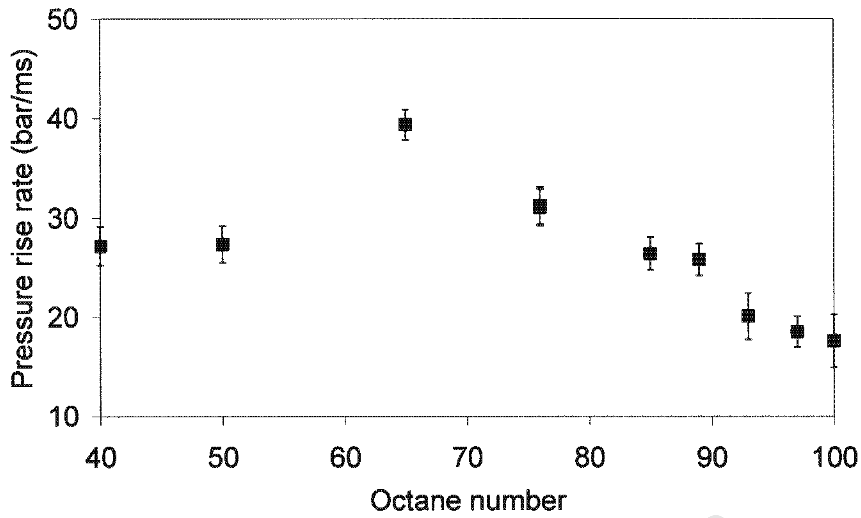

Figure 4-8: Pressure rise rate for a number of PRF blends under RON conditions at standard knock intensity§§.

The lack of a consistently smooth curve is not an undue concern, since the ASTM method allows for continuous adjustments to the knock measurement system. Significantly, the ranges of applicability without re-adjustment of the knock detection system settings are strictly prescribed by the test method and within those ranges, a linear response of knock intensity with octane number is assumed.

4.3.2. Compression ratio effect

PRF 100

For convenience of presenting the results, compression ratio is used in favour of octane number to discount the non-linearities introduced by the guide tables. The result of this representation is shown in Figure 4-9 for the RON PRF blends. Although the trend line suggest a more regular response of the pressure rise rate with respect to compression ratio, the arguments presented previously regarding the local linearity still holds. The data for the PRF pressure rise rate represents a definitive calibration curve for standard knock intensity at different compression ratios.

§§ In this graph, as with all of those presented henceforth, the error bars are +- one standard deviation. The range covered by the error bar thus represents the 68% confidence interval of the data.

Figure 4-9 shows another important feature of the calculated pressure rise rate, which is the behaviour at sub-critical compression ratios. The data for iso-octane at diminishing compression ratios indicates that up to a compression ratio of about 7:1, the pressure rise rate remains fairly constant, being associated with normal combustion. Above this compression ratio, however, a dramatic increase occurs in the pressure rise rate due to the emergence of the autoignition heat release.

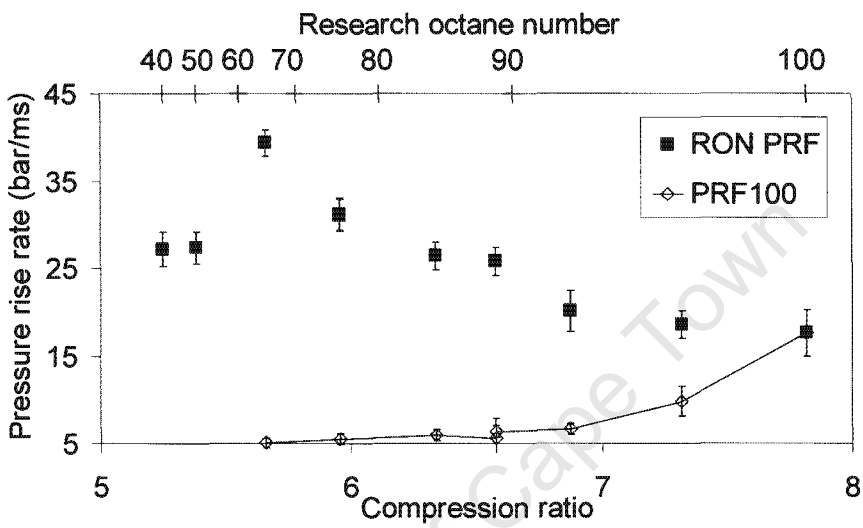

Figure 4-9: Pressure rise rates under RON conditions. The PRF blends in the range from 65 to 100 RON, shown by the square symbols, were tested at standard knock intensity. The open diamond symbols are for PRF100 at sub-critical compression ratios.

This behaviour at sub-critical compression ratios is further illuminated in Figure 4-10 where the relative growing amplitude of the filtered rate-of-change of pressure values can be seen as the compression ratio is increased. The results are presented for three individual pressure traces representing knocking operation at critical and sub-critical compression ratios as well as normal combustion. This picture is consistent when changing the compression ratio for any of the fuels considered, so individual results will not be shown.

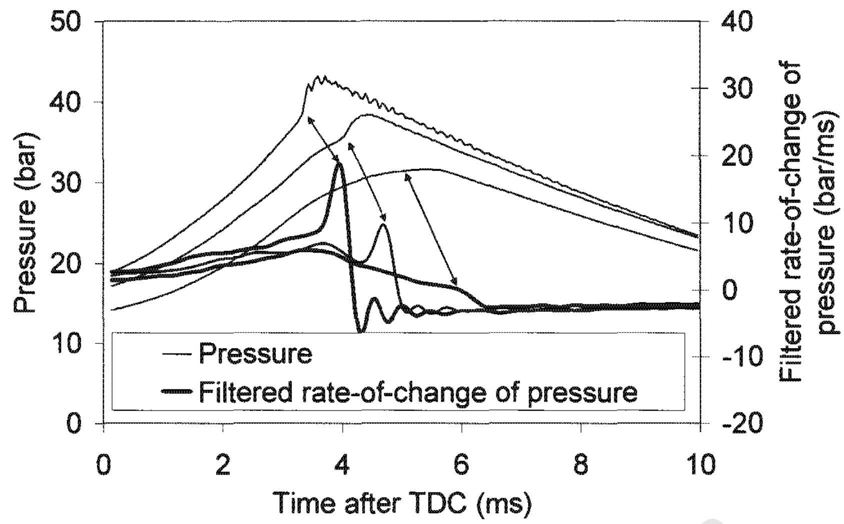

Figure 4-10: Cylinder pressure and filtered rate-of-change thereof for a PRF100 blend at CCR and two compression ratios lower than critical.

TSF blends

The effect of compression ratio of non PRF blends is presented for TSF and gasoline surrogate blends under RON conditions. The choice of the RON test condition for this study was one of convenience as it negated the need to reset the ignition timing as the compression ratio was changed.

The performance of the TSF blends is shown in Figure 4-11. Each of the fuels was rated at the relative air-fuel ratio that produced maximum knock and at the critical compression ratio. Thereafter, tests were performed at the same air-fuel ratio, but at progressively lower compression ratios. It is clear from the graph that the lower compression ratios produce progressively lower values for the pressure rise rate. For each of the TSF blends, the maximum value for the pressure rise rate approaches the calibration line defined by the PRF data.

The result for TSF998 can be used to explain the effect of the reduction of compression ratio allowed in favour of inlet air tuning. The maximum value of pressure rise rate is achieved at a compression ratio of 7.45 which corresponds to a RON value of 97.9 at the unadjusted inlet air temperature of 51.7 °C. Downward adjustment of the inlet temperatures would have resulted in a moderation of the end-gas conditions and a greater octane number rating.

The results for TSF934 when compared to TSFnatref (similar in composition but from a different source) are also very significant. In addition to speaking to the reproducibility of the blend preparation mentioned earlier, the TSFnatref result at maximum knock intensity is shown to be nearly co-incidental to the value achieved for a comparable PRF blend. The result for the TSF934 above the RON calibration line corresponds to the critical compression ratio for a 93.4 RON blend. At this compression ratio, the knock intensity was found to be 91 which was significantly higher than the required 50. This observation supports the notion that inlet air tuning would have been appropriate to correct the discrepancy.

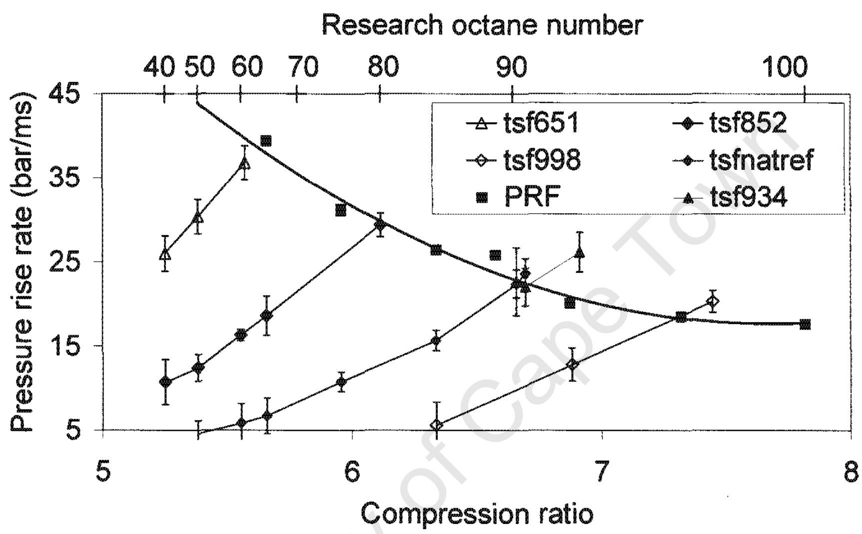

Figure 4-11: Pressure rise rates for a range of toluene standard fuel blends, compared to the calibration line defined by PRF blends under RON conditions. Tests were performed at varying, non-critical compression ratios.

The same picture was found to hold true for gasoline surrogate blends 5 and 6 (RON values of 90 and 95.6 respectively) as shown in Figure 4-12. The intersection of the lines of the pressure rise rate for the two blends with that of the PRF calibration curve suggests octane ratings about two to four lower than that measured by an independent laboratory.

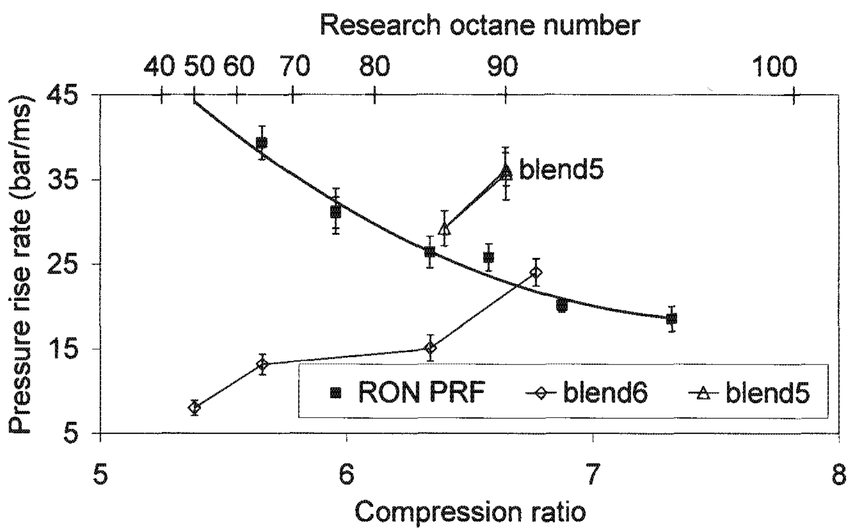

Figure 4-12: Pressure rise rates for gasoline surrogate blends, compared to the calibration line defined by PRF blends. Tests were performed at varying compression ratios. Blend 5 has RON of 90, whereas blend 6 has a RON of 95.6.

4.3.3. Air-fuel ratio effect

PRF93 example

The effect of changing air-fuel ratio can be explained with the aid of two pressure traces from the PRF93 example under RON conditions, shown in Figure 4-13. The graph shows the pressure trace and the filtered rate-of-change thereof for two values of the relative air-fuel ratio (λ=0.9 and λ=1). The former test condition is associated with standard knock intensity, viz. the air-fuel ratio where maximum knock intensity is observed at the CCR. The latter air-fuel ratio corresponds to a lower observed knock intensity (13) and a lower calculated rate-of-change value. The compression ratio for both operating conditions remained unchanged.

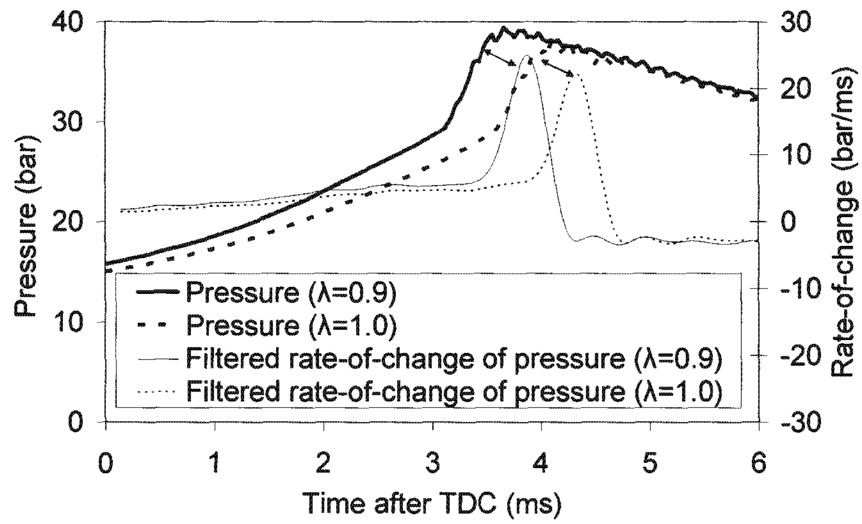

Figure 4-13: Pressure and filtered rate-of-change thereof for two values of the relative air-fuel ratio (rich and stoichiometric). Results are shown for a PRF93 tested at the same compression ratio under RON conditions at standard knock conditions.

TSF blends under MON conditions

The behaviour of non-PRF blends and the effect of changing relative air-fuel ratio are explained with reference to TSF and gasoline surrogate blends tested under MON conditions. The use of MON test data to illustrate this behaviour was convenient, since the fixed compression ratio used for each test condition negated the need to change the ignition timing. The results and conclusions hold equally well for the RON test condition and other fuels.

The results of the pressure rise rate values are shown in Figure 4-14. The values for the PRF blends again represent the calibration curve for standard knock intensity. Results of selected TSF blends are shown on the same graph, although errors bars are left out for clarity. An example of the values for the relative air-fuel ratio is annotated on the graph for the TSF887 blend.

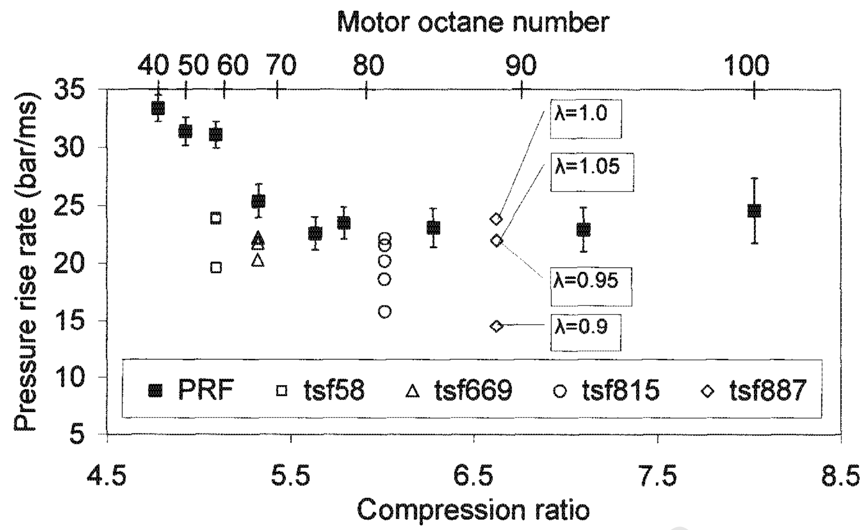

Figure 4-14: Pressure rise rates for selected toluene standard fuel blends, compared to the calibration line defined by PRF blends. TSF blends were rated at varying relative air-fuel ratios.

Figure 4-15 gives the pressure rise rate results corresponding to different relative air-fuel ratios for the toluene standard fuels tested under MON conditions. It is immediately apparent that the relative air-fuel ratio at which the maximum pressure rise rate value is achieved, differs between the different blends. This feature is also addressed later on in the chapter

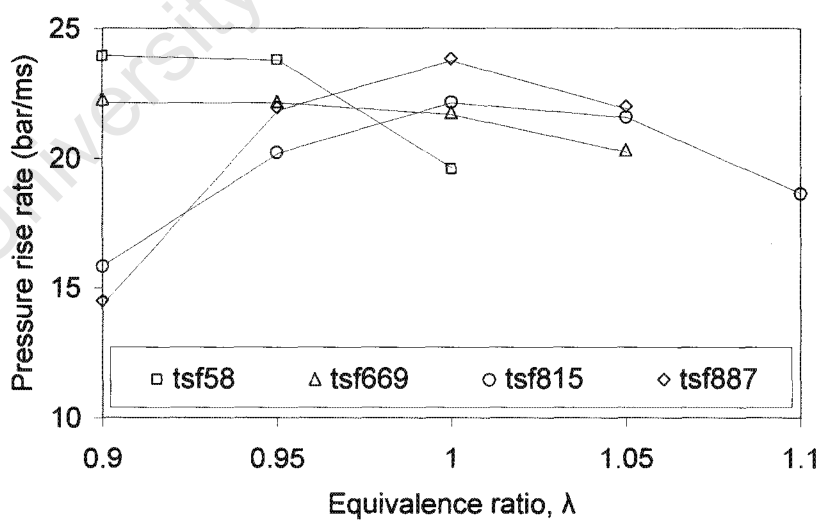

Figure 4-15: Pressure rise rate results at different relative air-fuel ratios for toluene standard fuels under MON conditions.

Gasoline surrogate blends

A similar picture emerges when the gasoline surrogate blends were rated at different relative air-fuel ratios. The results are given in Figure 4-16 where the pressure rise rate values again approach the PRF calibration values for the relative air-fuel ratio yielding maximum knock intensity.

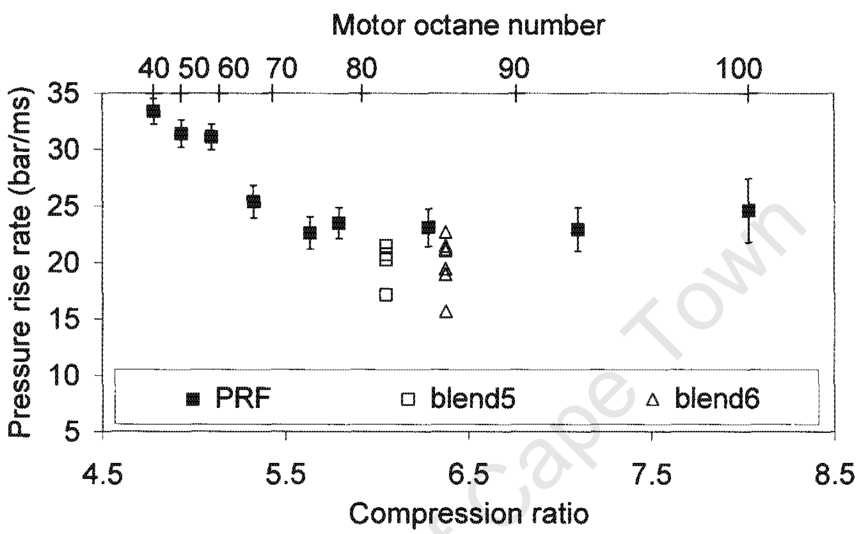

Figure 4-16: Pressure rise rates for the two gasoline surrogate blends, compared to the calibration line defined by PRF blends. Gasoline surrogate blends were rated at varying relative air-fuel ratios. Blend 5 has MON of 82 whereas blend 6 has a MON of 86.1.

Theoretical basis for air-fuel ratio effect

Although the autoignition reactivity response to air-fuel ratio is well documented and covered in Appendix B, the single biggest effect is changing the pressure development due to a slower burn rate. The slower burn rate leads to more moderate end-gas conditions and, although autoignition is not completely avoided, the autoignition is delayed. The results further suggest that the effect of the extended end-gas life-time and the time for autoignition reactions to progress is overshadowed by the more moderate operating conditions.

The effect of air-fuel ratio is explained by the fact that the flame speed and adiabatic flame temperature respond similarly to changes in air-fuel ratio. The effect of air-fuel ratio on adiabatic flame temperature is revealed by the theoretical prediction for a number of hydrocarbon species, shown in Figure 4-17. Noticeable is the adiabatic flame temperature of toluene, c7h8, as well as the TSF934 blend, containing 74 % by liquid volume, of toluene, that reaches a maximum value closer to stoichiometric when compared to the PRF blend components.

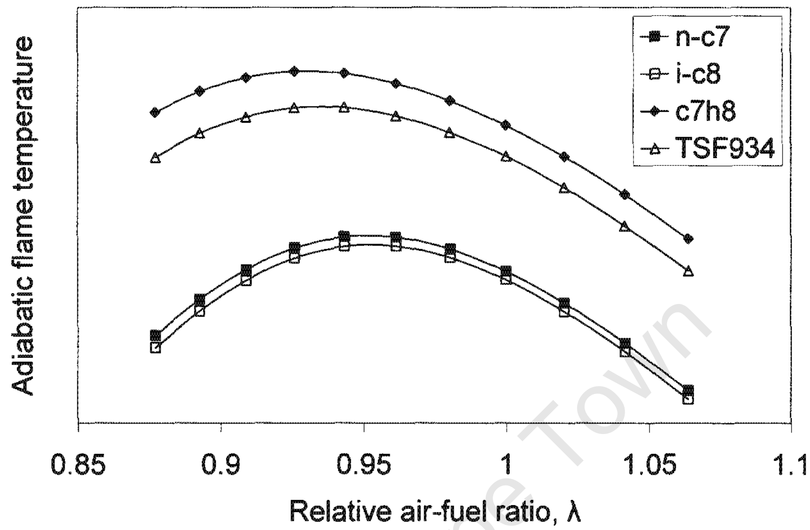

Figure 4-17: Calculated adiabatic flame temperature for a variety of hydrocarbons.

It was therefore expected that the effect of air-fuel ratio changes on the pressure rise rate during the octane rating tests will be different for the different fuel compositions tested. Figure 4-18 show selected tests from both RON and MON data sets and confirm the expectation. Three features are apparent from the graph:

- The maximum pressure rise rate is generally at richer mixtures for the lower speed RON condition for PRF blends. Only PRF40 contradicts the trend.
- Toluene containing blends (TSF and gasoline surrogates) generally have a flatter response to changes in relative air-fuel ratio.
- Toluene containing blends generally have the maximum pressure rise rate values closer to stoichiometric when compared to PRF blends. This was again expected based on by the adiabatic flame temperature response to relative air-fuel ratio.

All of the above observations based on the pressure rise rate values were confirmed by scrutiny of the observed recorded knock intensity values.

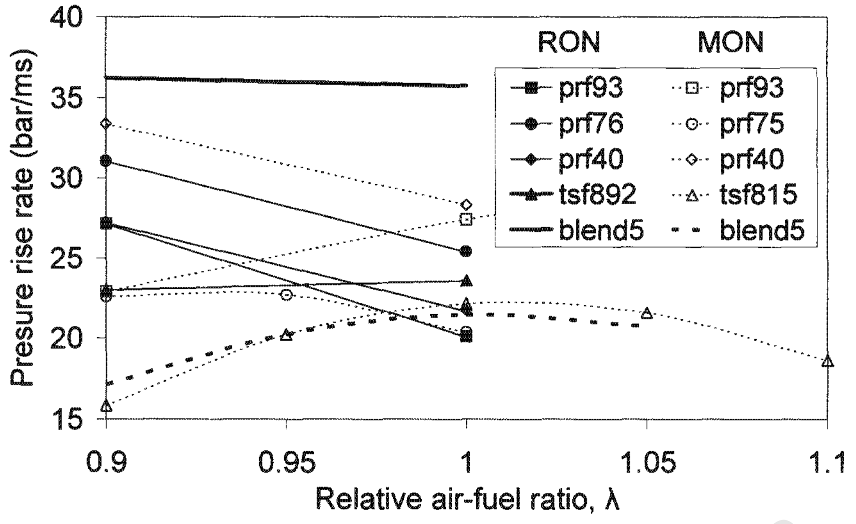

Figure 4-18: Pressure rise rates as a function of relative air-fuel ratio for selected blends.

4.3.4. RON and MON compared

The difference between the RON and MON test conditions are illustrated by considering the pressure rise rate values for PRF blends in Figure 4-19. The figure suggests that the pressure rise rate for RON conditions decreases more dramatically with octane number than for MON.

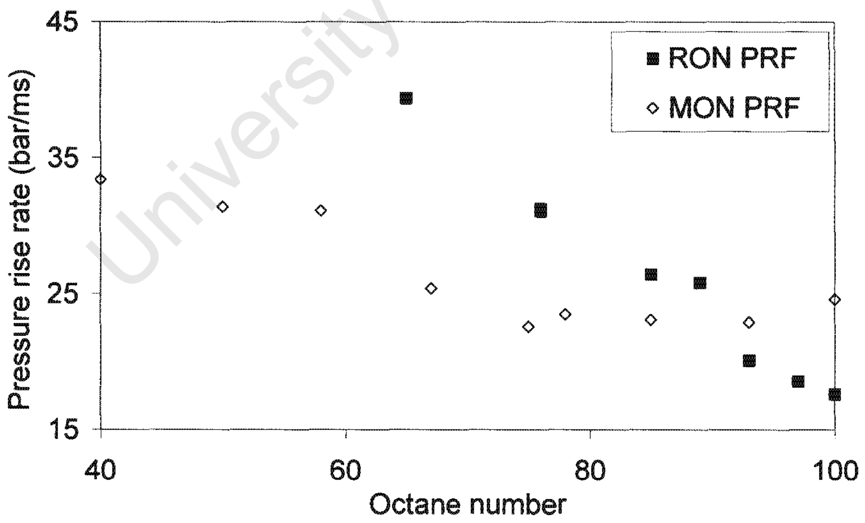

Figure 4-19: Comparative pressure rise rates for PRF blends for RON and MON test conditions.

The MON values appear fairly constant throughout the range of octane numbers, suggesting that the changing ignition timing in the MON tests manages to maintain fairly constant strength of autoignition throughout the octane number scale. This observation is echoed by the laboratory experience of less adjustment of the METER setting for the MON test condition. By comparison, RON tests required greater adjustment of the METER setting: a fact that is reflected in the greater range of the RON data in the graph. The "cross over" between the data for RON and MON at an octane number of about 90, is also evident by perusal of the guide table data for the two rating scales. (Yates et al., 2003)

4.4. Pressure fluctuations

The magnitude of the pressure fluctuations associated with knock in a spark ignition engine has been quantified by several different means in the past as summarised by Swarts et al. (2005). Since pressure fluctuations characterise potentially damaging knock in a SI engine, it was important to assess the pressure fluctuations present during octane rating at standard knock intensity. For this purpose, the minimum of the third derivative of pressure was taken to be indicative of magnitude of pressure fluctuations in the CFR engine (Checkel and Dale, 1986).

The relative ranking of fuels in terms of the third derivative indicator at a given operating condition is likely to be indicative of the expected knock performance in production spark ignition engines, where knock is characterised by pressure fluctuations.

4.4.1. RON results

An example of the calculation of the third derivative is illustrated below, where the minimum of the third derivative was shown to correspond to the position and relative size of the pressure fluctuations present in the pressure trace. Figure 4-20 portrays data for PRF93 blend at standard knock intensity as tested under RON conditions.

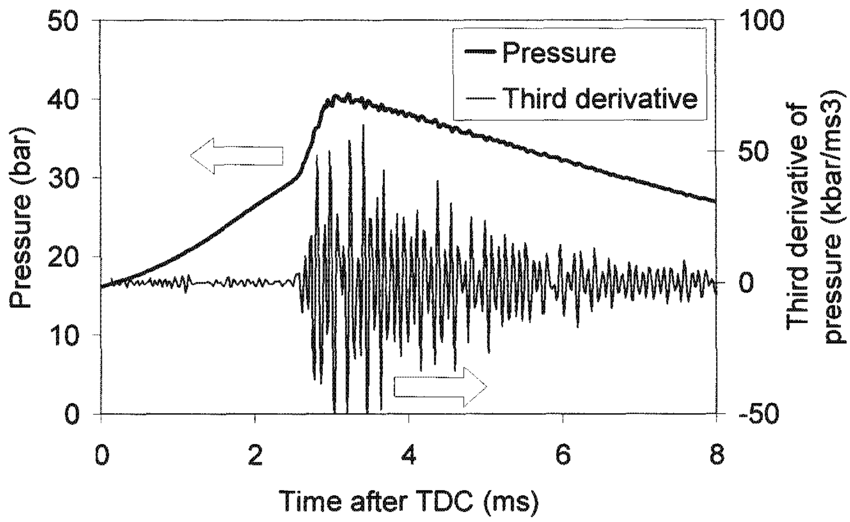

Figure 4-20: Third derivative of pressure with respect to time for a PRF93 blend under RON conditions at standard knock intensity.

The comparative strength of the pressure fluctuations were investigated for PRF, TSF and gasoline surrogate blends. Figure 4-21 shows that for RON conditions, the average of the minima of the third derivative*** data for individual PRF blends are contained in the range between 10 and 40 kbar/ms^3 for all compression ratios. Values at comparable compression ratios for the TSF blends are consistently lower than the PRF equivalent. It was also found that the value of the third derivative of about 10 kbar/ms^3 is associated with the noise of the underlying digitised pressure signal and indicates the absence of any noteworthy pressure fluctuations. The TSF blends are a case in point.

*** This average value will henceforth simply be referred to as the "Third derivative"

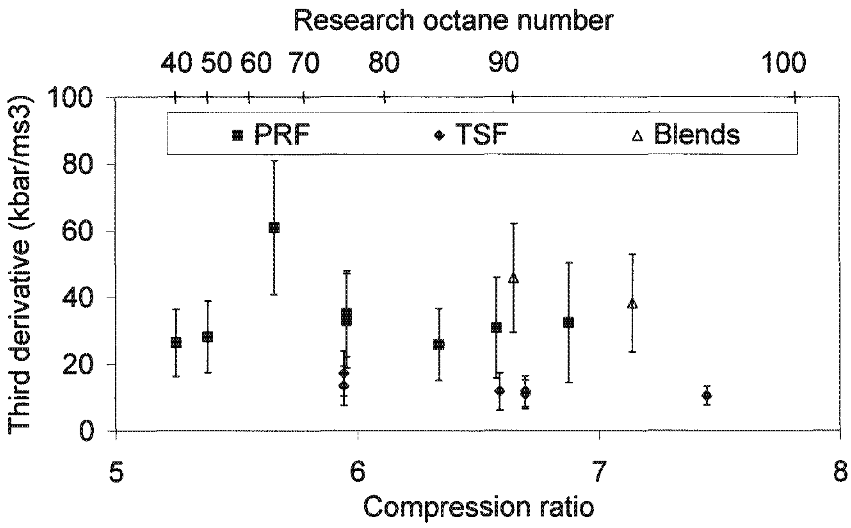

Figure 4-21: Third derivative with respect to time for all RON tests performed.

When considering the relationship between the third derivative of pressure and the Pressure rise rate, Figure 4-22 suggests a regular positive correlation between increasing levels of these two quantities for PRF blends and the gasoline surrogate blends. TSF blends can again be seen at the lower extremity of the third derivative scale.

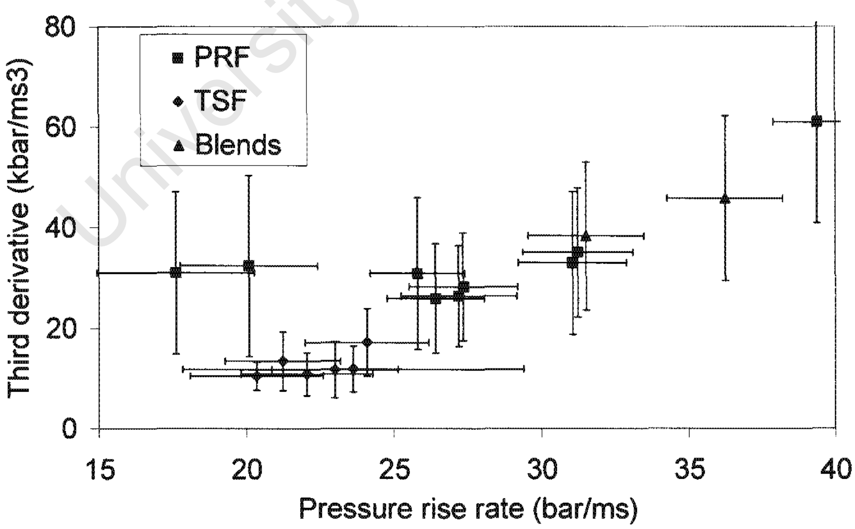

Figure 4-22: Third derivative for RON against the pressure rise rate.

4.4.2. MON results

The equivalent result for tests performed at standard knock intensity under MON conditions are shown in Figure 4-23. For all the fuel blends, there is a consistent reduction in the value of the third derivative of pressure with increasing compression ratios. The graph suggests that the pressure fluctuations are consistently higher for PRF blends when compared to non-PRF blends at the same compression ratio, as was seen for the RON results.

The comparatively high values of the third derivative for low octane fuels are probably due to the advanced ignition timing prescribed by the MON method, resulting in the location of the pressure fluctuations being closer to TDC when compared to RON.

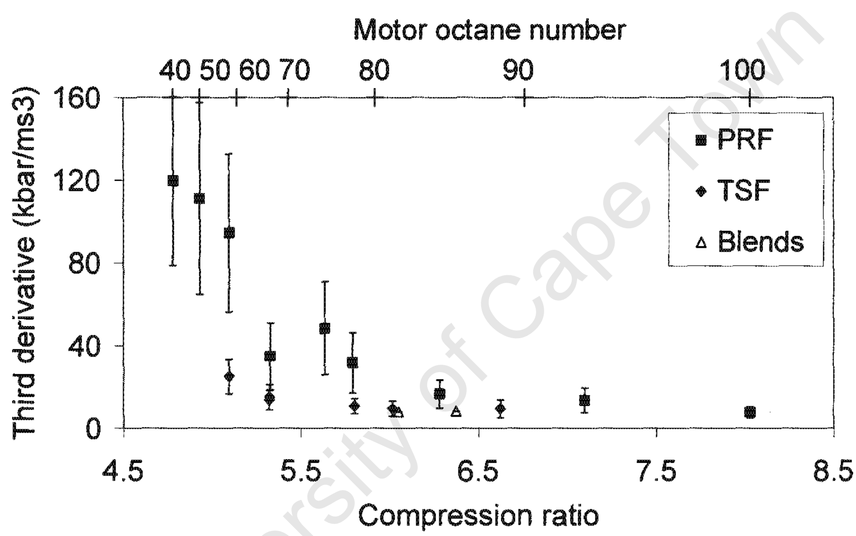

Figure 4-23: Third derivative of pressure with respect to time for all MON tests performed.

Figure 4-24 gives the relationship between the third derivative of pressure and pressure rise rate for MON test conditions. In this case, the positive correlation observed for RON was still visible, although the gasoline surrogate blends cluster with the TSF blend results. It is particularly insightful to see that the low octane PRF blends (the three data points furthest to the right) exhibit particularly severe autoignition by either metric. This is again attributable to proximity of the knock appearance to TDC.

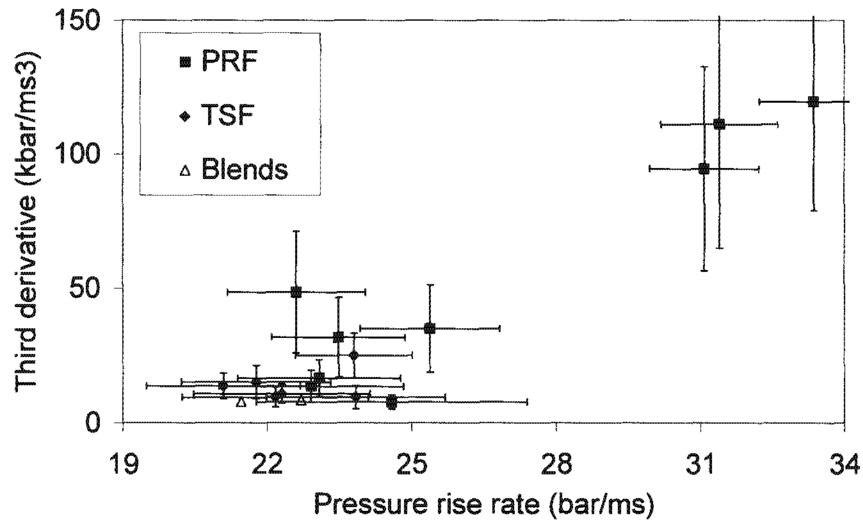

Figure 4-24: Third derivative shown against pressure rise rate for MON test conditions.

4.4.3. General discussion

The results for RON and MON both suggested an overall positive correlation between the third derivative of pressure and the pressure rise rate values. This means that, at standard knock intensity, increased pressure rise rate values corresponded to increased levels of pressure fluctuations (indicated by the third derivative values). Scrutiny of the data revealed a latent compositional effect, wherein the third derivative values for the TSF blends were consistently lower than the other blends tested. In many instances the third derivative indicator was at the noise level of the data, suggesting that the pressure fluctuations were negligible.

The implication for aromatics and aromatic containing fuels, in particular, is that their knock performance in production engines are likely to be *better* than the octane number suggests. This is due to diminished pressure fluctuations during octane rating, suggesting that the fuels are not operating close to the verge of the appearance of pressure fluctuations that would be detected in a knock-sensor equipped production engine. Anecdotal support of this notion stems from the Honda motor sport experience where the knock-limited boost pressure was much higher for aromatic containing fuels when compared to paraffinic fuels of the *same octane number*. (Otobe et al., 1994)

Douad and Eyzat (1978) distinguished between "moderate" and "heavy" for RON and MON conditions, respectively. Although it is not clear how the severity of the knock was quantified, there is sufficient evidence to confirm that autoignition in RON and MON tests are different. The differences are visible both in the pressure rise rate values, as well as the third derivative indicator.

4.5. Towards a pressure data based octane rating

It was entirely possible to replicate the operation of the knock detection system on the CFR engine by the appropriate post-processing of pressure data obtained from an in-cylinder piezo-electric pressure transducer. This fully digital system would apply the digital filters in real time to the time derivative of the pressure signal, much as the operation of the knock detection system had been emulated using recorded pressure data. Added benefits of such a digital system could include online statistics of the variation as well as reporting on pressure fluctuations. The latter could be done through the third derivative calculation or by means of a band pass filter, tuned to the appropriate characteristics.

The process for utilising such a digital system would be similar to the ASTM methods, whereby the PRF calibration curve of pressure rise rate values would be determined first to set up the local bracket values. The process for rating an unknown fuel would be to increase the compression ratio, vary the relative air-fuel ratio and track the increase of the pressure rise rate, until the PRF calibration line was encountered. The corresponding local value of the pressure rise rate would then be indicative of the appropriate octane number of the sample fuel.

The suggested methodology obviates the continuous adjustment of the METER and SPREAD settings as the eventual output would not be required to conform to the limited range of the knockmeter readout. Additional benefits would include seamless compression pressure checking without the need to fit the compression meter, as well as doing away with the ASTM knock measurement system altogether. This would be particularly useful with only one access point into the CFR engine.

5. Modelling interpretation

This chapter gives details of the theoretical model interpretation of phenomena observed in the engine.

5.1. End-gas condition estimation

Average temperature in the engine can be calculated by application of the ideal gas law:

$$T = \frac{P \bullet volume}{mass \bullet R} \qquad \textbf{(5-1)}$$

where *P* is the pressure and *R* is the specific gas constant. The changing average composition during the combustion phase reflects in a changing gas constant and invalidates the application of the ideal gas law in the presence of a flame front. Moreover, lack of quantitative information about the residual gas fractions and extent of blow-by introduces further uncertainties about the gas constant and mass, respectively.

The estimation of the end-gas temperatures, based on recorded pressure data, reverted to a calculation based on the polytropic compression according to:

$$\frac{T_i}{T_{IVC}} = \left(\frac{P_i}{P_{IVC}}\right)^{\frac{k-1}{k}} \qquad \textbf{(5-2)}$$

where the subscript *i* refers to any instant after IVC and *k* is the polytropic coefficient.

For isentropic (reversible, adiabatic) compression, the polytropic coefficient is equal to the ratios of specific heats, γ:

$$k = \gamma = \frac{Cp}{Cv} \qquad \textbf{(5-3)}$$

It can be readily shown from thermodynamic calculations that the ratio of specific heats decrease with increasing temperature. In addition, the value of the polytropic coefficient changes during the compression phase: from one larger than the ratio of specific heats to a value smaller. This is due to the change in direction of heat transfer: from taking up heat early during the compression to rejecting heat during the latter stages. The calculation of the instantaneous polytropic coefficient and the inferences that can be drawn from it is addressed in the paper by Swarts and Yates (2004).

For the purposes of the ensuing analysis, however, a constant value for the ratio of specific heats is assumed. The latter is calculated at an estimated temperature appropriate to the instant of spark discharge to account for the higher temperatures relevant at higher compression ratios. As such it is intended to provide relative ranking of fuel performance and not an absolute measurement. Details of the thermodynamic property calculations are given in Appendix D.

5.2. Ignition delay model implementation

The ignition delay for any combination of pressure and temperature can be calculated using the ignition delay expression:

$$\tau_{overall} = \frac{1}{\left(\frac{1}{\tau_1 + \tau_2} + \frac{1}{\tau_3}\right)} \tag{5-4}$$

Where $\tau_i = A_i p^{n_i} e^{\frac{B_i}{T}}$ *for* $i = 1,2,3$

Further details, as well as the parameters used in the ignition delay expression for the different fuel types are given in Appendix B.

The ignition delay development in the changing pressure and temperature engine environment is accounted for by integrating the ignition delay integral value in accordance to the logic presented in Section 2.2.3. Since the pressure used during the model interpretation is in discrete form, the calculation is performed as a discrete summation according to the expression below:

$$\sum_{i=1}^{peak} \frac{\Delta t}{\tau_i} \tag{5-5}$$

The index *i* corresponds to the discrete data points and autoignition is deemed to have occurred when the sum above reaches unity, whilst the index *peak* refers to the peak pressure point.

The application of the ignition delay model is demonstrated with reference to the experimental pressure trace of a PRF93 fuel tested under RON conditions at standard knock intensity. Figure 5-1 shows the recorded pressure trace and apparent reaction rate (inverse of ignition delay time) based on the adiabatic compression of the end-gas ($k = \gamma$). A rapid increase in the "reaction rate" is visible only during the start of the combustion phase, suggesting that the very early history contributes little to the overall reaction progress.

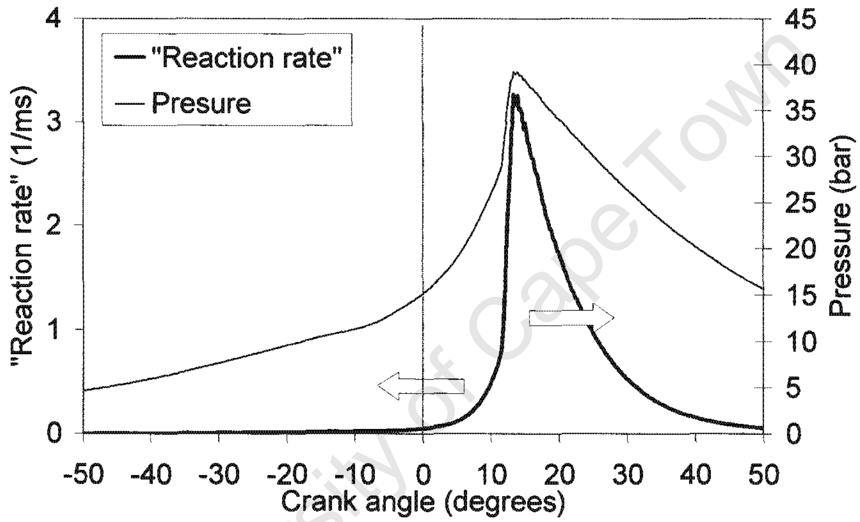

Figure 5-1: Recorded pressure for a PRF93 blend under RON conditions at standard knock. The calculated "reaction rate" (inverse of ignition delay time) is shown on left Y-axis.

The accumulation of the ignition delay integral value for the case presented in Figure 5-1 is shown in Figure 5-2 with emphasis on the conditions during combustion. It is clear that the integral value has accumulated somewhat by the time of spark discharge at 13 °BTDC due to the compression work done on the combustible mixture, but the significant accumulation of the integral value occurs predominantly during the combustion phase.

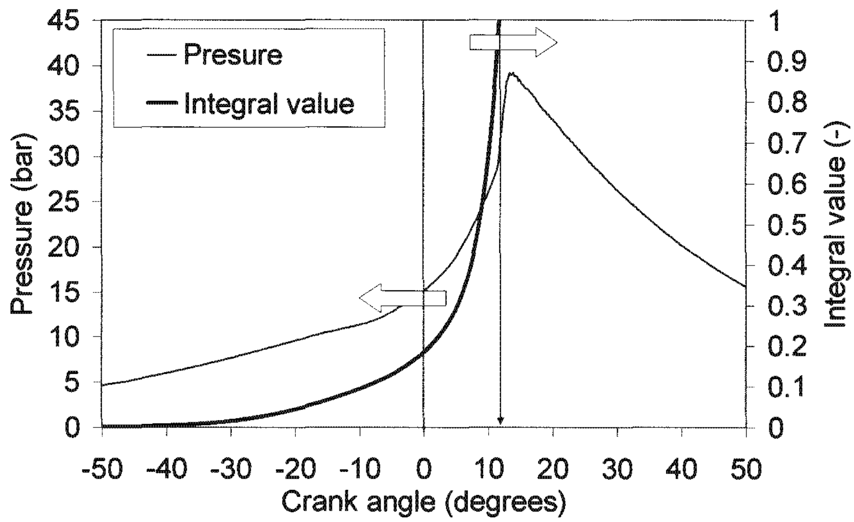

Figure 5-2: Recorded pressure trace and calculated reaction rate for PRF93 blend under RON conditions at standard knock intensity. The ignition delay integral value is shown on the right-hand y-axis and attains a critical value of 1.0 at autoignition at the knock point.

5.3. Cascading autoignition calculation

Building on the concepts presented in Section 2.1.3, it is hypothesised that the post knock-point pressure development in the CFR engine is a cascading autoignition in an inhomogeneous end-gas mixture, much as the autoignition development observed in HCCI engine. It is further suggested that the first autoignition occurs at the knock-point and that the autoignition in each of the autoignition "elements" involves only a finite fraction of the remaining end-gas. This gives rise to the observed pressure development which is more abrupt that a flame propagation but too weak to give rise to high localised pressures and pressure wave formation. As such the pressure in the cylinder can be regarded as being uniform.

One likely manifestation of this hypothesis requires distinctly different temperature histories for each of the different autoignition elements to bring about the progressive, non-instantaneous autoignition. Two thermal explanations exist for attaining the required differences in temperature histories for the different autoignition elements.

- The elements may share the same initial temperature (i.e. a truly homogeneous mixture) but experience different levels of heat loss during the compression. The extent of heat loss may range from adiabatic centres to the thermal boundary layer, where the intimate contact with the wall will result in a much greater heat loss.

- The autoignition elements may experience similar heat loss characteristics, but have an inhomogeneous temperature distribution at the instant of inlet valve closure (IVC) stemming from the gas-exchange process.

The reality is likely to be a combination of the two scenarios, as well as being compounded by the effects of mixing and the action of the flame front. To explore the concepts, however, variations in both the polytropic coefficient and the initial temperature were calculated.

The calculation methodology required the ignition delay integral value for each of the autoignition elements to be calculated. The initial temperatures (or heat loss gradient, where appropriate) was then adjusted to ensure autoignition occurs for each of the successive elements at the instant that coincides with the next available pressure data point. As such, the size of the autoignition elements corresponded to the resolution of the underlying pressure data. The concept is graphically represented with the aid of Figure 5-3 which shows ten autoignition elements relevant to a typical RON pressure trace.

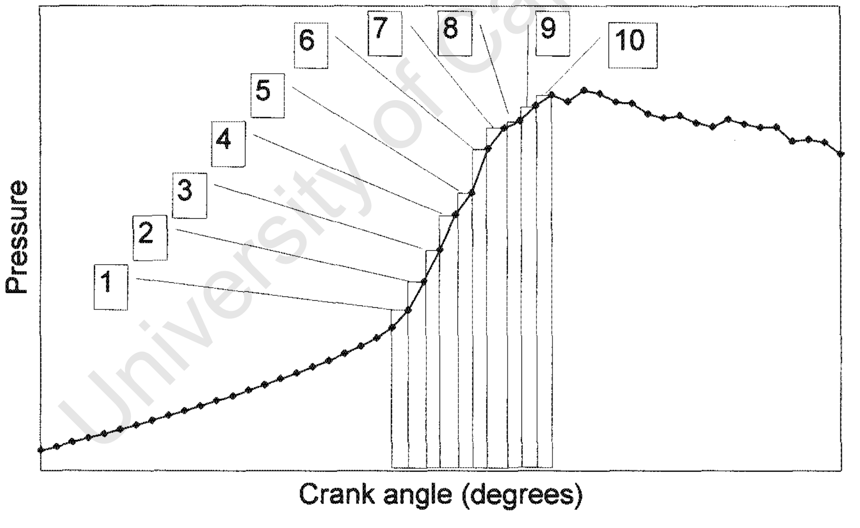

Figure 5-3: Illustration of the cascading autoignition concept, showing ten autoignition elements.

The calculation methodology and implementation of the interpretive model particular to this study is presented in the flow-diagram in Figure 5-4 and further details are provided in Appendix D.

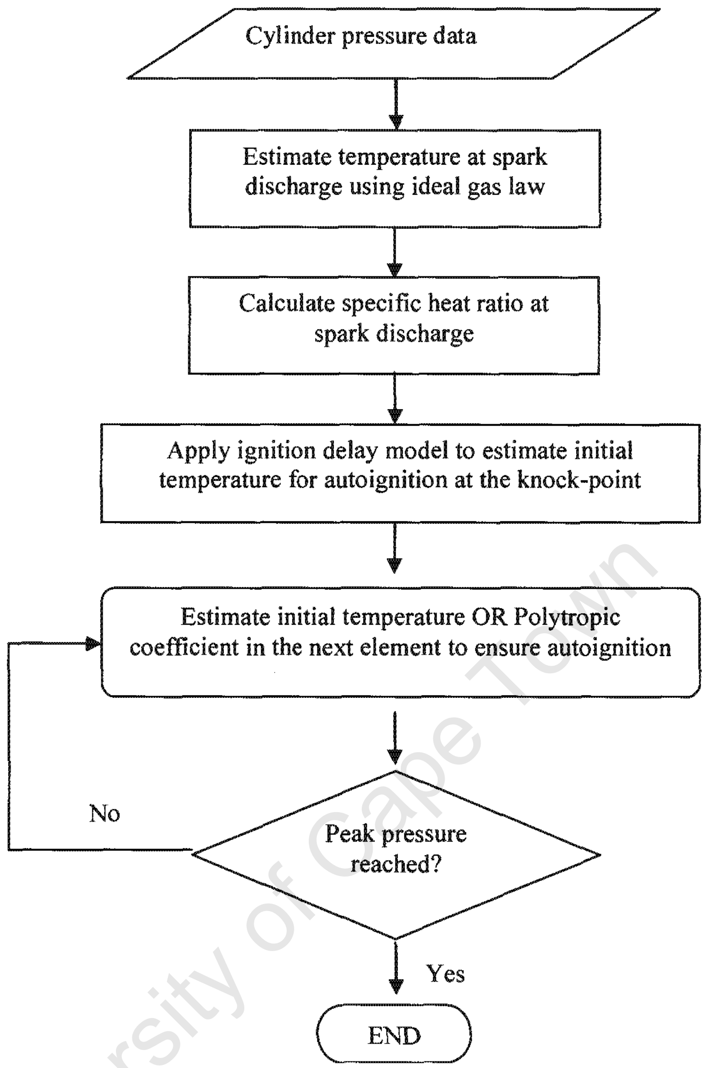

Figure 5-4: Flow diagram showing the implementation of the interpretive model

5.3.1. Initial temperature inhomogeneity concept

The inferred differences in initial temperatures (at IVC) required to sustain the cascading autoignition were quantified using the same ignition delay model as before. The results are given in Table 5-1 and suggest a variation of the initial temperature of about 40K for a PRF93 blend under RON conditions.

Table 5-1: Initial temperature required for cascading autoignition, based on data for a PRF93 blend at standard knock intensity under RON conditions.

Element number	Position ATDC (°CA)	Initial temperature (K)
1	10.2	452.9
2	10.4	450.3
3	10.6	447.4
4	10.8	444.1
5	11	440.4
6	11.2	437.0
7	11.4	433.7
8	11.6	430.5
9	11.8	427.6
10	12	424.8
11	12.2	422.3
12	12.4	419.8
13	12.6	417.7
14	12.8	415.6
15	13	413.5
16	13.2	411.7
17	13.4	409.8

To explore the sensibility of this predicted initial temperature difference, multi-dimensional modelling of the inlet process was performed using computational fluid dynamics (CFD). Results are contained in Appendix C and suggest that a variation of initial temperatures at IVC of 20 K may be more appropriate. Conceptually similar, although not directly applicable, is the work by Dec (2005) from Sandia who presented results of a multi-zone kinetic calculation. He found a thermal width at BDC of 20 K was required to ensure sequential autoignition of different temperature zones for HCCI applications.

5.3.2. Heat loss gradient concept

Under the alternative assumption of a thermally uniform mixture in the cylinder at the time of inlet valve closure, the temperature histories for all elements to autoignite can be calculated.

The first element to autoignite is assumed to be subject to adiabatic compression. The value for the polytropic coefficient of the final autoignition element is inferred to achieve the required autoignition timing.

Figure 5-5 shows the two distinct temperature histories of the first and last elements of the end-gas to autoignite for a PRF93 blend under RON conditions. These are termed "adiabatic" and "polytropic", respectively, on the graph and refer to autoignition at the knock-point and peak pressure points, respectively. The same graph also shows that the temperature calculation based on the ideal gas law appears closer to the adiabatic element temperature. The ideal gas calculation result is initially hotter than the adiabatic temperature, attributable to heat uptake early in the engine cycle. Significantly, the terminal temperature calculated from the ideal gas law is bordered by the temperatures in the two extreme calculation elements.

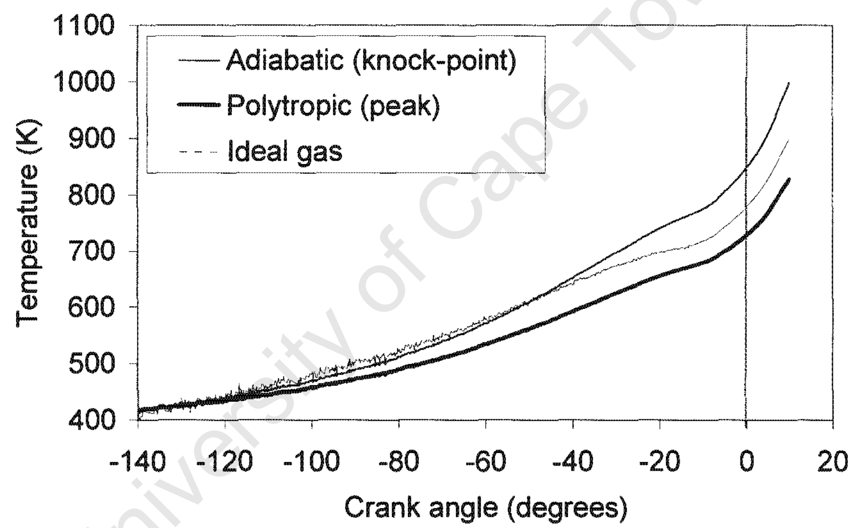

Figure 5-5: The effect of the polytropic coefficient on the end-gas temperature history.

Figure 5-6 shows the resultant ignition delay integral values for the autoignition at the knock-point and peak pressure, respectively, for the same data as in Figure 5-5. From the graph, the differences in temperature histories are evident, although both retain the features of the pressure development, including the knock-point, both share the same initial temperature (Estimated at 418 K but not shown on the graph).

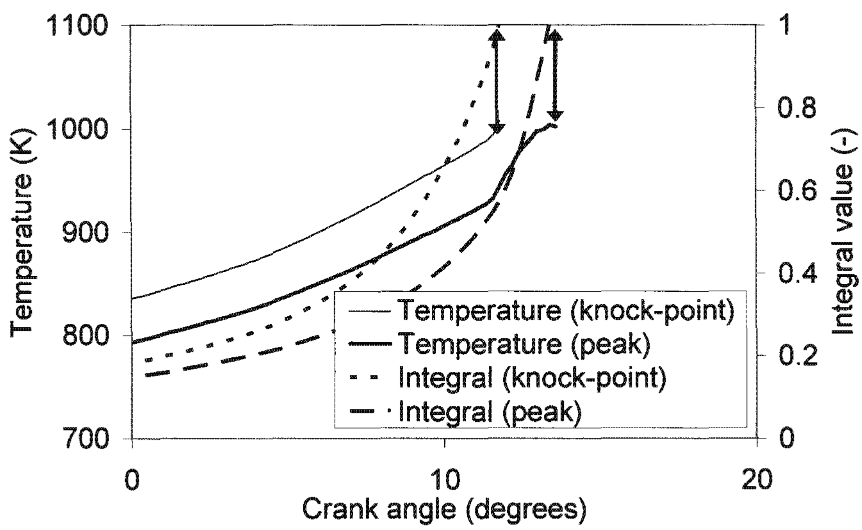

Figure 5-6: Two calculated temperature histories to coincide with autoignition at the knock-point and peak pressure. These are the first and last elements, respectively, to autoignite.

The values for the calculated polytropic coefficients for the PRF93 case, required to sustain the cascading autoignition in all of the autoignition elements, are given in Table 5-2. The size of the elements corresponds to the resolution of the underlying pressure data at 0.2 °CA. The table also contains the recorded pressures, calculated mass fraction burnt and calculated compression temperature for the individual elements. The effect of the heat loss is visible in the compression temperatures for the separate elements. Despite experiencing pressures that range from 30 to nearly 40 bar, the temperatures range between 974 and 1018 K.

The values in the table suggest that combustion is practically complete at peak pressure, with a mass fraction burnt of 99.4%. Subsequent to peak pressure, the mass fraction value approaches 100%, with some fluctuations present in the calculated values that stem from fluctuations in the underlying pressure data.

Table 5-2: Calculated values for the polytropic coefficient for autoignition elements corresponding to the angular pressure data recorded for a PRF93 blend under RON conditions at standard knock intensity.

Element number	Position ATDC (°CA)	Polytropic coefficient	Pressure (bar)	Final temperature in element (K)	Mass fraction burnt (%)
1	10.2	1.355	30.3	1018.8	66.6
2	10.4	1.351	32.0	1026.7	72.7
3	10.6	1.347	33.6	1031.5	78.3
4	10.8	1.343	35.2	1035.6	84.3
5	11	1.338	37.1	1039.7	91.2
6	11.2	1.334	37.3	1032.1	92.2
7	11.4	1.330	37.9	1027.9	94.8
8	11.6	1.326	38.4	1023.1	96.9
9	11.8	1.322	38.3	1014.7	96.6
10	12	1.319	38.6	1010.0	98.1
11	12.2	1.316	38.2	1001.5	97.1
12	12.4	1.313	38.7	999.2	99.4
13	12.6	1.311	38.2	990.4	97.7
14	12.8	1.309	38.2	986.0	98.3
15	13	1.306	38.5	983.2	99.9
16	13.2	1.304	37.8	974.7	97.6
17	13.4	1.302	38.3	973.9	100.0

For the remainder of the analyses, the combustion is assumed completed at peak pressure or a mass fraction burnt value greater than 99%. The results of this convention is shown in Figure 5-7, where the polytropic coefficient required for the sustained autoignition is shown as a function of the mass fraction burnt for the same PRF93 case used hitherto. The secondary X-axis is added to indicate the angular dependence of the polytropic coefficient.

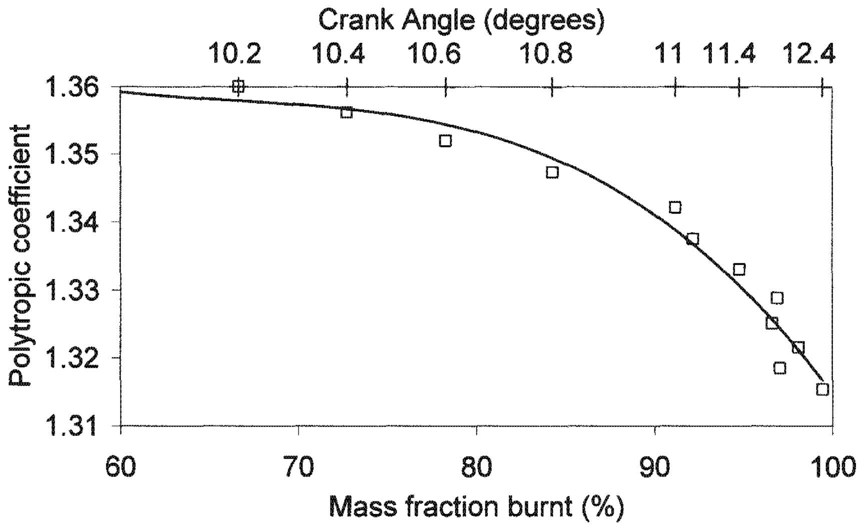

Figure 5-7: Polytropic coefficient required to sustain autoignition for a PRF93 blend tested under RON conditions, expressed as a function of mass fraction burnt.

5.3.3. Critical temperature gradient

The temperature distribution at the knock-point, resulting from the application of the heat loss gradient concept, was used to estimate the critical temperature gradient required for developing detonation. The estimation followed the description by Bradley et al. (2004), although the current formulation considers a discrete implementation of the equations.

The critical temperature gradient was calculated from the local sonic velocity, a, and the ignition delay gradient with respect to temperature:

$$\left(\frac{\Delta T}{\Delta r}\right)_c = a\left(\frac{\Delta T}{\Delta \tau}\right)_c \qquad \textbf{(5-6)}$$

The sonic velocity is calculated as:

$$a = \sqrt{\gamma RT} \qquad \textbf{(5-7)}$$

To find the required spatial dimension, the end-gas at knock-point is considered to be spherical, originating at an adiabatic centre and the radii and associated radial temperatures are the result of the individual polytropic compression progress. The ignition delay for each of the pressure and temperature points is calculated from the ignition delay model. The resultant quantities for the discrete calculation for PRF93 data under RON conditions are shown in Table 5-3.

Table 5-3: Critical and actual temperature gradients in the end-gas at the knock-point. Data shown for a PRF93 blend under RON conditions.

Radius (mm)	Temp. (K)	Ignition Delay (ms)	Sonic Velocity (m/s)	Ignition Delay Gradient (ms/K)	Critical Temp. Gradient (K/mm)	Actual Temperature Gradient (K/mm)	Dimension-less Temp. Gradient
r	T	τ	a	$\left(\frac{\Delta T}{\Delta \tau}\right)_c^{-1}$	$\left(\frac{\Delta T}{\Delta r}\right)_c$	$\left(\frac{\Delta T}{\Delta r}\right)_{actual}$	ξ
0.0	1000.5	1.06	572.8				
9.6	1000.9	1.30	572.9	0.052	0.034	0.4	12.6
11.7	993.1	1.58	570.7	0.041	0.043	4.3	101.1
13.3	984.7	1.96	568.2	0.054	0.033	6.2	188.4
14.6	975.2	2.54	565.5	0.038	0.047	10.0	215.0
14.8	966.8	2.63	563.0	0.021	0.083	27.3	328.9
15.2	958.7	2.89	560.7	0.031	0.057	21.9	382.4
15.5	951.1	3.12	558.5	0.014	0.128	35.0	274.4
15.5	944.3	3.09	556.5	0.010	0.178	44.5	249.7
15.7	938.0	3.26	554.6	0.005	0.386	19.1	49.6
15.5	932.3	3.14	552.9	0.013	0.134	19.2	142.9
15.9	926.8	3.41	551.3				

Although the current analysis is not as rigorous as that performed by the Leeds University researchers, the critical temperature gradient, calculated to be in the range of 0.03 to 0.13 K/mm, was in good agreement with temperature gradient reported by Bradley et al. (2004) for a 65:35 toluene:heptane blend under RON and MON conditions. The dimensionless temperature gradients are significantly higher than those required to sustain a developing detonation, suggesting that a *subsonic autoignitive deflagration* is the underlying mode of autoignition.

The calculated temperature gradients were also much greater than the intermediate temperature gradient of 12.5 K/mm previously found by Pan et al. (1998) relevant to a developing detonation.

5.3.4. Thermal boundary layer evaluation

Further evidence, corroborating the heat loss gradient concept, was found by viewing the instantaneous calculated temperature as a function of distance from the edge of the idealised, spherical end-gas region, next to the cylinder wall. This choice was made to enable comparison with published measurements and model results. The results are shown in Figure 5-8 for the knock-point instant. The temperature drop at about 2 mm from the edge was in fair qualitative agreement with measurements reported by Jenkin et al. (1996a) and corroborated by model results by Jenkin et al. (1996b). The ranges of the two y-axes have been set equal, although the absolute values are different due to differences in compression ratio and angular position between the current calculated and literature values.

The distance from the wall where the major temperature drop-off appears was also in agreement with the empirical prediction of the thermal boundary layer thickness using the correlations provided by Lydford-Pike and Heywood (1984).

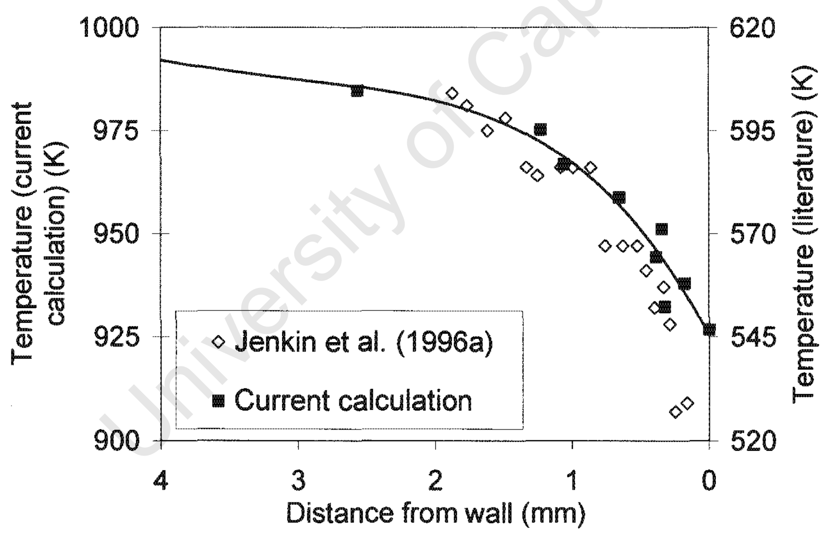

Figure 5-8: Radial temperatures at the knock-point for PRF93 in a spherically idealised end-gas. Experimental results from Jenkin et al. (1996a) are included for qualitative comparison.

5.4. *Setting the heat loss gradient*

To enable the geometric coupling between the flame propagation and autoignition development, there was a need to ascribe a geometric shape to the end-gas heat loss gradient.

The first challenge was to assess the expected location of the end-gas in the strongly swirling flow in the CFR engine. To this end, a transported flame model was developed and is presented in Appendix D. The model results suggest that the end-gas is always confined to a crescent shaped area almost diagonally across from the spark-plug. In this configuration, it is likely that autoignition may be initiated at adiabatic centres at the interface between the burnt and unburnt zones.

The heat loss gradient was found for each of the RON and MON configurations by estimating the polytropic coefficient required to sustain the cascading autoignition at low compression ratios (i.e. for the lowest octane number PRF blends with the largest mass fraction remaining at knock-point). The calculation was performed under the assumption of a thermally uniform mixture at IVC.

The results of the polytropic coefficient values are given in Figure 5-9 as a function of mass fraction burnt. The figure is further annotated with a conceptual geometry, suggesting that the adiabatic centres (with the highest polytropic coefficients) are in the in the vicinity of the flame front, whereas areas with the greatest heat loss (smallest polytropic coefficient) are found next to the cylinder walls. The figure further shows the remarkably similarity between RON and MON conditions when expressed as a function of mass fraction burnt.

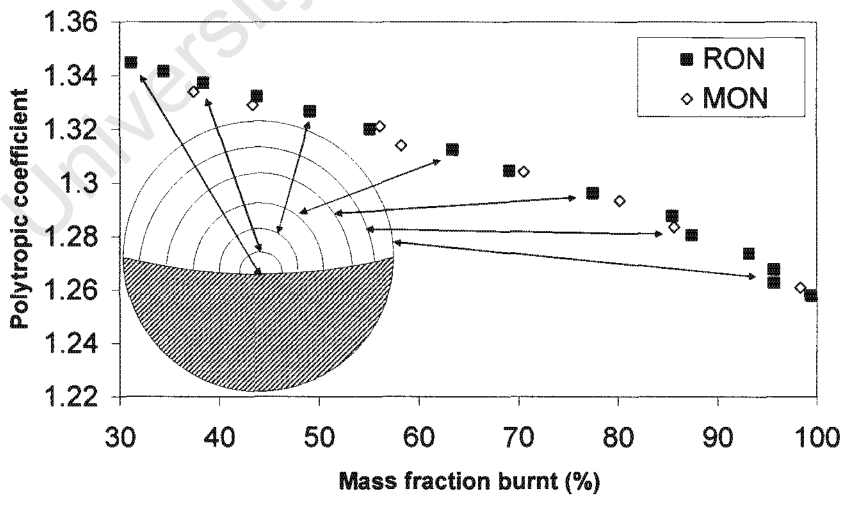

Figure 5-9: Polytropic coefficient expressed as a function of mass fraction burnt. The expected geometrical location in the engine end-gas is also annotated.

The heat loss gradient is expected to be a feature of the engine and should be independent of the fuel used. In the absence of autoignition, the normal flame propagation would also encounter the heat loss gradient. Evidence of what appears to be quenching of the flame was seen in the low compression ratio pressure development of PRF100 shown previously in Figure 4-10.

The heat loss gradient (polytropic coefficient values) dependence on mass fraction burnt was further expected to remain as the compression ratio was increased. With cognisance of the variation of the mass fraction burnt for different octane number fuels, it was expected that initial autoignition for higher octane number fuels (higher MFB at knock-point) would occur in non-adiabatic regions. For example, for a 100 RON fuel blend, the MFB at the knock-point is about 80 %, so the first autoignition is expected to occur in a region with a polytropic coefficient of about 1.3, according to the graph above.

5.5. Mapping to the pressure-temperature-time domain

When considering the matching between the autoignition characteristic and the temporal history of the end-gas in the engine, it is convenient to view the variables in the pressure-temperature domain. One of the first utilisations of this representation was by Rifkin and Walcutt (1957) who compared peak engine cycle points and lines of constant ignition delay from a RCM. A further extension to this concept was introduced by Gluckstein and Walcutt (1961) who considered the total pressure-temperature history in the engine.

The concept was explored and brought to fruition by Yates et al. (2005). In this view in the pressure-temperature domain, the fuel ignition delay character is shown as an iso-line of a chosen, constant ignition delay.

Figure 5-10 shows the result for the 4 ms ignition delay of the three blend components used in this study (Toluene, Iso-octane and n-Heptane). The parameters used in the ignition delay calculations can be found in Appendix A. In this view, components and blends with a greater resistance to autoignition are further away from the origin of the plot (i.e. higher pressures and temperatures required to attain the same ignition delay when compared to a more reactive blend). The graph also shows the variation in negative temperature coefficient behaviour for the different components in the range of temperatures and pressures considered relevant to the engine. Taking n-heptane as an example, the NTC region can be seen as a simultaneous reduction in pressure and temperature for the same ignition delay, whereas outside of the NTC region, a constant ignition delay is associated with a reduced temperature and increased pressure (or vice-versa).

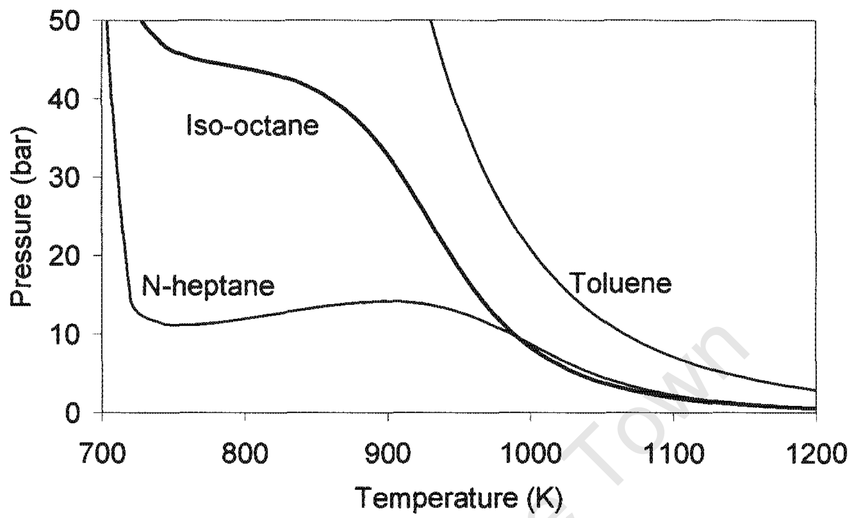

Figure 5-10: The 4 ms ignition delay for three pure components (Toluene, iso-octane and n-heptane).

Using the heat loss gradient introduced in 5-7, the end-gas histories of the different autoignition elements in the engine can be overlaid on (or mapped to) the ignition delay graph. An example is shown in Figure 5-11 for PRF93 under RON conditions at standard knock intensity. The end-gas history for the adiabatically compressed element is shown to experience higher temperatures for the shared pressure when compared to the final, polytropically compressed, element to autoignite.

The intersection of the end-gas trace and the ignition delay line provides a convenient mapping of the relative proximity of the end-gas in the engine to the NTC region of the fuel. The example in Figure 5-11 suggests that, for the final autoignition element, the slow-down due to the proximity to the NTC region was becoming more relevant.

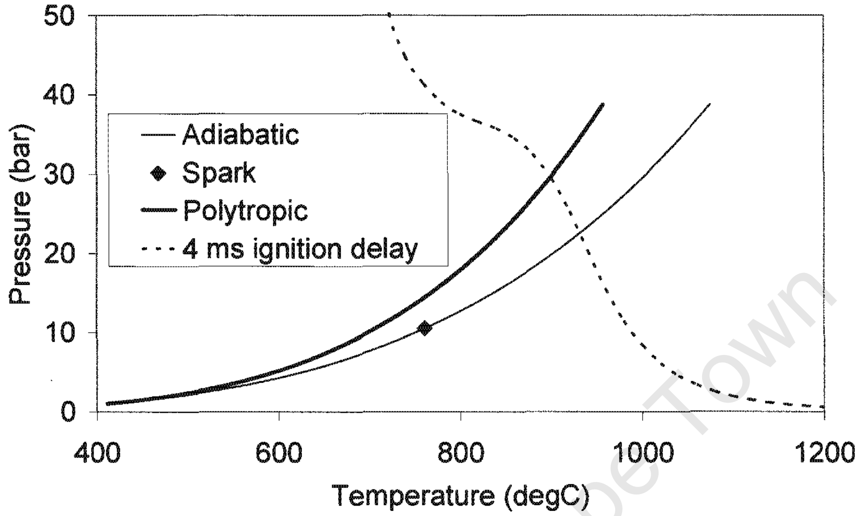

Figure 5-11: End-gas histories for the adiabatically and polytropically compressed elements in a cascading autoignition. Pressure data from a PRF93 blend tested under RON conditions at standard knock intensity.

The importance of choosing an appropriate time contour was explored with reference to Figure 5-12. In it, two different time contours are shown: a short time basis of 2 ms (which corresponds to 7 °CA at 600 rpm and is about a quarter of the typical combustion duration) and a long time basis of 8 ms (equal to the combustion duration). It is clear that the general conclusions about the relative relevance of the NTC region and mapping to the ignition delay characteristics do not change materially if the ignition delay contour time is chosen *within reason*. It must also be borne in mind that the graphical representation, including any conclusions drawn from it, does not detract from the rigour of the underlying ignition delay calculation.

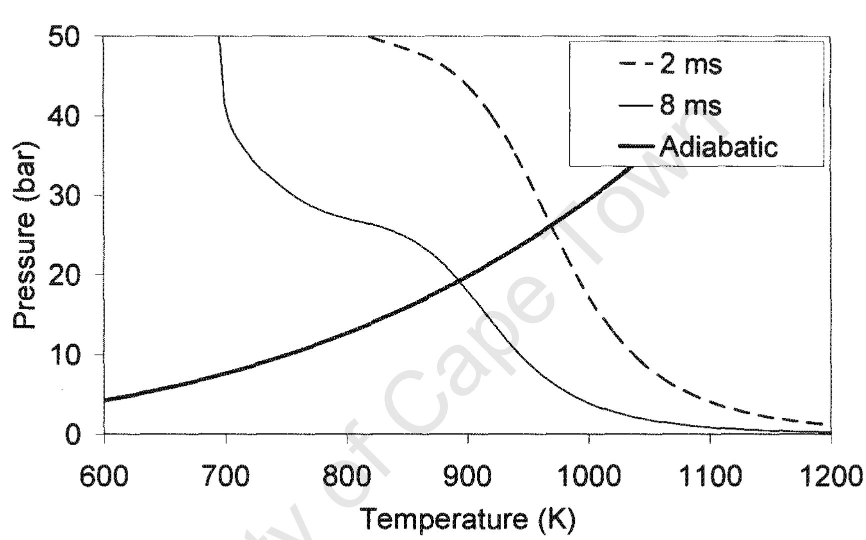

Figure 5-12: End-gas history for the adiabatic compressed element of a PRF93 blends under RON conditions at standard knock intensity. 2 and 8 ms ignition delay contours are shown.

Douaud and Eyzat (1978) suggested using a different time contour for the ignition delay for RON and MON, where the latter is 50% shorter due to the similarly faster engine speed. In the subsequent analysis however, only the 4 ms time contour will be used, which will allow for the back-to-back comparison for RON and MON test results.

The mapping of engine trace to the fuel autoignition delay characteristics provides a convenient vehicle to explore the effects of fuel composition and engine operating conditions on the interaction between the two during octane rating. The application of the modelling interpretation constitutes the next chapter.

6. Applications

This chapter explores selected applications of the model interpretation developed in the previous chapter.

6.1. Initial temperature estimation

Probably the biggest uncertainty surrounding the accurate prediction of knock and the application of autoignition models in engines is the knowledge of in-cylinder temperatures. There is as yet no simple, reliable and accurate technique to quantify temperatures in the internal combustion engine. The heat loss gradient concept was applied to estimate the initial temperature at IVC for each of the operating conditions and each of the fuels tested and for which results were presented in Section 4.3. Results of the initial temperatures to achieve the cascading autoignition are shown Figure 6-1 and Figure 6-2 for RON and MON test conditions, respectively.

For RON test conditions in Figure 6-1, the initial temperatures were found to generally increase with decreasing octane number. This is in part due to the reduced volumetric efficiency and increased levels of hot residual gasses at the lower compression ratios. Moreover, the absolute values of the initial temperatures are higher than the air inlet temperature of 51.7 ˚C (324.8 K), indicated by the broken line on the graph. This is attributable to heating of the inlet charge by engine hot surfaces during the gas exchange phase as well as mixing with hot residual gasses. The result cautions strongly against the use of inlet temperatures as estimates for the initial, in-cylinder temperatures.

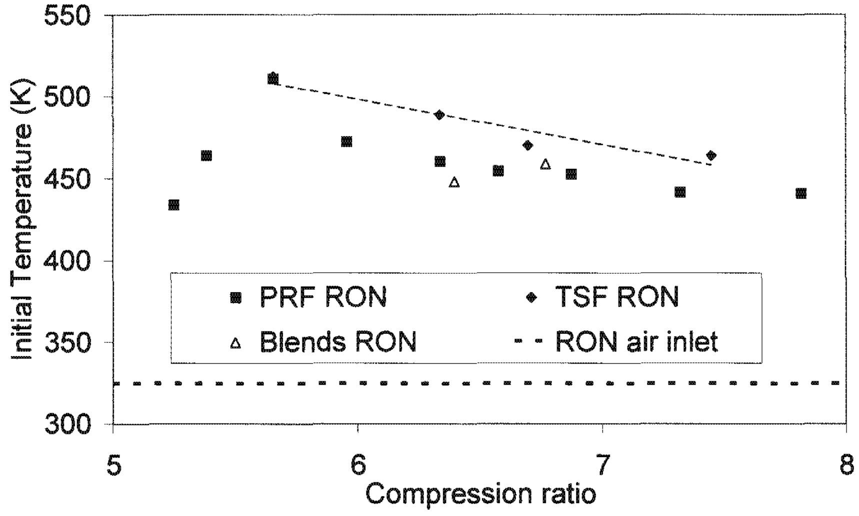

Figure 6-1: Estimated initial temperatures to ensure autoignition in adiabatic element at knock-point for all blends tested under RON conditions at standard knock intensity.

The initial temperature for the TSF blends can be seen to be consistently higher than that of PRF blends by a margin of about 20 to 40 K. Gasoline surrogate blends suggest initial temperatures very similar to that of PRF blends. The higher initial temperatures suggested for the TSF blends may originate from one of two sources:

- Toluene has a slightly higher normal boiling point and is thus expected to contribute less to the evaporative cooling of the inlet change. This effect was not taken into account during the modelling interpretation.
- The initial temperatures are inferred from the ignition delay model. It is conceded that any inaccuracies in the model will reflect as an apparent difference in the temperature required for autoignition, owing to the exponential temperature dependence.

Despite these reservations, the conclusions are believed to give a sufficiently accurate *relative* ranking of the fuel performance. One intriguing possibility is that the difference in initial temperature between the PRF and TSF blends can be ascribed to the lack of inlet air tuning (as highlighted in Section 3.1). The concept is tempting and would serve to align the initial temperatures of the different fuel blends, but was not explored further.

MON test results, shown in Figure 6-2, suggest similar trends as for RON, with similarly increasing initial temperatures with decreasing octane numbers. Again the initial temperatures for TSF blends are consistently higher than that of PRF blends with the thermal behaviour of the gasoline surrogate blends somewhere between the two. All initial temperatures are consistently higher than the inlet mixture temperature of 149 °C applicable to the MON test, shown as the broken line on the graph.

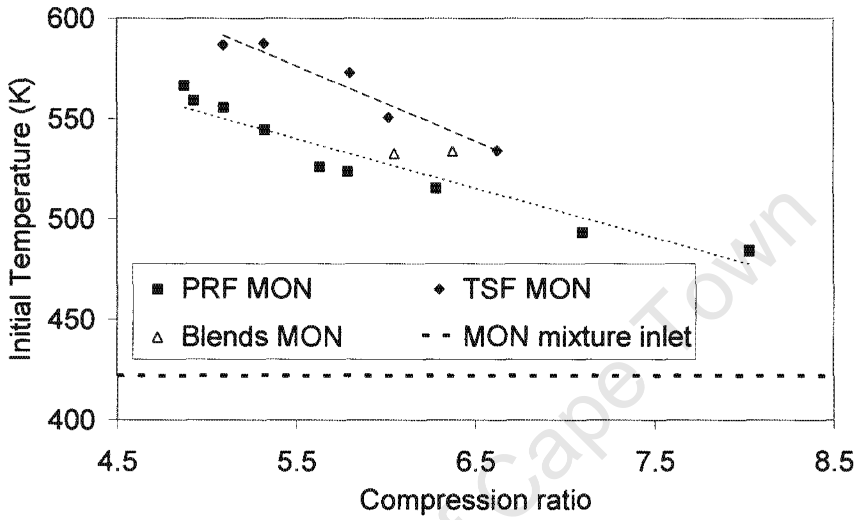

Figure 6-2: Estimated initial temperatures to ensure autoignition in adiabatic element at knock-point for all blends tested under MON conditions at standard knock intensity.

Despite MON having an inlet mixture temperature of nearly 100 K higher than the air temperature applicable to RON, the comparative results, given in Figure 6-3 suggest that the difference in initial temperature is only about 50 K. The reason is likely that the uptake of the mixture entering the engine under MON conditions is less than for RON due to the diminished driving force between the hot engine surfaces and the hotter inlet mixture. In addition there is a shorter contact time due to the higher engine speed. The typical engine component temperatures have been shown by Yates (1988) to typically be in the range of 130 to 190 °C (403 to 463 K), but this can be expected to be even higher due to the antiquated design of the cooling passages on the CFR engine and low flow velocities, and by extension heat transfer, of the evaporative cooling system.

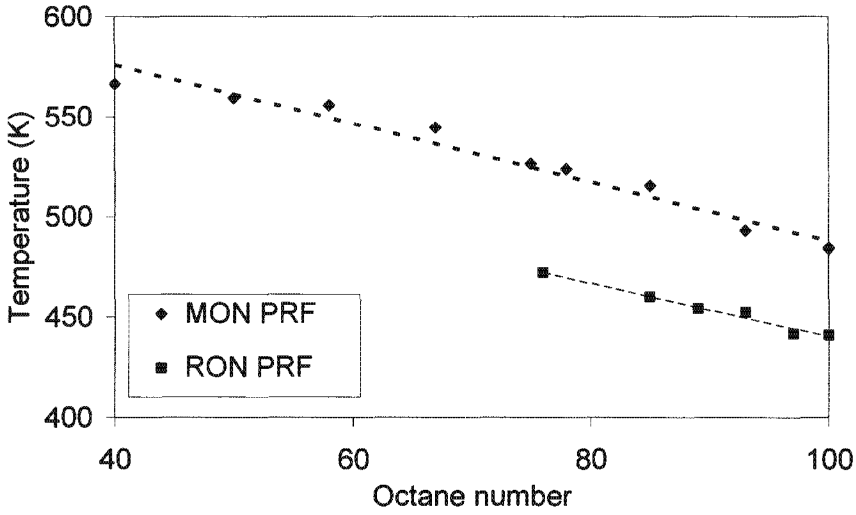

Figure 6-3: Comparative estimated initial temperatures of PRF blends under RON and MON conditions at standard knock intensity.

Dimpelfield and Foster (1986) found that end-gas compression subject to adiabatic compression needed to be further enhanced for the best comparison between measured and observed knock. It was conceded by them that the temperature correction may be compensating for inaccuracies in the reaction mechanism, but the current initial temperature estimation suggests another possibility, which is that Dimpelfield and Foster may have used an inappropriate initial temperature, especially if this was based on inlet conditions only.

6.2. Cascading autoignition applications

6.2.1. Non-standard knock intensity

To assess the robustness of the proposed heat loss gradient, the calculated autoignition position in degrees crank angle was plotted against the measured position. The latter quantity was then inferred from the measured pressure development, assuming a true cascading autoignition. The calculated position is the result of ignition delay model application when applied to the heat loss gradient proposed in Section 5.4.

Calculated autoignition positions are shown in Figure 6-4 for a PRF93 blend under RON conditions for two values of relative air-fuel ratio: λ=0.9 that gave standard knock intensity and λ=1.0 that gave a sub-standard knock intensity of 13. Given the calculation resolution of 0.2 °CA, this should be considered the accuracy of the estimated position and is included as an error bar on the parity line. The results clearly show that both relative air-fuel ratios exhibit cascading autoignition behaviour. The previously reported differences in pressure rise rate values (and by extension the knock intensity) are attributable to the delayed onset of autoignition and reduced mass participating in the cascading autoignition.

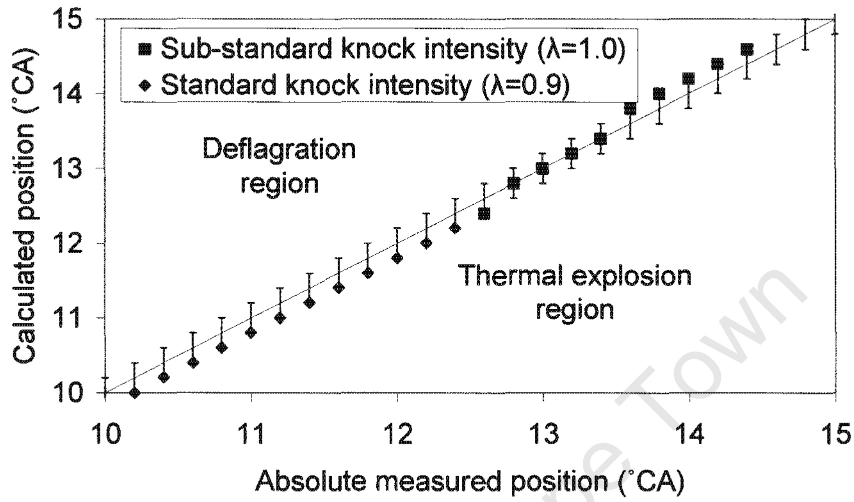

Figure 6-4: Calculated versus measured autoignition position for a PRF93 blend. Standard and sub-standard knock intensity conditions are shown.

The graph above can also be used to qualitatively assess the tendency to revert to either deflagration or a thermal explosion mode of autoignition. If the calculated autoignition point for any fuel is *earlier* than the measured point (i.e. below the parity line) the risk exists for a thermal explosion to occur. For a calculated autoignition point *later* than the measured position, deflagration autoignition is likely.

6.2.2. Different octane fuel blends

The behaviour of different octane PRF blends, as well as non-PRF fuels under standard knock intensity, was assessed using the methodology described above. The results for PRF blends tested under MON conditions are given in Figure 6-5. The calculation accuracy error bar is excluded for the sake of viewing clarity. It can be seen that most of the high octane fuels match the parity line exceedingly well. Low octane PRF blends, however predict an autoignition position earlier than the expected values, suggesting thermal explosion type behaviour. These deviations for the PRF58 and lower are clearly visible as pressure fluctuations (see Figure 4-23).

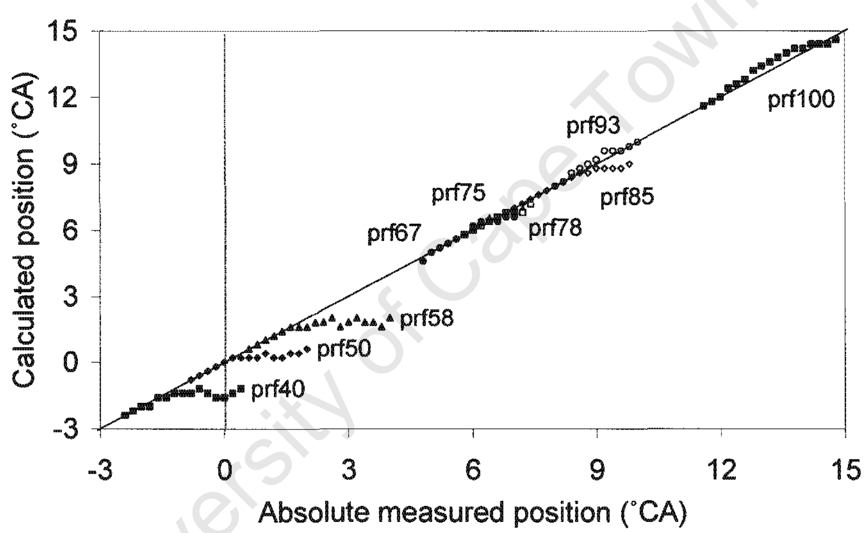

Figure 6-5: Calculated versus measured autoignition position for all PRF blends subject to heat loss gradient. Results are shown for MON test condition.

The same analysis was applied to non-PRF blends and these results are shown in Figure 6-6. All of these blends suggest an initial tracking of the parity line, followed by the eventual autoignition timing earlier than measured. Although this would suggest the tendency towards a thermal explosion, the lack of pressure fluctuations was ascribed to the presence of toluene in the blends. The diminished rate of heat release of the toluene fails to produce a high enough local pressure to cause pressure fluctuations.

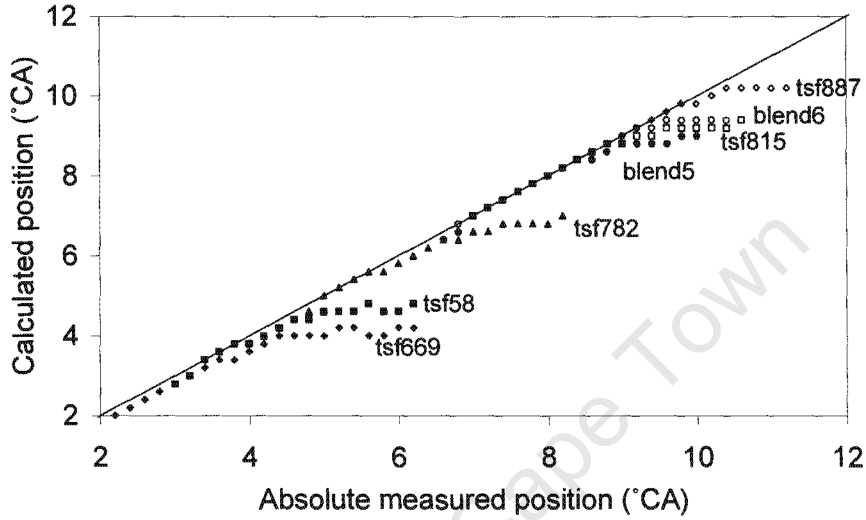

Figure 6-6: Calculated versus measured autoignition timing for non-PRF blends subject to heat loss gradient. Results are shown for the MON test condition.

6.3. Engine mapping to autoignition

6.3.1. High octane PRF blends

The difference between the RON and MON rating method can be illuminated by considering how the two test engine conditions map to the ignition delay character of a fuel. Figure 6-7 shows the results for a PRF93 fuel blend. The two engine traces for each of the RON and MON conditions signifies the initial and terminal autoignition elements (as in Figure 5-11): all of the autoignition events can be considered to be contained between these two lines. The higher initial temperature and consistently lower pressure for MON is apparent, when compared with RON. For the PRF93 example, both RON and MON conditions are contained in the high temperature regime and the NTC behaviour is not expected to feature strongly during the octane rating.

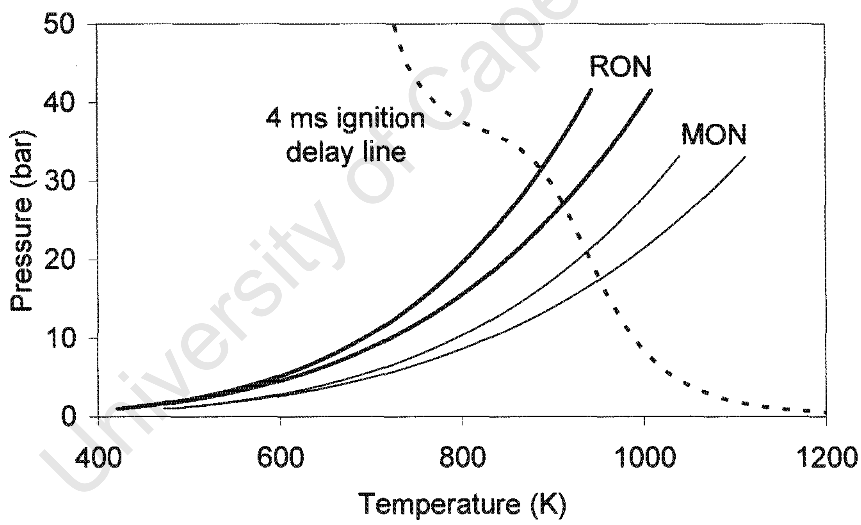

Figure 6-7: Engine pressure trace mapping to ignition delay for PRF93. RON and MON operating conditions are compared. 4 ms ignition delay shown as dotted line. The initial and terminal element traces are shown for each operating condition.

6.3.2. Low octane PRF blends

A similar analysis was performed for the lower extreme of the octane scale. The results for PRF40, with its known strong NTC character, are shown in Figure 6-8. From the graph, the RON test condition can clearly be seen to map to the NTC region of the fuel ignition delay character, whereas the MON test condition remains in the high temperature regime.

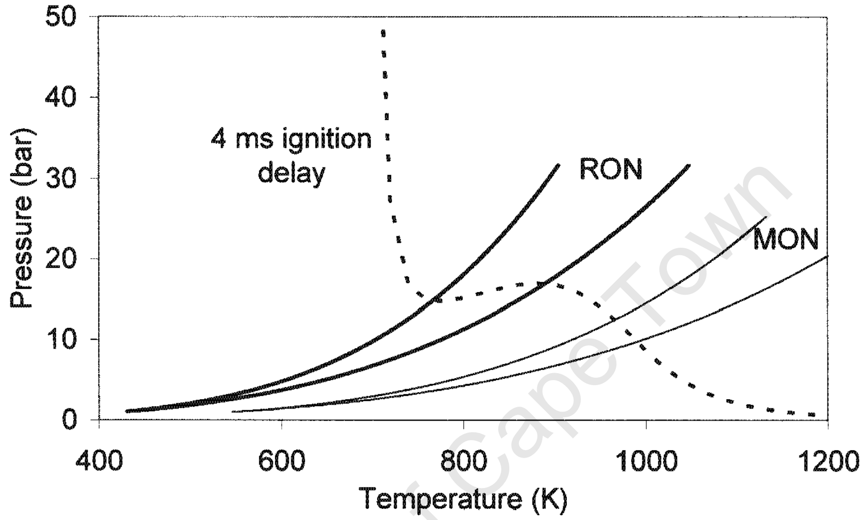

Figure 6-8: Engine trace mapping to 4 ms ignition delay line for PRF40. RON and MON operating conditions are compared. The initial and terminal element traces are shown for each operating condition.

This behaviour explains the distinctly different pressure fluctuation behaviour of the RON and MON tests for the low octane PRF:

- MON remains in the high temperature regime, moving to shorter ignition delays for higher temperatures as the autoignition progresses. This will expedite the autoignition reactions and possibly cause a rapid succession of autoignition reaction and strong pressure fluctuation observed.
- The RON operated around the NTC region where increasing temperature causes longer autoignition delays and a postponement of the subsequent autoignition reactions.

6.3.3. Non-PRF blends

Since the presence of the NTC behaviour for the PRF blends is entrenched in the guide curve of the octane rating scale, the different NTC character of non-PRF fuel blends warranted further investigation. The behaviour was explored with the aid of the TSF934 (TSF815 in MON nomenclature) blend comprising of 74:26 toluene:n-heptane on a liquid volume basis. The results of the mapping are shown in Figure 6-9 for RON and MON conditions. The graph reveals a strong NTC character associated with the presence of n-heptane, although the engine operation seems to be constrained to the high temperature region of the fuel ignition delay characteristic.

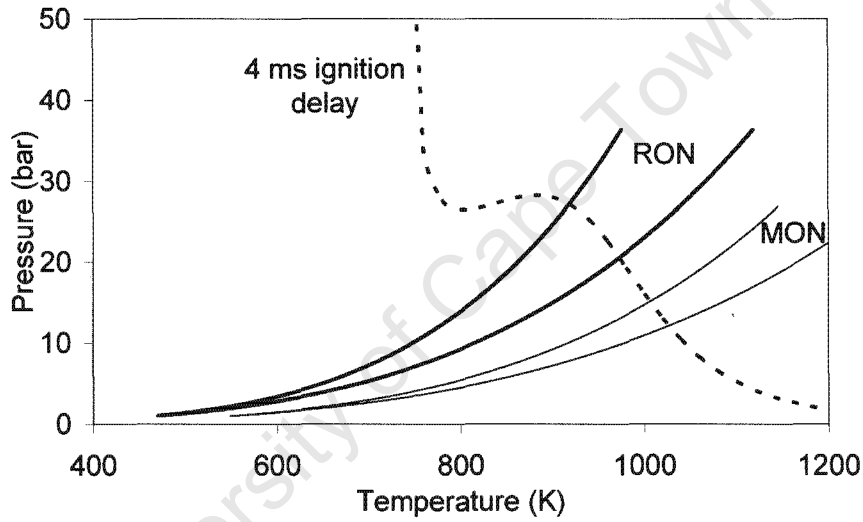

Figure 6-9: RON and MON test condition mapping to the 4 ms ignition delay line for TSF934/TSF815. The initial and terminal element traces are shown for each operating condition.

Since the TSF934 is matched to a PRF93 during octane rating, the comparative engine mapping is shown in Figure 6-10. The two engine traces for each fuel is again indicative of the first and last elements to autoignite. It is clear that both the PRF and TSF blends are confined to the high temperature region of the autoignition delay scale and overlap partially. Note that the differences are attributable, firstly to the different estimated initial temperatures and secondly to the different compression ratios used when the two fuels were tested. (Recall that the compression ratio adjustment was allowed in favour of inlet air temperature adjustment.)

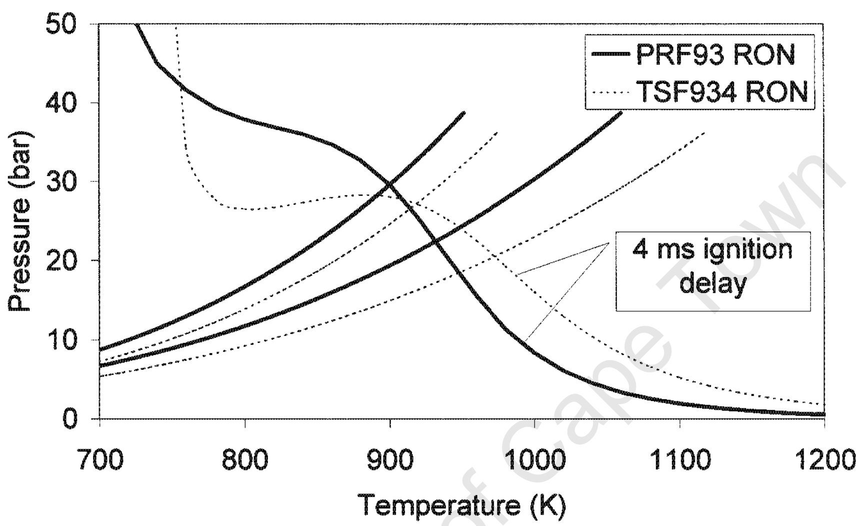

Figure 6-10: Mapping to the 4 ms ignition delay for the TSF934 blend and PRF93, both under RON conditions. The initial and terminal element traces are shown for each operating condition.

Perhaps more insightful is the comparison of matching the TSF blend to the respective PRF blends under both RON and MON conditions. For the sake of clarity, Figure 6-11 shows only the autoignition mapping associated with the knock-point and the 4 ms ignition delay line of the three fuel blends under consideration. Each of the four mapping points is shown on the graph, according to the legend:

- PR = PRF93 RON operating condition
- TR = TSF934 RON operating condition
- PM = PRF81 MON operating condition
- TM = TSF815 MON operating condition

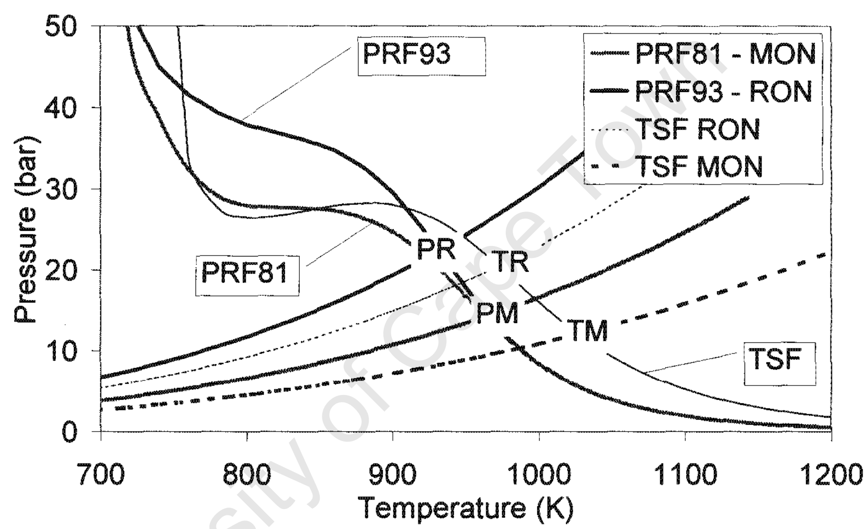

Figure 6-11: TSF blend compared to PRF blends for RON and MON rating. Only the initial element trace is shown for each operating condition.

From the graph above it can be seen that the high and low PRF blends, used to rate the TSF blends, exhibit distinctly different NTC behaviour. Differences in NTC behaviour between the reference and sample fuels are thought to be central to the phenomenon of fuel sensitivity, as alluded to by Yates et al. (2005). The preceding graph suggests that the difference in NTC behaviour may actually be more pronounced in the RON operating region than in the MON and is contrary to literature references on the subject of the chemical origins of octane sensitivity. Further exploration of this subject falls beyond the scope of the present study.

6.4. *Predictive modelling*

Part of the original aim of the thesis was to investigate the feasibility of a predictive model of the CFR engine that captures the essence of the interaction between the fuel autoignition and the engine operating features.

To explore the basis for such a predictive model, a two-zone thermodynamic engine model was developed and utilised to predict the pressures and temperatures in the CFR engine under knocking and non-knocking combustion. The model employed current best practices and further details are given in Appendix D. The model considers the normal combustion heat release and calculates, in addition, the autoignition development for five autoignition elements in the end-gas. Each of the elements was assumed to contain one fifth of the unreacted mass at any time during the calculation and each underwent a unique temperature history due to different polytropic coefficients (due in turn to the application of the heat loss gradient). The autoignition development was monitored by applying the ignition delay model used throughout the study. When autoignition occurred in any one of the elements, there was an instantaneous reaction from the unburnt, end-gas state to the equilibrium burnt gas state. The reaction was however limited to the mass contained in the element reaching the point of autoignition. By the application of an overall energy and mass balance, compression heating of the remaining elements was achieved, leading to the acceleration of the reactions in the remaining autoignition elements.

Three alternatives for the heat loss gradient are presented to ensure consistency with the observations so far:

- Small, indicating a zero gradient, causing the near-simultaneous autoignition of all the elements, similar in nature to a thermal explosion.
- Intermediate, causing a cascading autoignition.
- Large, causing a *very* slow autoignitive deflagration

The result of the predictive model is shown in Figure 6-12 and includes the predicted normal combustion pressure development at a calculation resolution of 1 ˚CA (i.e. no autoignition whatsoever). For a large temperature gradient, the pressure development due to the autoignition heat release is very similar to the normal combustion, as is apparent from the graph. For the large temperature gradient, a "misfire" (failure to autoignite) is visible for the last element, by which time the piston is already moving downwards. The smaller the temperature gradient gets, the more rapid the heat release, since autoignition events are much closer spaced. In fact, for the smallest temperature gradient, autoignition occurs simultaneously in all of the elements.

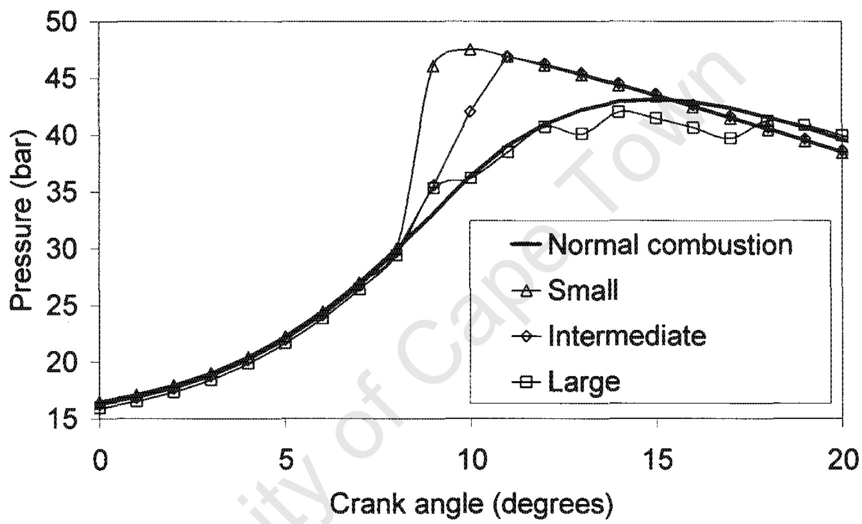

Figure 6-12: Modelled pressure development for normal combustion and cascading autoignition with small, intermediate and large temperature gradients.

To assess the prospects of applying the predictive model to actually replicate the operation of the knock measurement equipment on the CFR engine, the pressure rise rate values were calculated from the predicted pressure. Figure 6-13 shows typical results for the example given above and it is clear that the theoretical prediction was able to distinguish between normal combustion and autoignition propagation. Moreover, the effect of the heat loss gradient is clearly visible, since the difference between rapid and moderate autoignition is evident in the peak values of the pressure rise rate results.

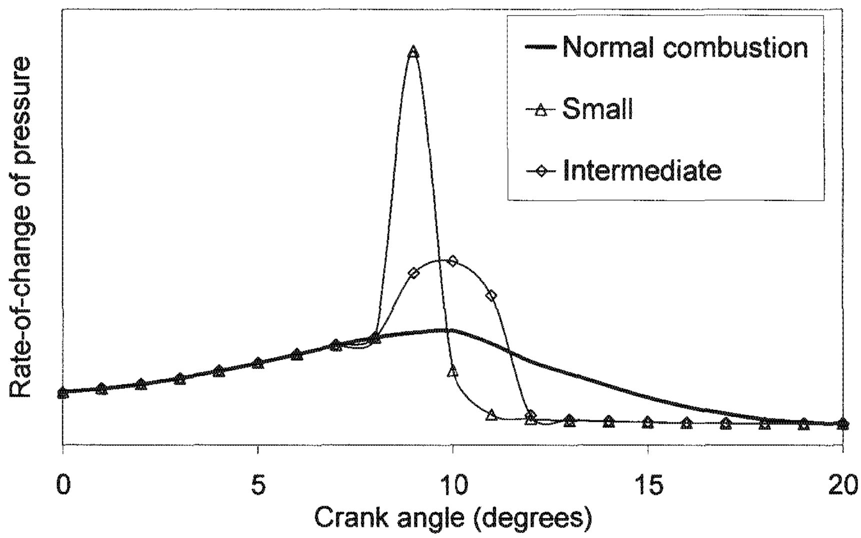

Figure 6-13: Typical pressure rise rate prediction. Normal combustion is compared to autoignition with small and intermediate heat loss gradients.

The predictive model was qualitatively compared to the pressure development measured in the CFR engine for a PRF93 blend under RON conditions. The comparison to measurements is shown in Figure 6-14, with excellent agreement visible. It must be noted that the flame propagation parameters in the model were adjusted to match the pressure during the normal combustion part, but the autoignition timing was calculated without a-priori knowledge of the pressure development. The only inputs for this part of the calculation were the fuel's ignition delay parameters and the previously derived heat loss gradient.

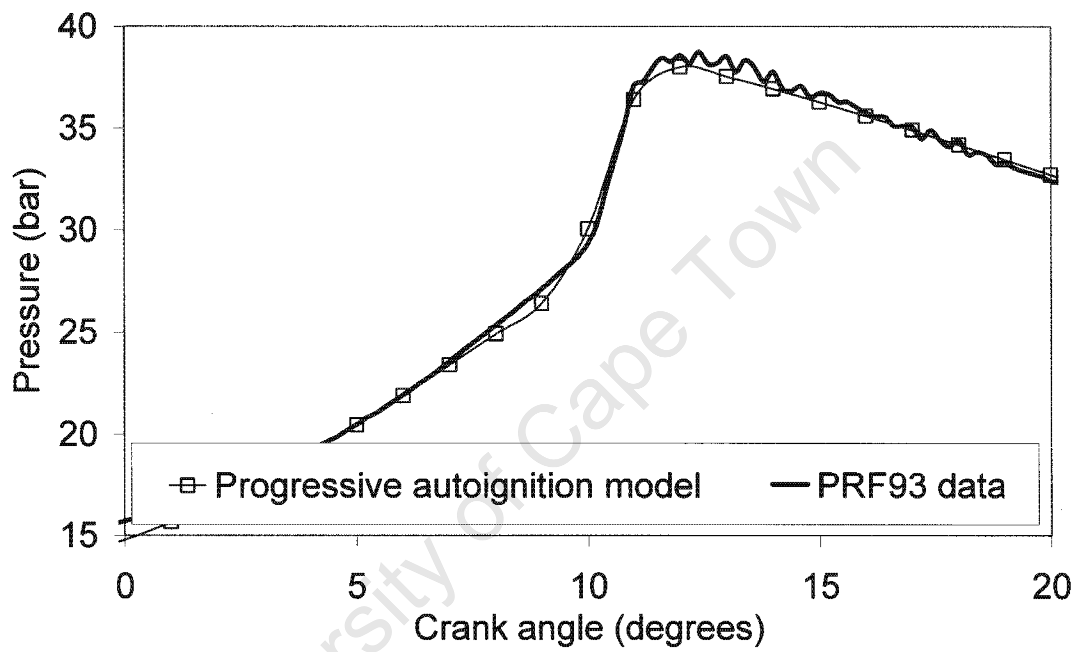

Figure 6-14: Modelled cascading autoignition compared to a measured pressure trace for PRF93 under RON conditions.

7. Conclusions and recommendations

This chapter concludes the thesis and provides a summary and recommendations for further work.

The measurements performed on the CFR engine allowed for the following conclusions to be drawn:

- All fuels tested during this study, including non-PRF blends, were confirmed to exhibit the peculiar pressure development under knocking operation in the CFR engine as was reported previously for PRF blends. This pressure development is characterised by the presence of a knock-point, where the pressure trace increases abruptly.
- The knock-point phenomenon was found to be present for both RON and MON test conditions over the range of octane numbers from 40 to 100. It was also confirmed to be present at sub-critical knock intensity.
- The operation of the ASTM knock measurement system was studied in detail and the design was found to filter out pressure fluctuations, characteristic of knock in a modern spark ignition engine. This feature was a deliberate effort to replicate the operation of the original bounding pin device with an electronic system.
- The operation of the knockmeter was replicated using recorded pressure data and applying the prescribed conditioning (applying a low pass filter to the rate-of-change of the pressure data). The results suggested that the absolute value of the pressure rise rate, defining the "standard knock intensity threshold" varied for different for octane number fuels and were different for RON and MON test conditions. The observation serves to explain the required adjustment to the METER setting on the knock measurement system, which serves as a scaling factor to produce a consistent output to the knockmeter (a voltmeter with a fixed range). This understanding addresses the objectives stated in Chapter 1.
- The basis for a digital knock measurement system was proposed, wherein the pressure data from the CFR engine can be used to generate the absolute values for the pressure rise rate information that defines the standard knock intensity at each octane level.
- It was found that the knock measurement system responded to a bulk heat release due to the autoignition of a significant fraction of the trapped mass (much greater than modern production engines). This pressure development was found to be best described by a cascading autoignition in an inhomogeneous end-gas. The cascading autoignition is

conceptually similar to the subsonic autoignitive deflagration mode of autoignition, but the distinction is proposed since the current analysis is not as rigorous as that of the originators of the three modes of autoignition. This clearly speaks to the problem statement and reaches the objectives of the research.

The application of a theoretical model to enable the interpretation of the observed phenomena yielded the following conclusions:

- A cascading autoignition was shown to be sustainable over the full spectrum of operating conditions in the CFR engine (both RON and MON over the full octane number scale) under the proviso of an inhomogeneous end-gas. The inhomogeneities were provided by enforcing a heat loss gradient. This heat loss gradient led to variations in end-gas histories in different elements of the end-gas, giving rise to variations in different autoignition development. These differences are central to the timing of the cascading autoignition.
- The overall ignition delay model gave reasonable results throughout the thesis and served to align the observations with fuel autoignition information.
- The extent of the pressure fluctuations at standard knock intensity, quantified by the maximum negative value of the third derivative of pressure, depended on the chemical composition of the fuel. It was found that the blends containing toluene exhibit smaller pressure fluctuations. This was attributed to the lower autoignition heat release rate known to characterise aromatics.
- The mapping of the engine pressure and temperature conditions to the autoignition delay behaviour revealed that the role of the NTC behaviour varied between RON and MON test conditions, as well as between different octane number fuels, as well as between fuels with different compositions. It was confirmed that differences in NTC behaviour between PRF blends and a sample fuels and is likely to explain the fuel's octane sensitivity.
- The role of differences in NTC behaviour appeared to be more prevalent under RON conditions than MON. This observation was contrary to the general wisdom on the role of NTC behaviour in determining octane sensitivity, although subject was not fully explored.

General conclusions that can be drawn include:

- The comparatively low compression ratio and large clearance volume under which the CFR engine operates is likely the reason for the lack of strong, potentially damaging, pressure fluctuations present under knocking operation. This serves to explain why the CFR engine can be run throughout the world under constant knocking conditions without sustaining damage.

- It was apparent that the knock resistance expected in production engines (which use control strategies based of pressure fluctuations) may be misrepresented by octane number measurement (that clearly does not consider pressure fluctuations).
- The CFR engine measurements were used in conjunction with the ignition delay model to estimate the temperatures at IVC. The results suggest that the initial temperatures were significantly higher than the inlet temperatures. Moreover, the difference in initial temperatures for RON and MON conditions were closer than the inlet conditions suggested. Both features are attributable to heat exchange with hot engine surfaces during the gas-exchange process, as well as residual gas mixing, and warn against the use of inlet temperature conditions for initial condition estimation.
- Researchers who equated the temperature at IVC with the inlet temperature would be led to infer, erroneously, that the incipient point of autoignition in the CFR engine occurs near the peak pressure. The recognition that the first manifestation of autoignition occurs relatively early in the combustion process (at lower pressure), in combination with the enhanced initial temperature, leads to a very different conclusion regarding the prevailing engine conditions at standard knock intensity.
- The basis for a predictive model was presented that described the interaction between the autoignition of the fuel and the inhomogeneous end-gas. The model proved able to predict all three modes of autoignition, depending on the temperature gradient in the end-gas.
- The cascading autoignition prediction, using the derived temperature gradient, was found to give a good quantitative comparison to measurements on the CFR engine at standard knock intensity for both RON and MON over the full octane scale.

Based on the conclusions, the following recommendations can be made:

- The continued study of chemical kinetic models, both detailed and reduced, is recommended. This is particularly relevant to the understanding and quantification of blending interaction between different types of molecules.
- The need for reliable autoignition data is undeniable. The continued pursuit of devices that are able to measure overall ignition delay times over a range of engine-relevant pressure and temperature is strongly recommended. Ignition delay data will serve, not

only for the verification of chemical kinetic models, but can also be parameterised for the ignition delay-type model used during this thesis.

- Given the prevalence of cool-flame heat release for paraffinic molecules, it is appropriate to recommend the quantification of the timing and magnitude of thereof to enable the further refinement of the autoignition delay model when applied in a predictive manner. This is particularly relevant if one considers the application of the ignition delay concepts to HCCI engine operation where the cool flame heat release is not insignificant.
- The role of autoignition characteristics, especially the difference in NTC behaviour of different fuels and the relation with fuel octane sensitivity, warrants further investigation.
- The chemical foundation for differences in the autoignition heat release rates, especially for aromatics, begs a chemical kinetics explanation and quantification, again with a view to enhancing the interpretative and predictive modelling abilities for octane numbers.

References

Adbel-Gayed, Bradley, Lung (1989) *Combustion and Flame* Vol. 76, pp. 213-218. 2-3

American Society for Testing Materials (1948) *ASTM Manual of Engine Test Methods for Rating Fuels* Philadelphia, PA: American Society for Testing Materials 2-16

Arendse (2004) *Speech by Arendse during the budget vote debate of the department of environmental affairs and tourism* http://www.anc.org.za/ancdocs/speeches/2004/sp0621b.html 1-2

Arrigoni, V., Cornetti, G.M., Spallanzani, G., Calvi, F. and Tontodonati, A. (1974) *High Speed Knock in S.I. Engines* SAE paper 741056. 2-24

ASTM (1973) *1973-74 ASTM Manual for Rating Motor, Diesel and Aviation Fuels* Philadelphia, American Society for Testing Materials 2-18

ASTM (1978) *1978 Annual Book of ASTM Standards, Part 47, Test Methods for Rating Motor, Diesel and Aviation Fuels* Philadelphia, American Society for Testing Materials 2-18

ASTM (2004a) *Standard Test Method for Research Octane Number of a Spark-Ignition Engine Fuel, ASTM Designation: D 2699-04a* ASTM International .... passim

ASTM (2004b) *Standard Test Method for Motor Octane Number of a Spark-Ignition Engine Fuel, ASTM Designation: D 2700-04a* ASTM International 2-20, 2-21, 3-2

Barton, R.K., Lestz, S.S. and Duke, L.C. (1970) *Knock intensity as a function of rate of pressure change* SAE paper 700061 3-5

Bood et al. (1950) *American Petroleum Institute Research Project 45: Eleventh annual report* Philadelphia, American Society for Testing Materials *1-3*

Bradley, D., Kalghatgi, G.T. and Golombok, M. (1996b) *Fuel blend and mixture strength effects on autoignition heat release rates and knock intensity in S.I. engines* SAE paper 962105 2-14, 2-25

Bradley, D., Kalghatgi, G.T., Golombok, M. and Yeo, J (1996a) 'Heat release rates due to autoignition, and their relationship to knock intensity in spark ignition engines' *Twenty-Sixth Symposium (International) on Combustion,* The Combustion Institute, 2653-2660. 2-4

Bradley, D., Morley, C., Gu, X.J. and Emerson, D.R. (2002) *Amplified pressure waves during autoignition: relevance to CAI engines* SAE paper 2002-01-2868 2-5

Bradley, D., Morley, C., Walmsley, H. (2004) *Relevance of Research and Motor Octane numbers to the prediction of engine auto-ignition* SAE paper 2004-01-1970 .. 2-25, 5-11, 5-12

Broeze, J.J. (unknown) *Combustion in piston engine.* Haarlem, De Technische Uitgeverij H. Stam N.V. 2-24

Burluka, A.A., Liu, K., Sheppard, C.G.W., Smallbone A.J. and Woolley, R. (2004) *The Influence of Simulated Residual and NO Concentrations on Knock Onset for PRFs and Gasolines* SAE paper 2004-01-2998.......... 2-7, 2-12

By, A., Kempinski, B. and Rife, J.M. (1981) *Knock in spark ignition engines* SAE paper 810147 2-4

Checkel, M.D. and Dale, J.D. (1986) *Testing a third derivative knock indicator on a production engine* SAE paper 861216. 4-18

Chomiak, J. and Skold, J. (1995) *Fuel effects on energy release and knock parameters in a SI engine* SAE paper 952404 2-5

Coetzer, R.L.J., Rossouw, R., Swarts, A and Viljoen, C.L. (2006) 'The estimation of knock-points of fuels by a weighted mean square error criterion' Due for publication in *Fuel*......... *3-5*

Corner, E.S. and Cunningham, A.R. (1971) *Value of high octane number unleaded gasoline* [ACS division of Petroleum Chemistry Inc. Los Angeles meeting, March-April 1971] 1-3

Dec, J.E. (2005) *Understanding HCCI charge stratification using optical, conventional and computational diagnostics.* [paper presented at the Homogeneous Charge Compression Ignition (HCCI) Symposium, September 18-20, 2005, Grand Hotel, Lund, Sweden] Society of Automotive Engineers 5-7

Dimpelfield, P.M. and Foster, D.E. (1986) *Predictions of autoignition in a spark-ignition engine using chemical kinetics* SAE paper 860322.......... 6-4

Djurisic, Z.M. (1999) MS thesis, University of Deleware.......... 2-14

Douaud, A.M. and Eyzat, P. (1978) *Four-Octane-Number Method for Predicting the Anti-Knock Behavior of Fuels and Engines* SAE paper 780080.......... 2-12, 4-22, 5-18

Downs, D. and Wheeler, R.W. (1951) *Recent Developments in 'Knock' Reseach*.......... *2-14*

Elmqvist, C., Lindström, F., Ångström, H., Grandin, B. and Kalghatgi, G. (2003) *Optimizing engine concepts by using a simple model for knock prediction* SAE paper 2003-01-3128. 2-25

Fitton, J.C. (1995) *Knock-erosion damage in spark ignition engines.* M.Sc. thesis, University of Cape Town.......... 2-2

Flowers, D., Aceves, S., Smith, R., Torres, J., Girard, J. and Dibble, R. (2000) *HCCI in a CFR engine: Experiments and detailed kinetic modelling* SAE paper 2000-01-0328.................2-23

Gauthier, B.N., Davidson, D.F. and Hanson, R.K. (2004) 'Shock tube determination of ignition delay times in full-blend and surrogate fuel mixtures' *Combustion and Flame,* Vol. 139, pp. 300-311 ....2-13, 3-2

Gluckstein, M.E. and Walcutt, C. (1961) 'End-gas temperature-pressure histories and their relation to knock' *SAE Transactions* Vol. 69, pp. 529-553.........................2-6, 2-12, 2-23, 5-15

Gogan, A., Sunden, B., Montorsi, L., Ahmedand, S.S. and Mauss, F. (2003) *Knock modeling: an integrated tool for detailed chemistry and engine cycle simulation* SAE paper 2003-01-3122 3-4

Golovitchev, V. and Ogink, R. (2003) *Numerical Evaluation of Main Features of Chemical Models for Motor Fuel Surrogates* [paper presented at ISCHIA 2003 Joint meeting of the Scandinavian-Nordic and Italian sections of the Combustion Institute] 3-2

Griffiths, J.F., MacNamara, J.P., Sheppard, C.G.W., Turton, D.A. and Whitaker, B.J. (2002) 'The relationship of knock during controlled autoignition to temperature inhomogeneities and fuel reactivity' *Fuel*, Vol. 81, pp. 2219-2225..2-4

Gu, X.J., Emerson, D.R. and Bradley, D. (2003) 'Modes of reaction front propagation from hot spots' *Combustion and Flame*, Vol. 133, pp. 63-74...2-5

Hajireza, S., Sundén, B. and Mauss, F (1999) *A Three-Zone Model for Investigation of Gas Behavior in the Combustion Chamber of SI Engines in Relation of Knock* SAE paper 1999-01-0219..*2-5*

Halstead, M.P., Kirsch, L.J. and Quinn, C.P. (1977) 'The autoignition of hydrocarbon fuels at high temperatures and pressures – Fitting of a mathematical model' *Combustion and Flame*, Vol. 30, pp. 45-60. 2-10

Halstead, M.P., Kirsch, L.J., Prothero, A. and Quinn, C.P. (1975) 'A mathematic model for hydrocarbon autoignition at high pressures'. *Proceeding of the Royal Society London*, Vol. 346, pp. 515-538. 2-10

Heywood, J.B. (1988) *Internal combustion engine fundamentals* New York, McGraw-Hill Book Company 2-1, 2-2, 2-3, 2-6

Horowitz, P. and Hill, W. (1980) *The art of electronics* Cambridge, Cambridge University Press 3-6

Hu, H. and Keck, J. (1987) *Autoignition of adiabatically compressed combustible gas mixtures* SAE paper 872110 2-10

Jenkin, R.J., James, E.H. and Malalasekera, W.M. (1996a) *Modelling near wall temperature gradients in 'motored' spark ignition engines* SAE paper 960070 5-13

Jenkin, R.J., James, E.H. and Malalasekera, W.M. (1996b) *Thermal boundary layer modelling in 'motored' spark ignition engines* SAE paper 961965 5-13

Jennings, B.H. and Obert, E. F. (1944) Internal combustion engines Analysis and Practice Scranton Pennsylvania: International Textbook Company 2-17

Kalghatgi, G.T (2001a) *Fuel anti-knock quality – Part I, Engine studies* SAE paper 2001-01-3584 1-3

Kalghatgi, G.T (2001b) *Fuel anti-knock quality – Part II, Vehicle studies – how relevant is motor octane number (MON) for modern vehicles* SAE paper 2001-01-3585 1-3

Kalghatgi, G.T. (2005) *Auto-ignition quality of practical fuels and implication for fuel requirements of future SI and HCCI engines* SAE paper 2005-01-0239 1-1

Konig, G, Maly, R.R., Bradley, D, and Lau, A.K.C. (1990) *Role of exothermic centres on knock initiation and knock damage* SAE paper 902136 .... 2-3, 2-4

Konig, G. and Sheppard, C.G.W. (1990) *End gas autoignition and knock in a spark ignition engine* SAE paper 902135 .... 2-3, 2-26

Leppard (1992) SAE paper 922325 2-23

Leppard, W.R. (1987) *The autoignition chemistry of n-Butane: An experimental study* SAE paper 872150 2-23

Leppard, W.R. (1990) *The chemical origin of fuel octane sensitivity* SAE paper number 902137. 1-4

Livengood, J. C. and Wu, P. C. (1955) 'Correlation of autoignition phenomena in internal combustion engines and rapid compression machines' *5th Symposium (International) on Combustion* The Combustion Institute, 347-356 .... 2-4, 2-12

Lydford-Pike, E.J. and Heywood, J.B. (1984) 'Thermal boundary layer thicknesses in the cylinder of a spark ignition engine' *International journal of heat and mass transfer,* Vol. 27, No. 10, pp. 1873-1878 5-13

Ricardo, H. R. (1953) *The high-speed internal-combustion engine* London: Blackie and Son Limited 2-1, 2-2, 2-15, 2-25

Rifkin and Walcutt (1957) 'A basis for understanding antiknock action' *SAE Transactions*, Vol. 65, pp. 552-565 .... 2-12, 2-23, 5-15

Ryan, T. (2005) *Fuel requirements for full time HCCI engines* [paper presented at the Homogeneous Charge Compression Ignition (HCCI) Symposium, September 18-20, Grand Hotel, Lund, Sweden] Society of Automotive Engineers 1-3

SAE HCCI conference (2005) [Held at the Grand Hotel, Lund, Sweden, 18-20 September 2005] 2-5, 2-26

Schreiber, M., Sadat Sakak, A., Lingens, A. and Griffiths, J.F. (1994) 'A reduced thermokinetic model for the autoignition of fuels with variable octane ratings' *Twenty-Fifth Symposium (International) on Combustion,* The Combustion Institute, pp. 933-940 2-11

Sheppard, C.G.W., Tolegano, S. and Woolley, R. (2002) *On the nature of autoignition leading to knock in HCCI engines* SAE paper 2002-01-2831 2-5

Stewart (1953) 'Predict octanes for gasoline blends'. *Petroleum Refiner.* December, 135-139. 2-29

Stone, A. and Bennett K () *A bulk model of emissions from South African diesel commercial vehicles.* [paper presented at the National Association for Clear Air conference] 1-2

Swarts, A. and Yates, A.D.B. (2004) *In-Cylinder Fuel Evaporation and Heat Transfer Information Inferred from the Polytropic Character of the Compression Stroke in a Spark-Ignition Engine* SAE paper 2004-01-1856 5-2

Swarts, A., Viljoen, C.L. and Coetzer, R. (2003) *The analysis of observed burn rates in a spark-ignition engine and the relation to fuel properties* SAE paper 2003-01-3125 .... 2-8, 3-3

Swarts, A., Yates, A., Viljoen, C. and Coetzer, R. (2004) *Standard kock intensity revisited: atypical burn rate characteristics identified in the CFR octane rating engine* SAE paper 2004-01-1850 .... passim

Swarts, A., Yates, A., Viljoen, C. and Coetzer, R. (2005) *A further study of inconsistencies between autoignition and knock intensity in the CFR octane rating engine* SAE paper 2005-01-2081 .... passim

Taylor, C.F. (1934) *SAE Journal.* Vol. 34, No. 2. 2-2

Taylor, C.F. (1985) *The internal combustion engine in theory and practice Volume II: Combustion, fuels, materials, design* Cambridge, The MIT press 2-24

Taylor, C.F. and Taylor, E.S. (1948) *The internal combustion engine* Revised Edition, Scranton Pennsylvania: International Textbook Company 2-3

Taylor, C.F. and Taylor, E.S. (1961) *The internal combustion engine* Second Edition, Scranton Pennsylvania: International Textbook Company 2-3, 2-13, 2-22

Twu, C.H. and Coon, J.E. (1997) 'Estimate octane numbers using an enhanced method' *Hydrocarbon Process,* Vol. 75, pp. 65. 2-29

Van Gulick, H. (1975) 'Refineries and engines as a technical system' *The Journal of Automotive Engineering,* April 1975, pp. 11-16..1-3

Viljoen, C.L. (2005) Private communication 2-26

Viljoen, C.L., Yates, A.D.B., Swarts, A., Balfour, G. and Möller, K. (2005) *Investigation of the ignition delay character of different fuel components and assessment of various autoignition modelling approaches* SAE paper 2005-01-2084...2-11

Warnatz, J. (2000) Hydrocarbon oxidation high-temperature chemistry *Pure Applied Chemistry,* Vol. 72, No. 11, pp. 2101-2110 2-7

Waukesha Engine Division (1982) *Detonation Meter Model 501-C (M-Series) and Associated Equipment, Operating and Maintenance Instructions* Wisconsin, Waukesha Engine Division. 2-19

Waukesha Motor Company (ca. 1946) *A brief history of fuel testing.* Wisconsin, Waukesha Motor Company 2-16

Westbrook, C.K. and Pitz, W.J. (1987) *Detailed Kinetic Modeling of Autoignition Chemistry* SAE paper 872107 2-8

Westbrook, C.K., Curran, H.J., Pitz, W.J., Griffiths, J.F., Mohamed, C. and Wo, S.K. (1998) 'The effects of pressure, temperature and concentration on the reactivity of alkanes: experiments and modelling in a rapid compression machine' *Twenty-seventh symposium (International) on Combustion.* The Combustion Institute, pp. 371-378 2-29

Yates, A.D.B (1988) *Abnormal combustion methanol versus gasoline* Ph.D. thesis, University of Cape Town. 6-3

Yates, A.D.B and Mkwanazi, S. (2002) *Methodology of determining octane response at different altitudes for vehicles equipped with knock sensors* SAE paper 2002-01-1663 1-3

Taylor, C.F. (1985) *The internal combustion engine in theory and practice Volume II: Combustion, fuels, materials, design* Cambridge, The MIT press 2-24

Taylor, C.F. and Taylor, E.S. (1948) *The internal combustion engine* Revised Edition, Scranton Pennsylvania: International Textbook Company 2-3

Taylor, C.F. and Taylor, E.S. (1961) *The internal combustion engine* Second Edition, Scranton Pennsylvania: International Textbook Company 2-3, 2-13, 2-22

Twu, C.H. and Coon, J.E. (1997) 'Estimate octane numbers using an enhanced method' *Hydrocarbon Process,* Vol. 75, pp. 65. ....*2-29*

Van Gulick, H. (1975) 'Refineries and engines as a technical system' *The Journal of Automotive Engineering,* April 1975, pp. 11-16..1-3

Viljoen, C.L. (2005) Private communication 2-26

Viljoen, C.L., Yates, A.D.B., Swarts, A., Balfour, G. and Möller, K. (2005) *Investigation of the ignition delay character of different fuel components and assessment of various autoignition modelling approaches* SAE paper 2005-01-2084..2-11

Warnatz, J. (2000) Hydrocarbon oxidation high-temperature chemistry *Pure Applied Chemistry,* Vol. 72, No. 11, pp. 2101-2110...2-7

Waukesha Engine Division (1982) *Detonation Meter Model 501-C (M-Series) and Associated Equipment, Operating and Maintenance Instructions* Wisconsin, Waukesha Engine Division. 2-19

Waukesha Motor Company (ca. 1946) *A brief history of fuel testing.* Wisconsin, Waukesha Motor Company..2-16

Westbrook, C.K. and Pitz, W.J. (1987) *Detailed Kinetic Modeling of Autoignition Chemistry* SAE paper 872107 2-8

Westbrook, C.K., Curran, H.J., Pitz, W.J., Griffiths, J.F., Mohamed, C. and Wo, S.K. (1998) 'The effects of pressure, temperature and concentration on the reactivity of alkanes: experiments and modelling in a rapid compression machine' *Twenty-seventh symposium (International) on Combustion.* The Combustion Institute, pp. 371-378 2-29

Yates, A.D.B (1988) *Abnormal combustion methanol versus gasoline* Ph.D. thesis, University of Cape Town. 6-3

Yates, A.D.B and Mkwanazi, S. (2002) *Methodology of determining octane response at different altitudes for vehicles equipped with knock sensors* SAE paper 2002-01-1663.....................1-3

Yates, A.D.B. and Cilliers, C.T. (2002) *A fundamental study of the relationship between altitude and research octane number* SAE paper 2002-01-1662 .... *1-2*

Yates, A.D.B., Swarts, A. and Viljoen, C.L. (2003) *An Investigation of Anomalies Identified Within the ASTM Research and Motor Octane Scales* SAE paper 2003-01-1772.2-10, *2-30,* 4-18

Yates, A.D.B., Swarts, A. and Viljoen, C.L. (2004) *Understanding the Relation Between Cetane Number and Combustion Bomb Ignition Delay Measurements* SAE paper 2004-01-2017. 2-13

Yates, A.D.B., Swarts, A. and Viljoen, C.L. (2005) *Correlating auto-ignition delays and knock-limited spark-advance for different types of fuel* SAE paper 2005-01-2083.1-3, 2-13, 5-15, 6-12

Zel'dovich, Y.B. (1980) 'Regime classification of an exothermic reaction with nonuniform initial conditions' *Combustion and Flame*, Vol. 39, pp. 211-214 2-5

A. Experimental set-up

A.1. Engine and ancillaries

Tests were performed on the CFR engine at the University of Cape Town. The engine was substantially rebuilt prior to the commencement of the tests to include a new head, piston and rings. The CFR engine was connected to a direct current motor and regenerative drive that included a feedback speed control.

Although the engine was modified to include horizontal line-of-sight optical access into the top of the cylinder, all engine standardisation checks were performed according to the ASTM methods D2699 and D2700 and included adherence to the compression pressure requirements (ASTM, 2004a and ASTM 2004b).

Inlet air, mixture and oil temperatures were controlled by the use of a CAL3200 temperature controller with set-point accuracy of 0.1° Celcius. A number of additional temperatures were monitored, including, coolant and exhaust. The exhaust fuel-air equivalence ratio was checked by a Horiba MEXA 110λ lambda meter.

A.2. Data acquisition

AVL shaft encoder, provided clock pulses at 0.2° intervals and a marker at top dead centre (TDC). The position of the top-dead-centre marker was set in by means of the motored pressure trace by taking thermodynamic considerations into account.

In-cylinder pressure was measured by means of an AVL QC32C piezoelectric pressure transducer with natural frequency of 75 kHz and sensitivity of 25.8 pC/bar, connected to a Kistler charge amplifier. The transducer was fitted through one of the optical access ports.

The detonation pick-up was retained in its original position on the CFR engine, allowing for the simultaneous measurement of cylinder pressure and the knock intensity according to the ASTM methods. The spark discharge was monitored by a Fluke inductive pick-up on the high tension lead.

Three analogue channels were sampled using a National Instruments model PCI 6071E, 12 bit data acquisition card. The channels sampled were:

- Cylinder pressure
- TDC marker
- Spark discharge marker OR Filtered rate-of-change of pressure

The data acquisition software was developed in Labview™ and allowed for the easy selection between external and internal clocking. The former used the clock pulse from the shaft encoder, whilst the latter employed the internal clock on the data acquisition board at rates of up to 250kHz.

Operation of the knock measurement equipment was done according to the prescribed methods and meter and spread settings, as well as the knock intensity value was recorded.

During the first round of screening tests, 255 successive pressure traces were captured and stored. Where applicable, the data set was treated as a whole and descriptive statistics were presented. Previous research, employing much more rigorous statistical methods concluded that the number of samples in individual data sets and the variation therein were sufficient to draw meaningful conclusions from the data (Swarts et al., 2003).

A.3. Test fuel blends

The composition and octane numbers of the fuels blends tested, in addition to PRF blends, are givenTable A-1. Properties of the Toluene Standard Fuels were taken from the ASTM manuals (ASTM, 2004a and ASTM, 2004b). These blends, as well as the PRF blends, were prepared using the graduated burettes.

Table A-1: Composition and properties of the Toluene Standard Fuels.

MON designation	MON	Toluene (vol %)	Iso-octane (vol %)	N-heptane (vol %)	Bubble point (˚C)	RON	RON designation
TSF58	58	50	0	50	102.4	65.1	TSF651
TSF669	66.9	58	0	42	103.3	75.6	TSF756
TSF748	74.8	66	0	34	104.2	85.2	TSF852
TSF782	78.2	70	0	30	104.7	89.2	TSF892
TSF815	81.5	74	0	26	105.3	93.4	TSF934
TSF852	85.2	74	5	21	105.6	96.9	TSF969
TSF887	88.7	74	10	16	105.9	99.8	TSF998
TSF926	92.6	74	15	11	106.1	103.3	-
TSF966	96.6	74	20	6	106.2	107.6	-
TSF998	99.8	74	24	2	106.3	-	-

The two gasoline surrogate blends, designated blend 5 and blend 6, were prepared by volume addition and the octane numbers determined by an independent laboratory according to the prescribed methods. The composition of these is given in Table A-2.

Table A-2: Composition and properties of gasoline surrogate blends.

	Blend 5	Blend 6
RON	90	95.6
MON	82	86.1
Ethanol (vol%)	10	0
1-Hexene (vol%)	30	10
Toluene (vol%)	10	40
N-heptane (vol%)	12.5	12.5
Iso-octane (vol%)	37.5	37.5
Bubble point (˚C)	66.0	95.6

References A

ASTM (2004a) *Standard Test Method for Research Octane Number of a Spark-Ignition Engine Fuel, ASTM Designation: D 2699-04a* ASTM International.. A-1, A-2

ASTM (2004b) *Standard Test Method for Motor Octane Number of a Spark-Ignition Engine Fuel, ASTM Designation: D 2700-04a* ASTM International.. A-1, A-2

Swarts, A, Viljoen, C.L. and Coetzer, R (2003) *The analysis of observed bum rates in a spark-ignition engine and the relation to fuel properties* SAE paper 2003-01-3125 .... A-2

B. Autoignition delay model

B.1. Mathematical model of ignition delay

The ignition delay can be combined from three individual ignition delay times:

$$\tau_{overall} = \frac{1}{\left(\frac{1}{\tau_1 + \tau_2} + \frac{1}{\tau_3}\right)} \qquad \textbf{(B-1)}$$

Each of the ignition delay times can be conveniently described by the exponential function of temperature:

$$\tau_i = A_i p^{n_i} e^{\frac{B_i}{T}} \; for \; i = 1,2,3 \qquad \textbf{(B-2)}$$

Each of the ignition delay expressions required three parameters A, n, β. These provide tacit information about the overall scaling, pressure sensitivity and temperature sensitivity, respectively.

Furthermore, the effect of the fuel-air equivalence ratio, ϕ, can be added as a power law correction according to (Yates et al., 2005):

$$\tau = \tau_{\phi=1} \phi^m \qquad \textbf{(B-3)}$$

It is acknowledged that residual gasses will affect the ignition delay times as well, but this effect was neglected since only the natural residual fractions were expected.

B.2. Calculation of fuel model parameters

Using the model described above, the ignition delay for any fuel can be characterised by 10 parameters (three each for the three exponential functions and single exponent for the fuel-air equivalence ratio)

Parameters for the ignition delay model were found by the least fit regression to available data for the pure fuel components that constitute the fuel blend components used. The use of data from RCM devices was used with great caution due to the known phenomenon of reactions during the compression stage (Griffiths et al., 1997) and the fact that ignition delays are not consistently quoted from either the start or end of compression.

B.1.1. n-Heptane

Ignition delay data for n-heptane was found from measurements made by:

- Ciezki and Adomeit (1993)
- Gauthier et al. (2004)
- Fieweger et al. (1997)
- Warnatz (2000)

Data was found for a range of pressures, temperatures and fuel-air equivalence ratios. A sample of some of the ignition delay values at stoichiometric conditions and at different pressures is shown in Figure B-1 below.

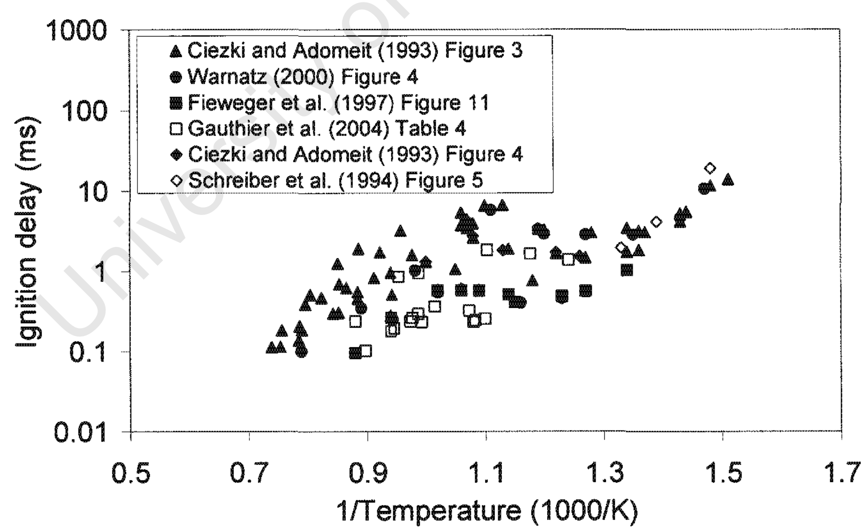

Figure B-1: Literature values for the ignition delay of n-heptane. Taken from Tao et al. (2000) and Curran et al. (1998).

Table B-1 shows the tabulated result of best the fit to all the available data.

Table B-1: Parameters applicable to the ignition delay model of n-heptane.

	Ln(A1)	n1	B1	Ln(A2)	n2	B2	Ln(A3)	n3	B3	m
N-heptane	-23.5	-0.19	17973.5	12.2	-2.07	-4553.7	-12.3	-0.93	15900.2	-0.46

Knowledge of the pressure coefficients allowed for the ignition delay data to be transformed to a pressure of choice to allow for the individual measurements to be visually compared, as indicated by the relationship below:

$$\tau_{p2}\Big|_{Corrected} = \frac{\tau_{p2}}{\tau_{p1}}\Bigg|_{Calculated} .\tau_{p1}\Bigg|_{Measured} \quad \textbf{(B-4)}$$

The result of the transformation of the data to 12 bar is shown in Figure B-2. Also included is the parameterised ignition delay model at the same pressure.

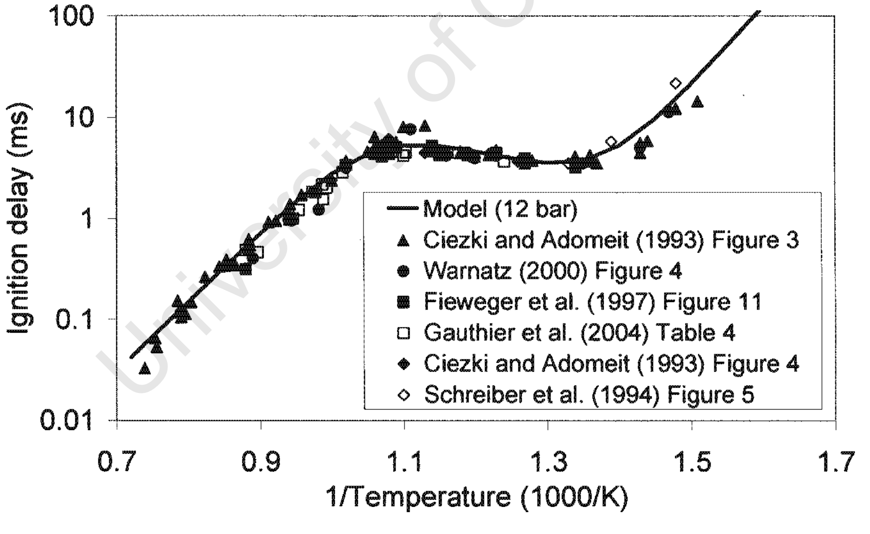

Figure B-2: Ignition delay data for n-heptane transformed to a pressure of 12 bar. The result of the ignition delay model is also shown.

B.1.2. Iso-octane

Similar ignition delay data for iso-octane (2,2,4-trimethylpentane) was found from literature references by:

- Fieweger et al. (1997)
- Curran et al. (2003)
- Davidson et al. (2005)
- Schreiber et al. (1994)
- Hu and Keck (1987)

The results are shown in Figure B-3 below with data transformed to 12 bar for the sake of clarity. The less pronounced negative temperature coefficient behaviour of iso-octane is immediately apparent.

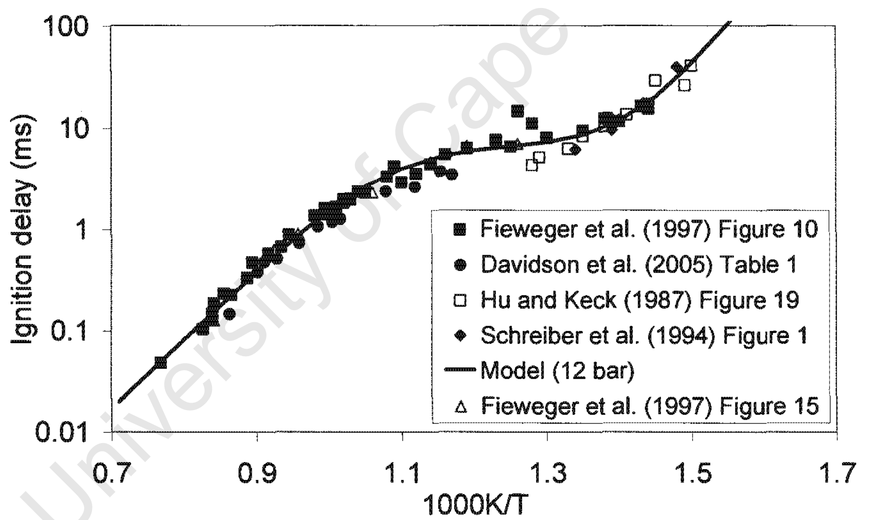

Figure B-3: Literature values for the ignition delay of iso-octane transformed to 12 bar.

A similar least squares fit to the literature data reveals the parameters as contained inTable B-2:

Table B-2: Parameters applicable to the ignition delay model of iso-octane.

	Ln(A1)	n1	B1	Ln(A2)	n2	B2	Ln(A3)	n3	B3	m
Iso-octane	-23.6	-0.79	19769.4	4.0	-0.67	-0.8	-12.0	-1.01	15820.9	-0.52

B.1.3. Toluene

Experimental ignition delay data for toluene is unfortunately less common than that of the primary reference fuel blend components. One of the main reasons is the very long ignition delays of toluene that limits access to low temperature (long ignition delay) measurements. The following references to toluene ignition delay measurements were used:

- Davidson et al. (2005)
- Golovitchev and Ogink (2004) referenced the data by Burcat et al. (1986), but this is limited to low pressure and high temperature (less than 6.81 bar and more than 1400 K) and Lemaire et al. (2001), but the data is limited to a temperature range between 910 K to 923 K.
- Pitz et al. (2001)
- Bounaceur et al. (2004)

The pressure corrected data is shown in Figure B-4, together with the ignition delay model prediction at 12 bar.

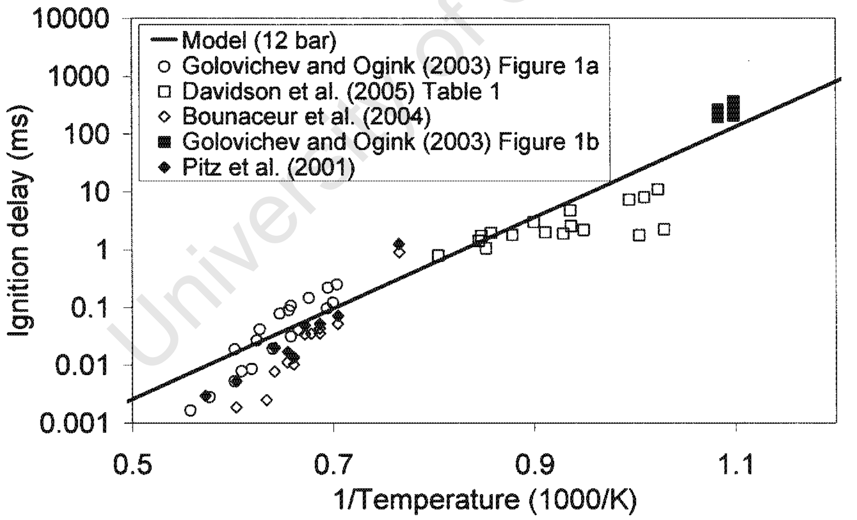

Figure B-4: Literature ignition delay values for toluene transformed to 12 bar.

Given the expected single stage reaction pathway of toluene, the parameters for each of the three ignition delay stages were set equal, as is apparent in Table B-3. Moreover, since there was contradictory literature information regarding the effect of fuel-air equivalence ratio on toluene ignition delay, all non-stoichiometric ignition delay information was disregarded and the fuel-air equivalence ratio exponent assigned a value of 0. This assumption was deemed acceptable given the narrow range of fuel-air equivalence ratios tested. The assumptions will require a review if the same model is to be applied at extreme values for fuel-air equivalence ratio.

Table B-3: Parameters applicable to the ignition delay model of toluene.

	Ln(A1)	n1	B1	Ln(A2)	n2	B2	Ln(A3)	n3	B3	m
Toluene	-12.0	-1.80	20128.4	-12.0	-1.80	20128.4	-12.0	-1.80	20128.4	0.0

B.1.4. Other blend components

The ignition delay data for other fuel molecules tested during this project were found by utilising chemical kinetic modelling with the Chemkin™ software. Details of the kinetic models for ethanol and 1-hexene can be found in Viljoen et al. (2005). The parameterisation of the ignition delay model followed the same methodology described previously.

B.3. Rule for fuel blends

To allow for the calculation of ignition delay times for fuel blends, the blending rule proposed by Yates et al. (2005) was employed. The rule combined the liquid volume fraction of the blend constituents, *v*, according to:

$$\tau_{Blend} = \frac{\sum v_i^P}{\sum \left[\frac{v_i^P}{\tau_i} \right]} \qquad \textbf{(B-5)}$$

The blending rule required a-priori knowledge of the ignition delay model parameters of blend components and the magnitude of the blending exponent, *P*, was found through the best fit to literature data for known fuel blends.

The fit to the PRF data from Fieweger et al. (1997) is shown in Figure B-5 and yielded an exponent value *P=1.05*.

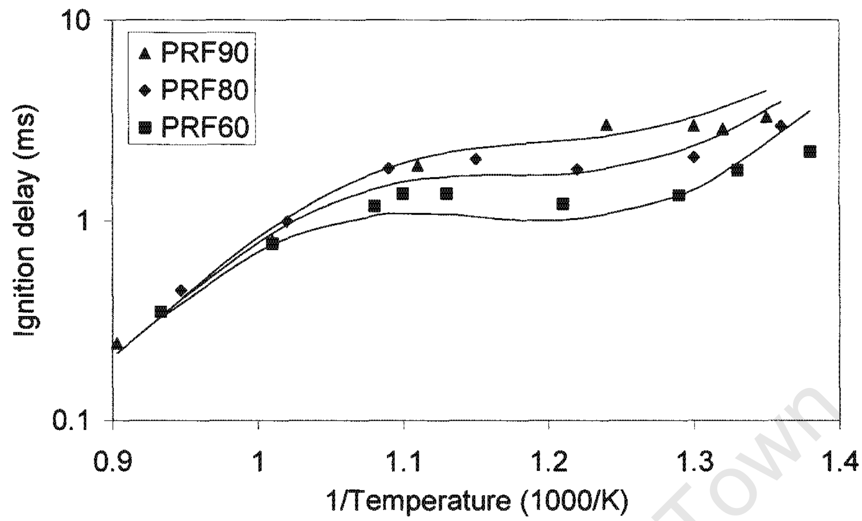

Figure B-5: PRF ignition delay behaviour at 40 bar from Fieweger et al. (1997).

The blending rule was further optimised by considering ternary fuel blends. Gauthier et al. (2004) performed shock tube experiments on two gasoline surrogates comprising of iso-octane, n-heptane and toluene. The data was available in two pressure ranges and is presented as low and high pressures in Figure B-6. The same graph includes the resulting current blending rule model predictions: low pressure for surrogate A and high pressure for surrogate B. In this instance, the blending exponent was adjusted to provide the best overall fit, including the PRF data, and yielded a value of 1.15.

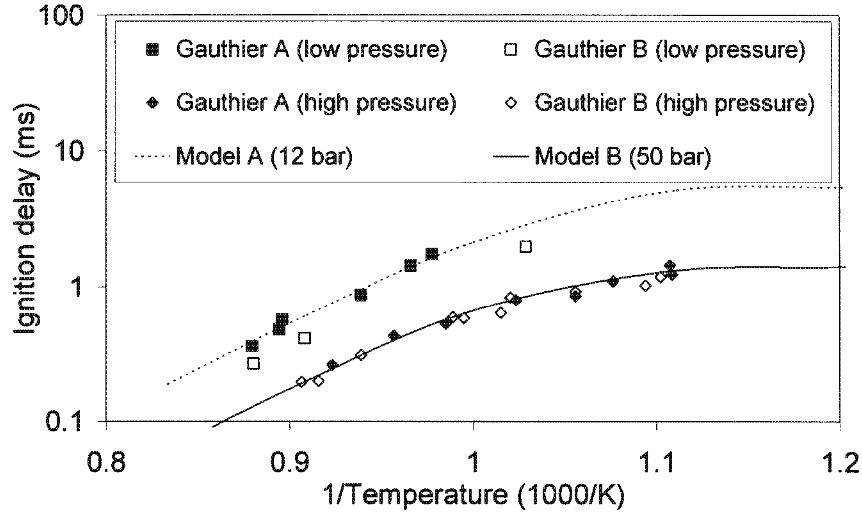

Figure B-6: Ignition delay data for two gasoline surrogates from Gauthier et al. (2004) is compared to the current blending rule model.

It is acknowledged that the Gauthier data is confined to the high temperature side of the temperature scale. To explore this concern, chemical kinetic model results for a 10:55:35 n-heptane:iso-octane:toluene blend was taken from Golovitchev and Ogink (2004) and compared to the blending rule prediction. The result is shown in Figure B-7 for a pressure of 15 bar and confirms good agreement throughout the temperature range. The graph further reveals the strong NTC character of the blend.

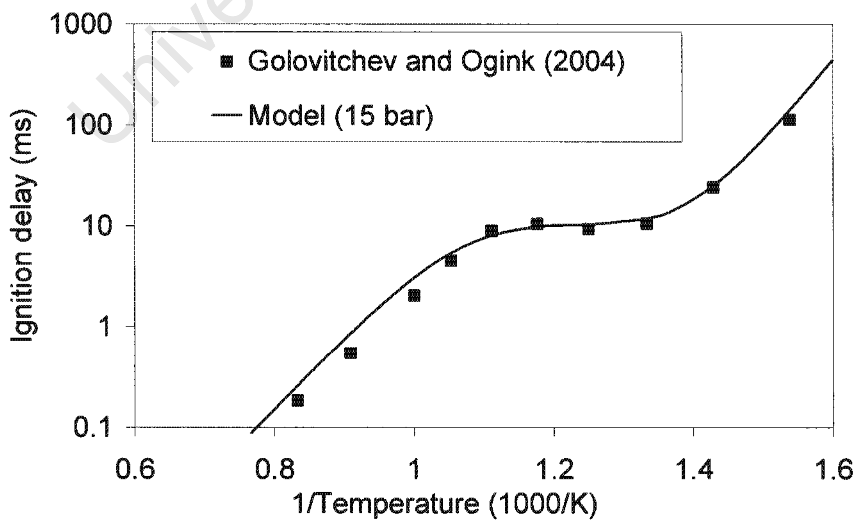

Figure B-7: Kinetic model predictions for a ternary blend compared to blending rule model prediction at 15 bar.

Since the kinetic model data did not constitute part of the training set for either the model fuel parameters or blending exponent, the result gave good confidence in the ignition delay model description and parameters and blending rule formulation. The same blending rule was applied to more complex blends, such as gasoline surrogate blends 5 and 6 used in the present study. Details of the blends are given Appendix A.

B.4. Fuel characteristic in the Pressure-Temperature domain

The combined effect of pressure and temperature on the ignition delay time is shown as a surface plot of ignition delay in Figure B-8 below:

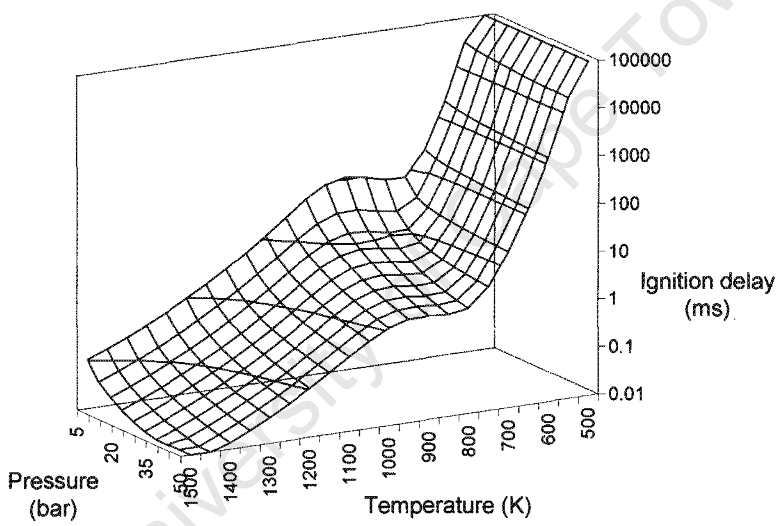

Figure B-8: Ignition delay surface for PRF93 blend.

If the surface is viewed in plan, contours of constant ignition delay can be seen in Figure B-9:

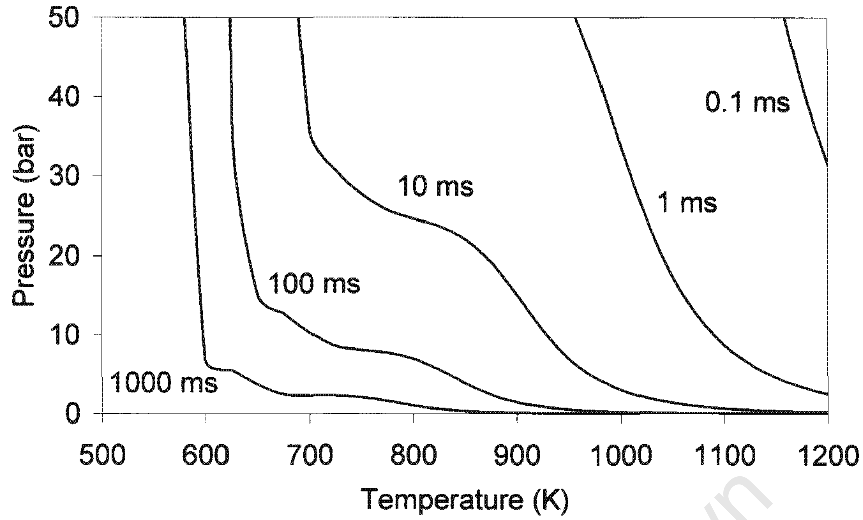

Figure B-9: Plan view of the ignition delay surface, showing contours of constant ignition delay.

References B

Bounaceur, R., Da Costa, I., Fournet, R., Billaud, F. and Battin-Leclerc, F. (2004) 'Experimental and modeling study of the oxidation of toluene' *International Journal of Chemical Kinetics* Vol. 37(1), pp. 25-49 .... B-5

Burcat, A., Snyder, C. and Brabbs, T. (1986) *Ignition delay times of benzene and toluene with oxygen in argon mixtures* Technical memorandum 86-87312 NASA B-5

Ciezki, H.K. and Adomeit, G. (1993) 'Shock-tube investigation of self-ignition of n-heptane-air mixtures under engine relevant conditions' *Combustion and Flame* Vol. 93, pp. 421-433 ... B-2

Curran, H.J., Gaffuri, P., Pitz, W.J. and Westbrook , C.K. (2003) 'A comprehensive modelling study of iso-octane oxidation' *Combustion and Flame* Vol. 129, pp.253-280. .... B-4

Davidson, D.F., Gauthier, B.M. and Hanson, R.K. (2005) 'Shock tube measurements of iso-octane/air and toluene/air at high pressures' *Proceedings of the Combustion Institute* Vol. 30, pp. 1175-1182. .... B-4

Davidson, D.F., Gauthier, B.M. and Hanson, R.K. (2005) 'Shock tube measurements of iso-octane/air and toluene/air at high pressures' *Proceedings of the Combustion Institute.* Vol 30, 1175-1182 .... B-5

Fieweger, K, Blumenthal, R, Adomeit, G. (1997) 'Self-igntion of S.I. engine model fuels: a shock tube investigation at high pressure' *Cobustion and Flame* Vol. 109, pp. 599-619 .... B-2, B-7

Fieweger, K, Blumenthal, R, Adomeit, G. (1997) 'Self-igntion of S.I. engine model fuels: a shock tube investigation at high pressure' *Cobustion and Flame*. Vol. 109, 599-619 .... B-4

Gauthier, B.N, Davidson, D.F and Hanson, R.K. (2004) 'Shock tube determination of ignition delay times in full-blend and surrogate fuel mixtures' *Combustion and Flame.* Vol 139, 300-311 .... B-2, B-8

Griffiths, J.F., Halford-Maw, P.A. and Mohamed, C. (1997) *Combustion and Flame*. Vol. 111, 327-337 .... B-2

Hu, H. and Keck, J. (1987) *Autoignition of adiabatically compressed combustible gas mixtures.* SAE paper 872110 .... B-4

Lemaire, O., Cocq, R., Roubaud, A., Minetti, R., Faravelli, T and Ranzi, E. (2001) Taken from *Combustion and the Environment* Ed. S. Margherita, pp. IV-15 .... B-5

Schreiber, M., Sadat Sakak, A., Lingens, A and Griffiths, J.F. (1994) 'A reduced thermokinetic model for the autoignition of fuels woth variable octane ratings' *Twenty-Fifth Symposium (International) on Combustion,* The Combustion Institute, 933-940 .... B-4

Viljoen, C.L., Yates, A.D.B., Swarts, A., Balfour, G. and Möller, K. (2005) *Investigation of the ignition delay character of different fuel components and assessment of various autoignition modelling approaches* SAE paper 2005-01-2084 .... B-6

W.J. Pitz, R. Seiser, J.W. Bozzelli, I. Da Costa, R. Fournet, F. Billaud, F. Battin-Leclerc, K. Seshadri and C.K. Westbrook (2001) *Proceedings of the 2nd Joint Meeting of the U.S. Sections of the Combustion Institute* B-5

Warnatz, J. (2000) 'Hydrocarbon oxidation high temperature chemistry' *Pure App. Chem.* Vol. 72, No. 11, 2101-2110 .... B-2

Yates, A.D.B., Swarts. A and Viljoen, C.L. (2005) *Correlating auto-ignition delays and knock-limited spark-advance for different types of fuel.* SAE paper 2005-01-2083 .... B-1, B-7

C. CFD model results

Multi-dimensional fluid dynamic analysis of the inlet process in the CFR engine was performed using Fluent CFD software. Details of the model are contained in the MSc thesis by Hsiao due for publication in 2006 (Hsiao, 2006)

C.1. Temperature results

Figure C-1 shows the temperature values at inlet valve closure (146 °BTDC) for a compression ratio of 7.5:1. The colour plate on the left shows a horizontal section at the level of the spark plug, about 15 mm from the top of the cylinder. The plan position of the inlet valve, shroud and spark plug is indicated for reference. The right hand colour plate shows a vertical section through the inlet valve. The variation in temperatures at this time ranges between 335 K and 355 K for both the horizontal and vertical viewing planes.

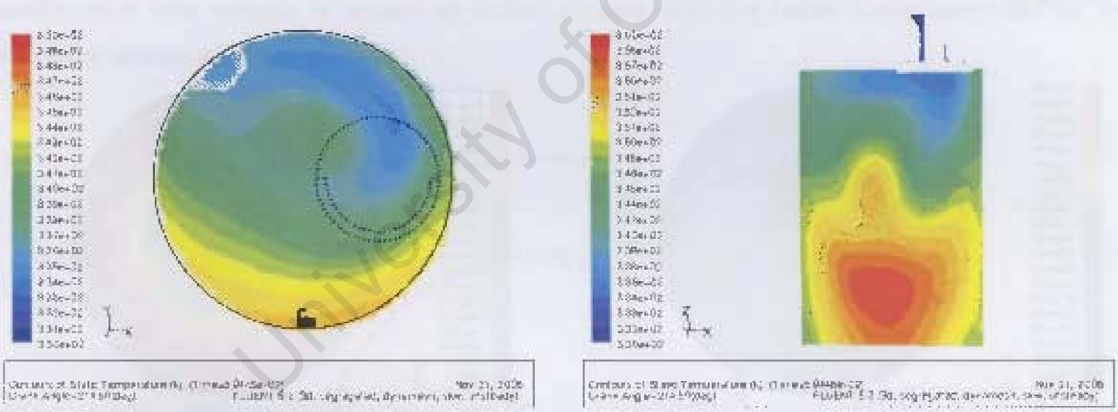

Figure C-1: Predicted temperature values at IVC during gas exchange in CFR engine

Figure C-2 shows the predicted temperatures at TDC during the compressions stroke and reveals that the temperature range has diminished to about 10 K in the horizontal plane and slightly more in the vertical plane, with thermal stratification clearly visible. Note that the model considered only gas exchange and that the effect of combustion and flame propagation was not taken into account.

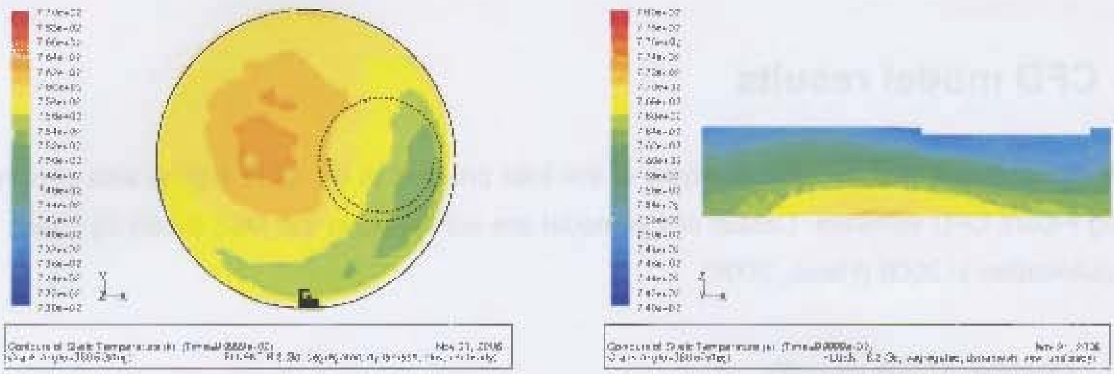

Figure C-2: Predicted temperature values at TDC during the compression stroke in CFR engine

C.2. Velocity results

The same model was used to predict the magnitude of the velocity at TDC in order to assess the effect of the shrouded inlet valve on the flow pattern inside the cylinder. The results, presented in Figure C-3, show strongly swirling flow on a horizontal plane at the level of the spark plug for a compression ratio of 5.25:1. Two conditions are show: IVC on the left and TDC on the right.

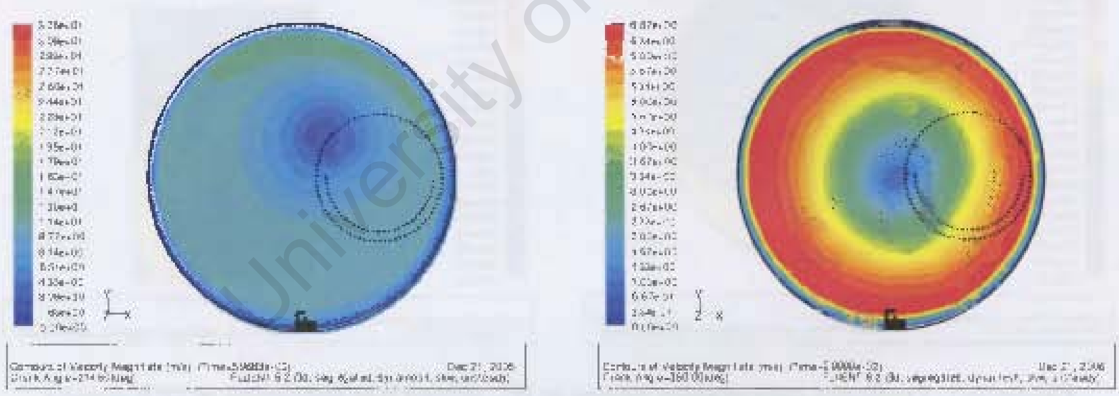

Figure C-3: Velocity contours at IVC (left) and TDC (right) for a compression ratio of 5.25:1.

Figure C-4 show similar results as previously, but for a compression ratio of 7.5:1. As with the low compression ratio example, the velocity magnitude at TDC varies with radius: from close to zero at the centre to ~6.5 m/s at the cylinder wall

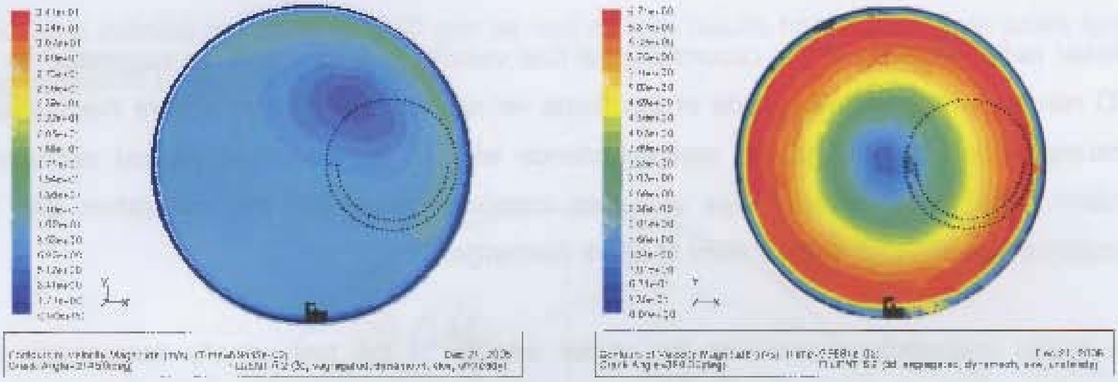

Figure C-4: Velocity contours at IVC (left) and TDC (right) for a compression ratio of 7.5:1.

C.3. Transported flame model

The knowledge of the velocity magnitude at TDC allows for the calculation of the flame front position in two dimensions using a transported flame assumption. The model considers a number of "packets" on an initial semi-circular flame kernel with velocity vectors directed radially outward from the spark plug. This is illustratively represented in Figure C-5, where the circumferential flow velocity is shown as dotted arrows; with the radial flame velocities for three packets are shown as solid arrows.

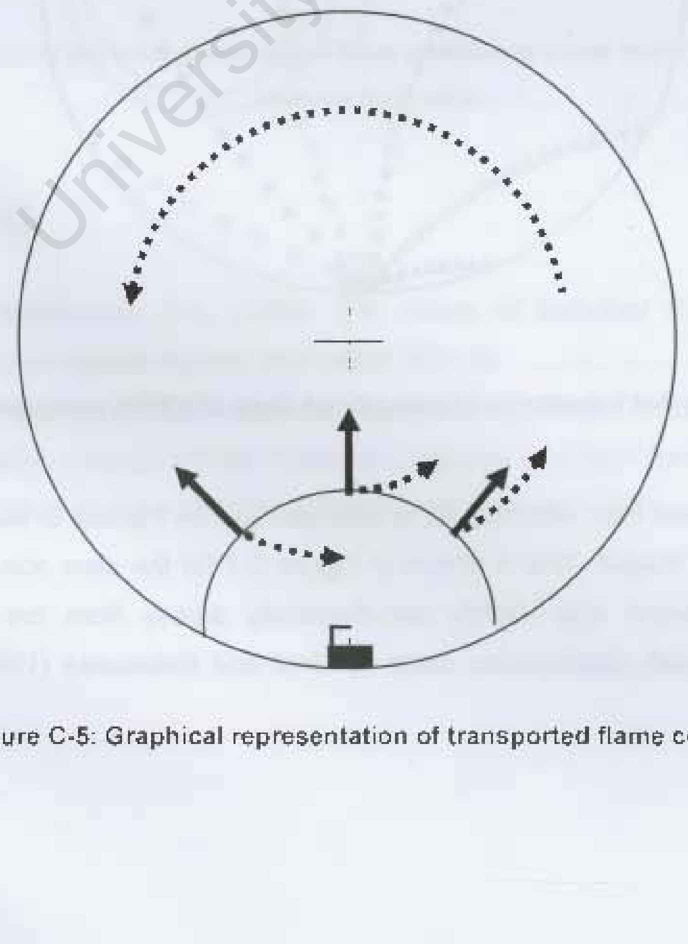

Figure C-5: Graphical representation of transported flame concept

A linear radial variation of the circumferential flow velocity was imposed, as suggested by the CFD results, whilst the magnitude of the flame velocity was chosen to ensure the complete consumption of the end-gas in correspondence with to the observed normal combustion duration. The flame velocity was assumed constant throughout the calculation and the calculation was initiated at the instant of spark discharge.

The model methodology considers the vector addition of the two velocity components and tracks the progress of each of the packets. An example is shown in Figure C-6 for a compression ratio of 7.5:1. The increment between successive symbols corresponded to an angular increment of 1 °CA at 600 rpm.

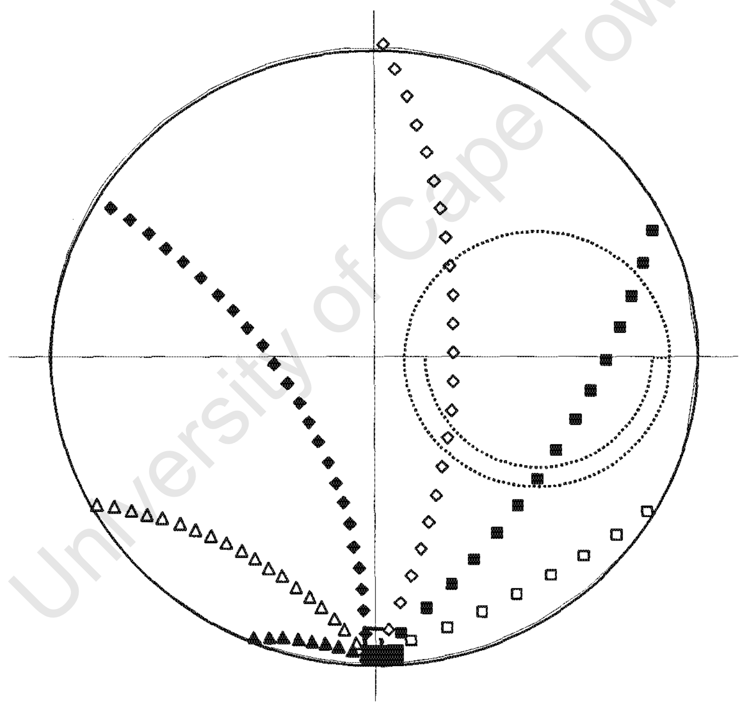

Figure C-6: Packet trajectories of transported flame at a 7.5:1 compression ratio.

The position of the flame front with respect to time can also be tracked to visualise the location of the end-gas at any instant. This is shown in Figure C-7 for the case above and indicates a crescent shaped end-gas only slightly non-diagonally across from the spark plug. The observation is in line with observations made by Groff and Matekunas (1980) for a shrouded inlet valve cylinder operated at 2000 rpm as well as with results from a high swirl spark ignition engine studied by Kumar et al. (1988)

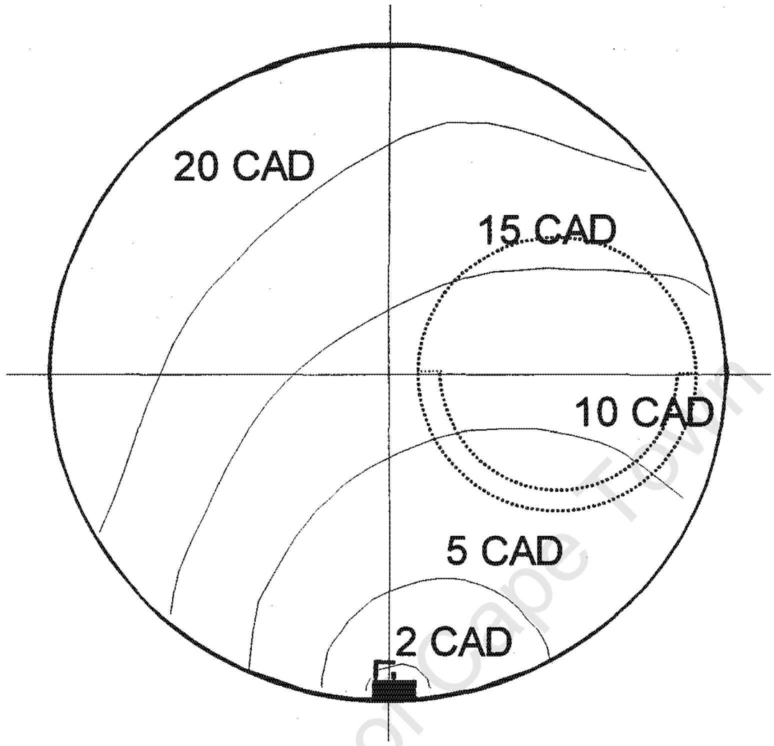

Figure C-7: Position of the transported flame front at different crank angle increments for a 7.5:1 compression ratio.

References C

Groff, E.G. and Matekunas, F.A. (1980) *The nature of turbulent flame propagation in a homogeneous spark-ignited engine.* SAE paper 800133 .... C-4

Hsiao, T. (2006) Unpublished MSc thesis, University of Cape Town C-1

Kumar, Ahary, Lambe, Watson (1988) 'Flame propagation in a high-speed variable swirl spark ignition engine' *Journal of the Institute of Mechanical engineers.* C61 .... C-5

D. Engine model details

D.1. Interpretative model

To enable the interpretation of recorded pressure data, the ignition delay model was applied according to the flow-charts given in Figure D-1 and Figure D-2 for the estimation of initial temperature inhomogeneity and heat loss gradient, respectively. The different polytropic coefficients in the latter give rise to the proposed heat loss gradient.

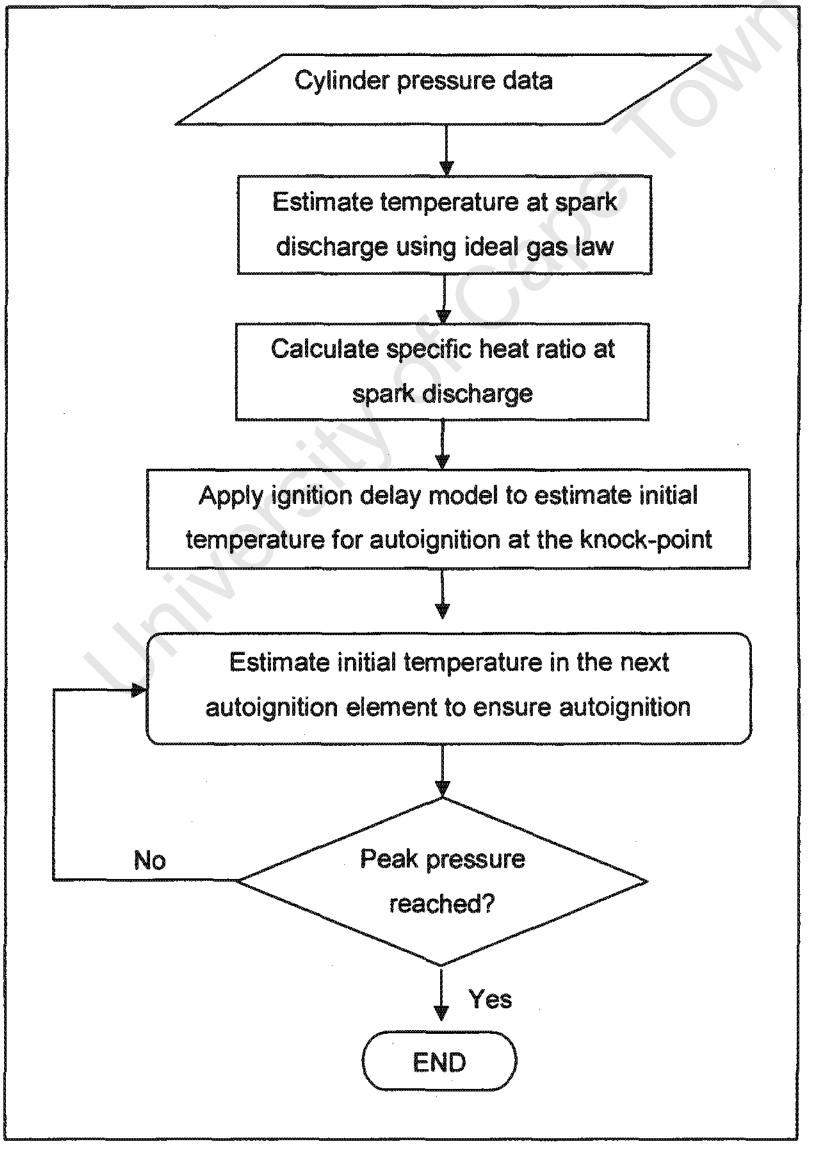

Figure D-1: Flow diagram for the estimation of the initial temperature inhomogeneities.

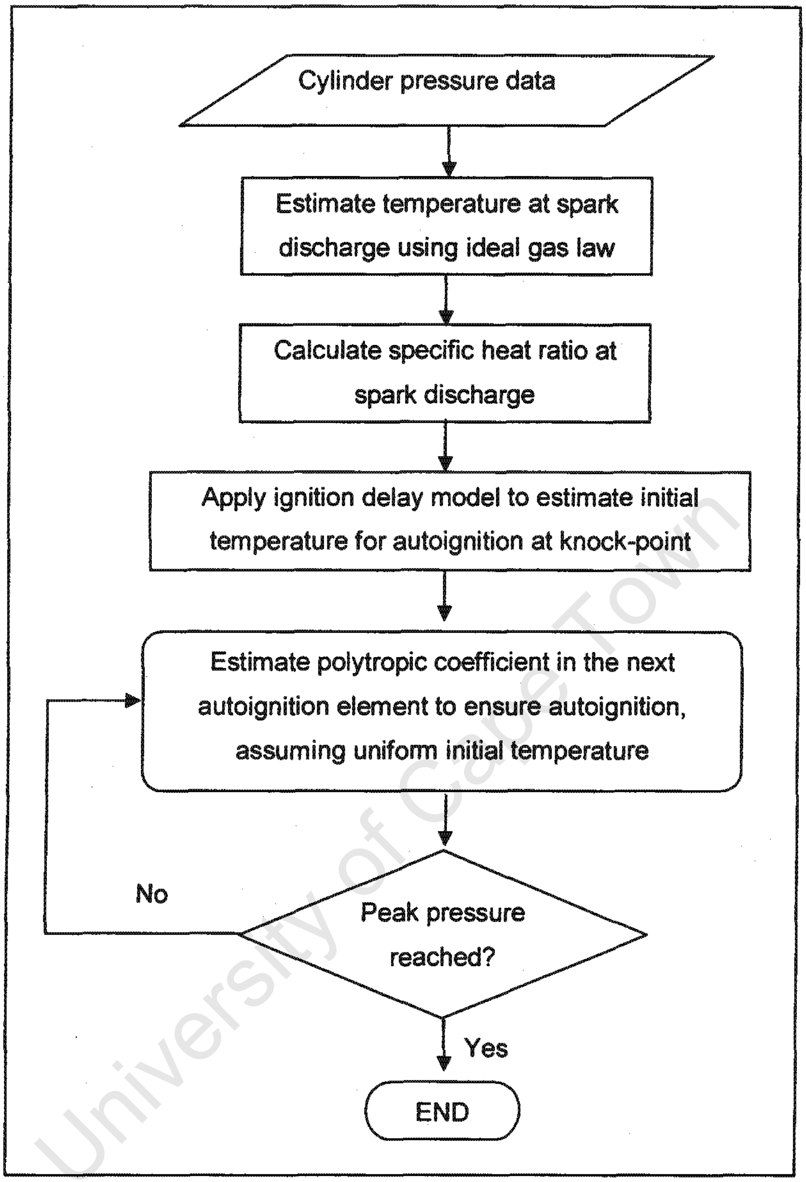

Figure D-2: Flow diagram for the estimation of the polytropic coefficient, giving rise to the heat loss gradient.

D.2. Predictive model

General description

A two-zone thermodynamic engine model was used for the predictive part of thesis. The model solves the overall energy balance in accordance with standard textbooks on the subject. (Heywood, 1988)

Assumptions

The following assumptions were made:

- The two zones are each homogeneous and well mixed
- The two zones are separated by a flame front of negligible thickness
- Blow-by and crevice volume effects were ignored
- The cylinder pressure was uniform at all times
- The fuel was fully evaporated and well mixed.

Mass fraction burnt (normal combustion)

The mass fraction burnt, attributable to normal flame propagation, was calculated according to the fuel-life function (Oppenheim, 1998)

$$x_\theta = \frac{\exp\left[-\alpha(1-\Theta)^\beta\right]-\exp(-\alpha)}{1-\exp(-\alpha)} \qquad \textbf{(D-1)}$$

where

$$\Theta = \left(\frac{\theta-\theta_0}{\Delta\theta}\right) \qquad \textbf{(D-2)}$$

with θ the position in °CA, $\Delta\theta$ the burn duration, θ_0 the instance of spark discharge. The balance of the symbols are empirical constants.

Thermodynamic properties

All thermodynamic properties were calculated using data from the JANAF thermodynamic tables (National Bureau of Standards, 1971)

D.2. Predictive model

General description

A two-zone thermodynamic engine model was used for the predictive part of thesis. The model solves the overall energy balance in accordance with standard textbooks on the subject. (Heywood, 1988)

Assumptions

The following assumptions were made:

- The two zones are each homogeneous and well mixed
- The two zones are separated by a flame front of negligible thickness
- Blow-by and crevice volume effects were ignored
- The cylinder pressure was uniform at all times
- The fuel was fully evaporated and well mixed.

Mass fraction burnt (normal combustion)

The mass fraction burnt, attributable to normal flame propagation, was calculated according to the fuel-life function (Oppenheim, 1998)

$$x_\theta = \frac{\exp\left[-\alpha(1-\Theta)^\beta\right] - \exp(-\alpha)}{1-\exp(-\alpha)} \qquad \textbf{(D-1)}$$

where

$$\Theta = \left(\frac{\theta - \theta_0}{\Delta\theta}\right) \qquad \textbf{(D-2)}$$

with θ the position in °CA, $\Delta\theta$ the burn duration, θ_0 the instance of spark discharge. The balance of the symbols are empirical constants.

Thermodynamic properties

All thermodynamic properties were calculated using data from the JANAF thermodynamic tables (National Bureau of Standards, 1971)

Burnt gas composition

The effect of dissociation reactions in the burnt gas was included by allowing for the equilibrium of the water-gas-shift and CO2 dissociation reactions:

$$2CO_2 \Leftrightarrow 2CO + O_2 \qquad \textbf{(D-3)}$$

$$H_2O + CO \Leftrightarrow CO_2 + H_2 \qquad \textbf{(D-4)}$$

The equilibrium composition was assumed "frozen" at temperatures below 1750 K.

Ignition delay model incorporation

The ignition delay model was incorporated according to the flow diagram given in Figure D-3:

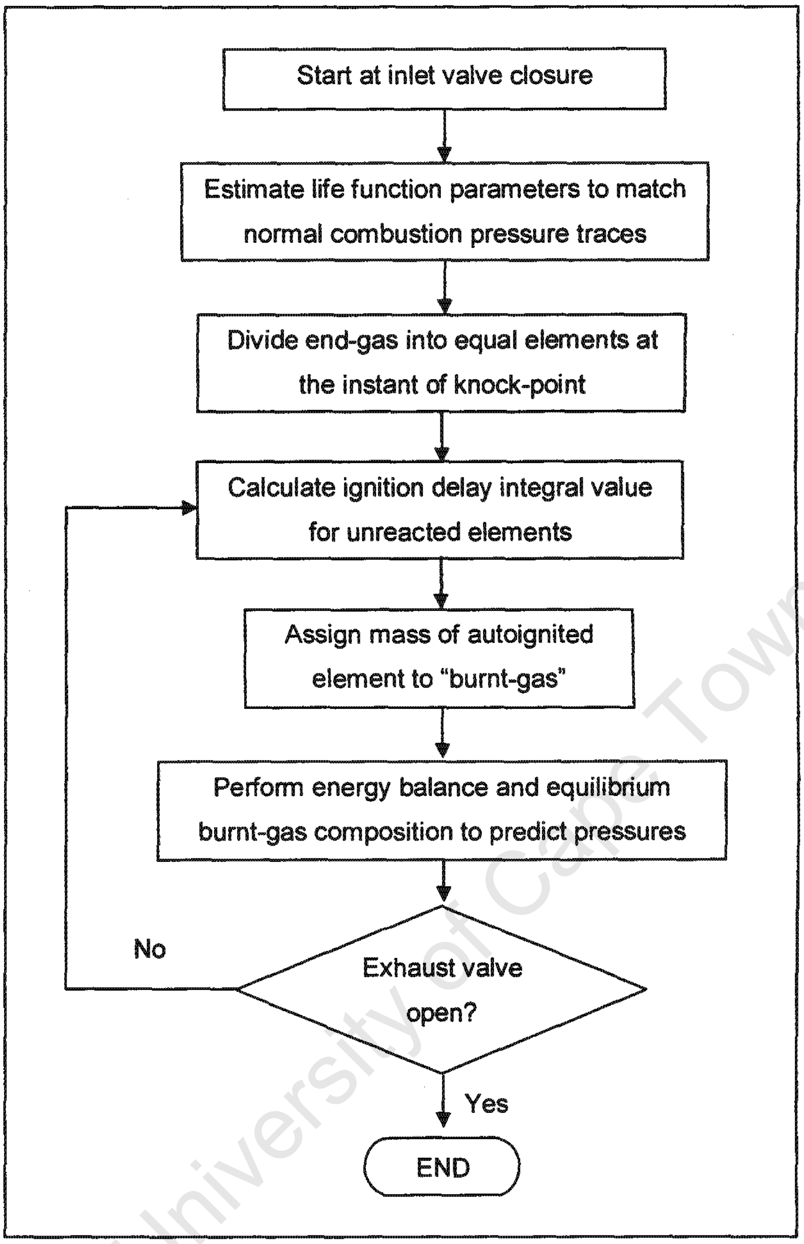

Figure D-3: Flow diagram for the incorporation of the ignition delay model with the predictive engine model.

References D

Heywood, J.B. (1988) *Internal combustion engine fundamentals* New York, McGraw-Hill Book Company. D-3

National Bureau of Standards (1971) NSRDS-NBS37 *JANAF thermochemical tables* National Bureau of Standards D-3

Oppenheim, A.K. and Kuhl, A.L. (1998) *Life of fuel in engine cylinder* SAE paper 980780 .... D-3